Università Ca'Foscari Venezia

Corso di Dottorato di Ricerca in

SCIENCE AND MANAGEMENT OF CLIMATE CHANGE

Ciclo XXXII

Tesi di Ricerca

Halogens in ice core as potential proxies for past sea ice reconstructions

Coordinatore del Dottorato

Ch. Prof. Carlo Carraro

Supervisore

Ch. Prof. Carlo Barbante

Co-Supervisore

Dr. Andrea Spolaor

Dottorando

Federico Scoto

Matricola: 956300

CONTENTS

Abstract (Italiano)

Da circa cinquanta anni, il ghiaccio marino in Artico sta progressivamente diminuendo, sia in estensione che in volume, ad un tasso di gran lunga più veloce rispetto a quanto previsto dai modelli numerici. Sebbene a partire dai primi anni '70 (ovvero la cosiddetta "era satellitare"), siano state acquisite numerosissime informazioni sul suo stato, vi è ancora una mancanza di conoscenza circa la sua evoluzione prima dell'utilizzo di misurazioni strumentali. Per colmare questa lacuna, vengono comunemente utilizzati paleo-archivi come sedimenti marini e carote di ghiaccio. In particolare, alcuni studi hanno identificato nel bromo contenuto all'interno di carote di ghiaccio un potenziale indicatore di condizioni di ghiaccio di neoformazione (o di 1° anno). Durante la primavera polare, infatti, a causa di reazioni fotolitiche che avvengono in prossimità della superficie del ghiaccio marino stagionale, vi è un efficiente riciclo di bromo inorganico che ne determina un aumento delle sue concentrazioni in fase gassosa (BrO) rispetto a quella misurata al di sopra della superficie dell'oceano, del ghiaccio marino pluriennale o del suolo artico. Ogni anno le cosiddette "esplosioni di bromo", possono essere osservate sia da satellite che da misure in-situ durante un periodo compreso fra i primi di marzo fino a fine maggio. Dopo l'emissione, il plume gassoso arricchito in bromo viene preso in carico dalle circolazioni cicloniche presenti nella bassa troposfera polare fino a quando, una volta raggiunta la terraferma, può precipitare sotto forma di HBr, attraverso deposizioni nevose. Quest'ultima sarà anch'essa arricchita in bromo rispetto al rapporto costante fra Br/Na in acqua di mare. Utilizzando l'arricchimento di bromo misurato in diverse carote di ghiaccio artiche, questa tesi è stata ideata seguendo una duplice prospettiva. Da un lato, mira a validare e calibrare il tracciante proposto con immagini satellitari del ghiaccio marino artico per il periodo 1984-2016. Dall'altro, una volta validato il tracciante, lo si applica ad un caso di studio sul paleoclima che ha come obiettivo principale quello di valutare la risposta del ghiaccio marino alle brusche instabilità climatiche dell'ultimo periodo glaciale (note come eventi DO).

Abstract (English)

In the last five decades, Arctic sea ice is experiencing a constant decline faster than forecasted by the most advanced numerical models. Despite we can rely on a consistent amount of sea ice observations that have been acquired since the early 70ies (the so-called "satellite era") there is still a lack of knowledge about its past conditions. To fill this gap, paleo-records such as marine sediments and ice cores are commonly used. In particular, recent studies have identified bromine in ice cores as a potential indicator of seasonal ice conditions. During polar springtime, in fact, the photochemical recycling of bromine is extremely efficient over first-year sea ice, resulting in enhanced concentrations of inorganic gas-phase bromine (e.g. BrO) compared to the ocean surface, multi-year sea ice or snow-covered land. This process is commonly known as "bromine explosion" and is seasonally detected by satellite and in-situ observations from early March to late May. After emission, the BrO plume can be carried for several days by high-latitude atmospheric circulation and in some cases also by cyclones formed in the lower polar troposphere until it reaches land and falls in the form of bromine enriched snow compared to seawater Br/Na ratio. Considering the bromine enrichment records from several Arctic ice cores, this thesis has been thought with a dual perspective. From one side, it aims at validating and calibrating the proposed proxy with remote-sensed Arctic sea ice maps for the period 1984-2016. After validation, the second goal is to apply the sea ice proxy to a paleoclimatic study case which aim to investigate the sea ice response to abrupt climate instabilities of the last glacial period (known as Dansgaard-Oeschger events). Thus, combining remote sensing and paleoclimate records this work aims to move forward from a qualitative to a quantitative link between halogens in ice core and sea ice conditions of the past.

1. Motivation and Outline

Since the second half of the last century, numerous remote and in-situ observations have showed a constant decrease in Arctic sea ice extent and thickness with a pronounced acceleration in the last four decades (Fig.1). The information retrieved are constantly used by climate models to constrain future climate simulations which, in general, agree on expected ice-free conditions of the Arctic Ocean (< 1 million km^2) in the next decades. Therefore, due to its high impact on global climate, wildlife and socio-economic systems (IPCC, 5th AR) there is a growing interest by climate scientists and modellers to use detailed sea ice time series able to provide more reliable climate predictions in view of the ongoing anthropogenic global warming. However, if on the one hand, a massive amount of remote-sensed sea ice data has been collected during the so-called "satellite era" (the period going from early 70ies to present day), on the other hand, there are very rare long-term reconstructions of the natural sea ice variability before the instrumental period. This is the main reason why collocating the current sea ice decline within a multi-decadal-to-millennial natural oscillation still remains a hard challenge, yet upon which paleoclimatic studies can shed some light.

A great effort, in this sense, was done by Kinnard et al. (2011) that, based on a circum-Arctic array of high-resolution sea ice proxies from terrestrial and marine cores, were able to reconstruct the past 1,450 years of summer Arctic sea ice extents. The conclusion of the study was that the current decline is unprecedent and it is consistent with the anthropogenically forced warming occurring in the Northern Hemisphere since early 1950s. However, there are still some open issues such as:

- *Which is the causality and the timing between atmospheric warming and sea ice decrease in the higher Arctic?*
- *Are there any evidences of past sea ice changes in response to abrupt climate instabilities of the last glacial period?*

This work aims to answer these questions, using for the first time, bromine and iodine enrichments from different Arctic ice core records as potential proxies for discriminating past sea ice conditions. The manuscript is structured in a logical way and can be divided in 3 parts. The introduction, consisting of *Chapters 2 and 3*, is a general overview on sea ice, the modern sea ice observations techniques and the proxies commonly used to reconstruct its past evolution.

The second part, corresponding to *Chapter 4*, is dedicated to the novel method developed with this PhD thesis to calibrate the bromine enrichment record of two different Arctic ice cores from Greenland (namely ReCAP and SIGMA-A) with satellite sea ice observations for the modern period

1984-2016. In addition, a detailed study with back-trajectories analysis was carried to isolate the potential bromine source areas and evaluate the role of the transport in modulating the glaciochemical signal of an ice core. The main outcome of this study was the evidence of a statistically significant correlation between seasonal sea ice extent (or first-year sea ice, FYSI) and the amount of bromine in terrestrial ice core.

Finally, once validated the proxy, it is applied to a paleoclimate study case, described in *Chapter 5* which targets to answer the open questions presented before. Based on a previous study new trace halogens and sodium ICP-MS measurements from a glacial portion of the NEEM ice core are used to investigate, with unprecedent sub-decadal resolution, the Canadian Arctic sea ice response to a series of repeated atmospheric warmings (the DO events) occurred in Greenland about 34-42 ky BP. The results are successively treated with two robust statistical methods that provide new information about the *causality, the timing and the magnitude of each warming event from the sea ice perspective*. Finally, *Chapters 6* presents the preliminary results from two additional studies initiated during the PhD and still under investigation. The first work aims to better understand the role of transport on halogen deposition based on analytical measurements on surface snow collected during a traverse over Central Greenland (NEEM to EastGRIP, 2015). The second work instead, shows the 110-year record of sodium, calcium and halogens measured from the SIGMA-A ice core drilled in 2017 on the North West Greenland Ice Sheet. Being located close to the North Water Polynya (NOW), the very high-resolution (sub-seasonal) halogen measurements obtained could provide new insight about the use of iodine as an indicator of phytoplanktonic activity.

Chapters 7 is dedicated to overall conclusions and future outlooks including a summary of the work and activities carried on during the PhD.

All the figures have been produced by the author, unless specified in the caption.
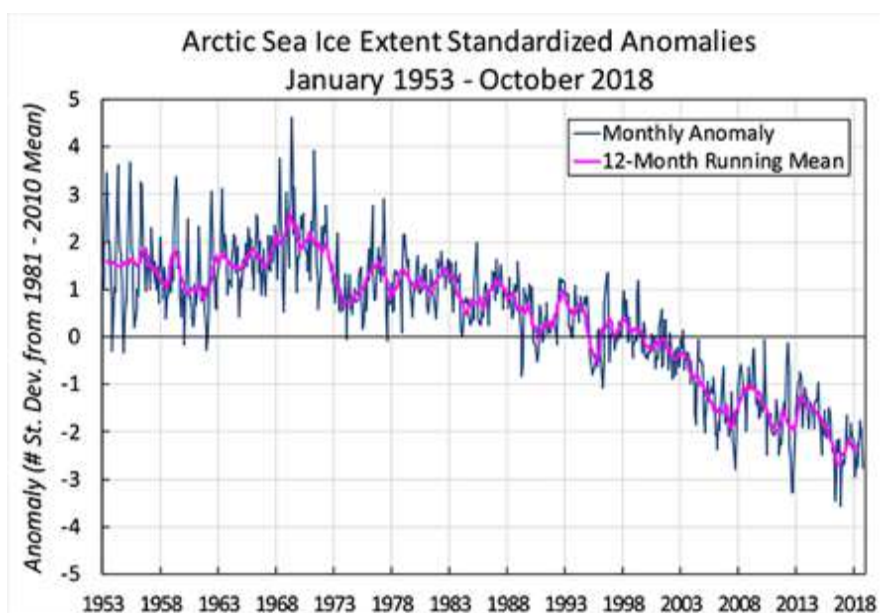
Figure 1: Mean sea ice anomalies, 1953-2018: Sea ice extent departures from monthly means for the Northern Hemisphere. For January 1953 through December 1979, data have been obtained from the UK Hadley Centre and are based on operational ice charts and other sources. For January 1979 present, data are derived from passive microwave satellite sensors. Image by Walt Meier and Julienne Stroeve, National Snow and Ice Data Center, University of Colorado, Boulder.

2. Arctic Sea ice and its role in the Earth's System

In the IPCC-AR5 Artic sea ice was identified as one of the tipping elements for global temperature increase. Because of its albedo, during polar day it cools down the high-latitude troposphere by reflecting the incoming solar radiation while, in the dark winter, it acts as a physical barrier limiting the heat and moisture fluxes from the warmer ocean to the colder atmosphere (Fig.2). Through the brine release process, it affects Arctic water stratification setting the intensity of the Atlantic Meridional Ocean Circulation (AMOC) and, by extension, regulating the global heat transport from the tropics to the North Atlantic and Arctic Region. It is also fundamental resource for wildlife and indigenous people. Hundreds of marine and terrestrial species, from big mammals to micro-algae adapted themselves to survive above and below it. Last but not least, in the next future, Arctic sea ice will play a crucial role also for geopolitics issues. Due to recent decline in its summer extent, new shipping routes have been already opened to link eastern and western civilizations and, being no more covered by frozen sea, new portions of the Arctic ocean have been identified and exploited for offshore energy and fishing businesses.

Figure 2: On the left-side the water vapor emitted from the Arctic ocean while on the right the sea ice edge.
Screenshot extracted from the movie "The big freeze" edited by National Geographic.

2.1 Sea ice formation and evolution

At polar latitudes, when the sea level atmospheric temperature is below -1.8 °C the ocean water starts to freeze, expelling salt from the ice matrix and realising it in the liquid phase. The newly formed fresh-water ice crystals (of 3-4 mm in diameter) are called *frazil* ice. Subsequently, they bond together forming a frozen layer that, depending upon the climatic and ocean conditions, can develop in two different pathways. In calm water conditions the so-called *grease* ice (composed by very thin and smooth ice forms) can progressively develop forming a continuous thin ice layers called *nilas* (up to 5 cm thick) that, pushed by currents or light winds, slide over each other in a process known as *rafting* (Fig. 3A). The final result of this process is a ticker smooth-bottomed congelation ice (up to 30 cm thick) that grows vertically under the sheet ice with slow formation of elongated crystals. In presence of rough conditions instead, the ocean waves push the *frazil* crystals each other creating slushy circular shapes, called *pancake ice*. If the ocean motion is particularly strong and the sheets ice colliding are thick enough another physical process, the *ridging* (Fig 3B*)*, produces lines of *ridges* on the surface where the sea ice fractures and piles on top of itself and its corresponding structure below the surface called the *keels*.

Figure 3: Rafting (A) and Ridging (B) are the main physical mechanism that allow sea ice to thicken.

The life cycle of Artic sea ice goes from its formation which start at the end of September, until March when it usually reaches its maximum extent (Fig.8). Exactly the opposite occurs in the Southern Hemisphere where the maximum extent is reached in September and the minimum in February (Fig. 8). If winter is the favourable season for sea ice's growth, during spring and summer sea ice is subjected to melting. When the newly formed ice (first-year sea ice, FYSI) is thick enough to resist to the melting season, it will grow over the next winter and will be classified according to its age

(second, third…, n-year sea ice) or generally as multi-year sea ice (MYSI >1-year old sea ice). Through a series of mechanisms (described in the next paragraph), the repeated melting cycles experienced by older sea ice determine a progressively loss of salty brine that, as final result, make of MYSI much fresher and less porous than FYSI (Fig.6). The difference in salinity affects the electromagnetic properties of each sea ice type, thus, satellite sensors may use this information to distinguish the two from a distance.

2.2 Salinity and Brine

By definition the salinity is a measure of the concentration of dissolved salts in a solution. It can be defined as kg of salt dissolved in 1,000 kg of water or in a nearly equivalent way based on electrical conductivity properties as Practical Salinity Units (PSU). Just as an example, 35 PSU correspond to 35 kg of salt dissolved in 1,000 kg of solution. Global seawater average salinity varies from 32 to 37 PSU, with highest values in the close basins such as the Red Seas (43 PSU) and lowest values in polar regions (average ~32 PSU or even less depending on the rivers inflow influence). The most concentrated salt ions in seawater are Chloride (55% of the total salts dissolved) and Sodium (30.6%), followed by Sulphates (7.7 %), Magnesium (3,7%), Calcium (1.2%), Potassium (1.1%) and minor constituents (0.7%) including Bromine (0,19%) and Iodine (0,0003%). As widely known, Sodium chloride (NaCl) is the most abundant salt present in the ocean water.

Salinity also affects the freezing point of a solution. According with thermodynamics laws, pure water freezes at 0 °C, however, for an increase of 1 PSU the freezing point of the solution decreases of -0.056 °C thus, in polar regions, where the ocean salinity is about 32 PSU, the water begins to freeze at around -1.8 °C. When _frazil_ ice crystals form, salt accumulates into microscopic droplets called _brine_ (Fig.4), which over time are gradually expelled from the ice matrix back into the ocean increasing the water salinity and contributing to the dense water sinking that regulates part of the global oceanic circulation. Due to their high salinity, brine droplets can concentrate inside the inclusions between the ice crystals remaining in a liquid state in respect to the ice lattice that is in a solid phase. This mechanism led to an increase of the sea ice salinity up to 15 PSU for first year ice while, when sea ice ages and the brine is gradually drained out the salinity decreases up to 1-2 PSU for multiyear sea ice. Brine can move out of sea ice following three different mechanisms: gravitational drainage, pressure stress and temperature gradients.

Figure 4: Brine pockets forming within sea ice lattice. From "Sea ice 3ʳᵈ ed. D.Thomas"

The first process common especially when sea ice is relatively young. Aided by gravity, the brine migrates downward through holes and channels in the relatively warmer and more porous sea ice until it reaches the ocean. The second way to brine

expulsion is linked with the pressure stress exerted on the brine pockets due to the thermal expansion of the ice matrix that breaks the brine pockets, allowing the brine to migrate to the ocean through the cracks formed.

In addition, summertime surface melting can also enhance salt loss because the melting water accumulated in small freshwater surface ponds (Fig. 5) can percolate through the crack widening the existing capillaries in the ice matrix and washing out the remaining brine.

Finally, the last mechanism for brine removal is the temperature gradient that forms during wintertime when due to colder temperatures brine channels shrink and, as consequence, the brine increases its salinity to the point at which it can melt the ice from the underside. This leads to a downward migration of brine droplets, ultimately allowing the brine to escape into the ocean below the ice sheet. Although is not the most effective mechanism for brine removal, this last process explains the typically c-shape salinity profile of sea ice (Fig. 6).

Figure 5: Melt ponds forming over sea ice floes, the darker colour of water decreases the albedo promoting further melting. Credit: NASA
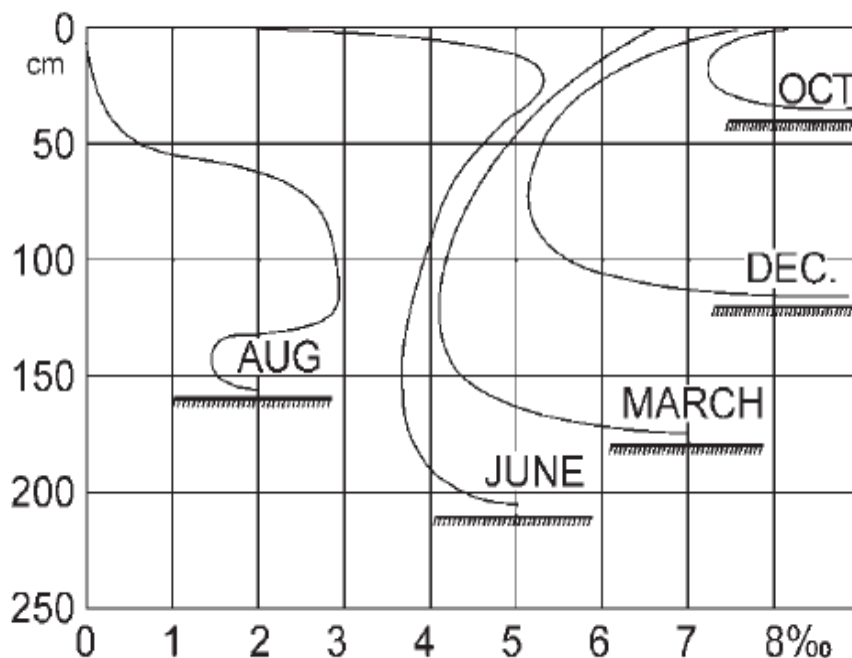

Figure 6:Evolution of sea ice salinity profiles (from Malmgren, 1927). Note the characteristic C-shape of the young sea ice during the winter growth (from October to March).

2.3 Arctic and Antarctic sea ice

Although they are might appear very similar, Arctic and Antarctic sea ice differs each other for many factors. The main difference is the geographic conformation of the two basins. Indeed, except for the Fram Strait, the Arctic Ocean is a closed basin (with a mean depth of 1361 m) surrounded by the boreal continents. Antarctica instead is exactly the opposite being a land-and-marine based continent encircled by the vast Southern Ocean (on average 4,000-5,000 m depth). The difference in their geography strongly affects sea ice growth and dynamics.

In the Arctic, wintertime formation mainly occurs in the shallow and fresher waters of Chucki Sea. Subsequentially, sea ice moves in the Arctic Ocean transported by the two main wind-driven pathways. One of them is the Beafourt Gyre (BG), a clockwise oceanic gyre located in the Canada basin that can traps sea ice up to 6 years. In this period, sea ice ages and, through rifting and ridging processes, increases its original thickness from 0.30 m up to 5 m. The other preferential pathway is the Trans Polar Drift (TD), an oceanic current crossing straight the Artic basin from the Laptev Sea and the East Siberian Sea towards Fram Strait (Fig 7A). The average TPD speed is 2.4 km per day, thus to cover the whole distance sea ice takes 1-2 years. According to residence time, Arctic sea ice is classified as first-year sea ice (FYSI) when, due to seasonal melting or export, the new-formed sea ice does not grow for more than one year. When it survives to the first-year, it became gradually fresher and stiffer and it's referred to as multi-year sea ice (MYSI). As said before, Antarctic sea ice is no land-locked such as in the Arctic basin thus it's free to grow symmetrically around the pole and move, with higher drift speed, around the continent. The prevalent ocean current of the Southern Ocean is the Antarctic Circumpolar Current

Figure 7:(A) The Arctic region. Blue arrows represent cold currents and red arrows the infl owing Atlantic Water. BG – the Beaufort Gyre, TD – the Transpolar Drift, AW- Atlantic Water. (B) The Antarctic region. Black arrows indicate the schematic circulation of Antarctic Circumpolar Current (ACC), WG – the Weddell Gyre and RG – the Ross Gyre In both figures the darker grey shows the mean maximum winter ice extent from 1979-2007 however Arctic sea ice reached a new minimum in 2012. From "Sea ice" 2° ed. D. Thomas.

(ACC) that transports the sea ice from west-to-east direction isolating and cooling the polar atmosphere. When sea ice edge grows enough at the end of spring (corresponding to September in the SH) and reaches the warmer waters (approximately located at 50-60 °S) where most of the ice start to melt. The remnant ice is transported by the persistent anti-clockwise gyres in the Weddell Sea and Ross Sea which led to the accumulation of sea ice floes in the eastern side of the Antarctic Peninsula forming the rare MYSI present in the Southern Ocean. (Fig 7B)

Table 1: Summary of the differences between Arctic and Antarctic sea ice from NSIDC website.

Summary of differences between Arctic and Antarctic sea ice characteristics

	Arctic	Antarctic
Average Maximum Areal Extent	15 600 000 km^2	18 800 000 km^2
Average Minimum Areal Extent	6 500 000 km^2	3 100 000 km^2
Typical Thickness	~2 m	~ 1 m
Geographic Distribution	Asymmetric	Symmetric
Snow Thickness	Thinner	Thicker
Trend, 1979-2008	Significant decrease of 4.4% (~520,000 km^2) per decade	Small increase of 1.8% (~219,000 km^2) per decade

Figure 8: Arctic and Antarctic sea ice concentration climatology from 1981-2010, at the seasonal maximum and minimum levels based on passive microwave satellite data. From NSIDC, University of Colorado, Boulder.

3. *Modern sea ice observation and past reconstructions*

Due to extreme climatic conditions and remote locations sea ice monitoring still remains a great challenge for technicians and scientists who undergo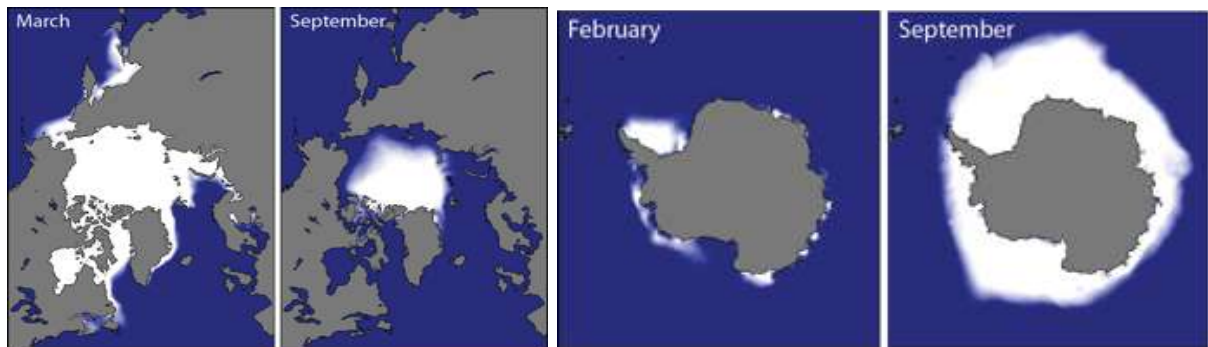 an impressive logistic effort to carry on their observations. Multidisciplinary research vessels (RV) and submarines operate year-round opening their ways through the pack to gather in-situ information about the physical state of the ocean, but also to install remote camps over the ice where collect precious measurements of the polar atmosphere, sea ice-related biogeochemical cycles and eventually also sea ice motion.

The principal limitation of the observations retrieved is the relatively reduced area covered by RV's routes if compared to great vastity of Arctic and Antarctic sea ice. Nevertheless, this information is essential to calibrate and validate another typology of measurements conducted from a distance widely referred as to *remote sensing*. Thanks to accurate sensors installed on orbiting satellite and/or flying aircrafts, it is possible to observe every single square meter of the globe, including the sea ice cover of the Polar Regions. A great variety of information can be inferred from distance such as the sea surface temperature (SST) of the ocean, sea ice drift, chlorophyll concentration, winds direction and many other variables that are constantly implemented in Earth system models to produce more realistic sea ice projections (Fig. 9). However, if on the one hand we can rely on a massive amount of sea ice data from polar-orbiting satellite collected over the last five decades, on the other hand, there are very scarce or no information about past sea ice coverage prior to the instrumental period. In this sense, an aid to investigate sea ice long-scale variability (i.e centennial to millennial variations) is provided by paleoclimatic studies that use biomarkers and geochemical proxies from marine and terrestrial archives.

Figure 9:Summer sea ice extent ensemble-model predictions (red and blue bands) vs observations (black). From Stroeve et al., 2007.

Divided in three parts, this chapter aims to provide a general overview about modern sea ice observation techniques and introduce the main proxies used to reconstruct past sea ice evolution (*Paragraphs 3.1 and 3.2*). Among terrestrial proxies, the last part of the chapter (*Paragraph 3.3*) is dedicated to a focus on the use of halogens in polar ice as past sea ice indicators that will constitutes the theoretical background on which this thesis is based.

3.1 Remote sensed sea ice observation

The remote sensing technology uses the ability of the sensors installed on satellites or aircrafts to detect the electromagnetic (EM) radiation of an object on the Earth's surface or in the atmosphere.
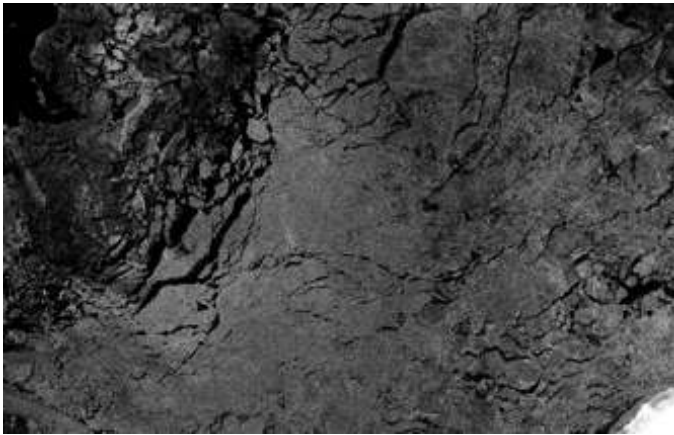
Figure 10:SAR Image of sea ice cracks from Copernicus Sentinel-1 Satellite.

Every day since late 1979, polar-orbiting satellites have been largely measured sea ice in several regions of the EM spectrum including the visible, infrared, and microwave.

As it will be showed in the next paragraphs, the choice of a spectral region rather than another strictly depends on different factors such as the solar radiation and weather conditions. This introductive part about sea ice monitoring from satellite will not deal about technical sensor specification and unprocessed data (Level 0,1, 2 of satellite products) because it will be out of the topic of this work. Rather, it aims to give a general overview about repeated sea ice observations (Level 3 - 4) freely available as time series analysis for scientific purposes.

3.1.1 Visible and infrared sensors

Visible, infrared and near-infrared imagery collected by sensors such as MODIS (Moderate-Resolution Imaging Spectroradiometer) and VIIRS (Visible Infrared Imaging Radiometer Suite) are broadly used to create operational sea ice products. However, their performance is strictly limited to particular circumstances such as in presence of sunlight and no cloud's coverage. In these conditions, sea ice reflects around 50-70% of the incoming solar radiation (McEvoy, 2003) resulting to be easily distinguished by visible optical satellites (Fig. 11A). In contrast, during polar night or in presence of clouds, occurring for the 70-90% of the time in the Artic, other sensors are required. Sea ice measurements in absence of sunlight can be conducted using infrared sensor taking advantage of the physical principle that infrared emission is proportional to the heat of an object. Indeed, wintertime sea ice temperature can be from 20 to 40 °C lower than surrounding ocean which is above the freezing point. This temperature

Figure 11: (A) True colour Terra-MODIS image taken March 6, 2003 in the Arctic Ocean north of Alaska. (B) Terra MODIS ice surface temperature map product of the same area at the same date and time. The colour scale represents ice surface temperature in Kelvin. Image from D.K. Hall et al. (2004)

difference allows infrared satellite also to capture sea ice features like cracks (Fig. 11B) or leads, however, during summertime some problems may occur due to formation melt ponds forming over sea ice surface. The water contained in the pond has, in fact, approximately the same temperature of the ocean water making sea ice hard to distinguish from the surroundings. Also gasses and water vapour contained in clouds emit infrared radiation so, also in this case, infrared observations have to be accompanied by other measurements.
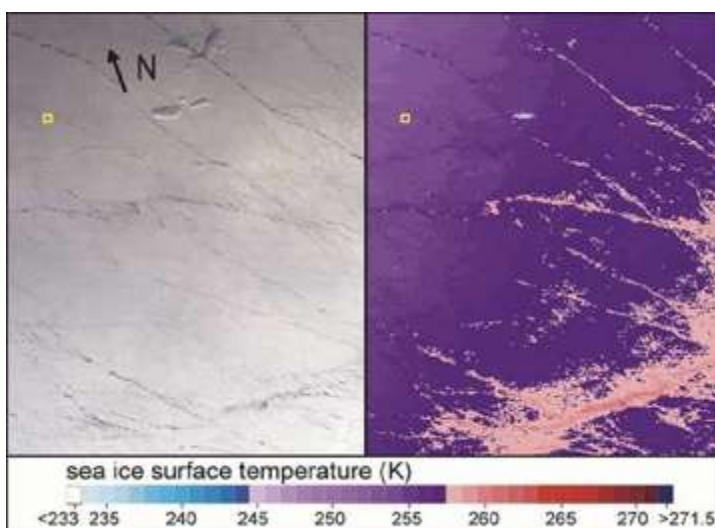
3.1.2 Passive and active microwaves sensors

A way to collect sea ice observation regardless of daylight conditions and the presence of clouds is employing microwaves sensors. Differently from infrareds, which are strictly depending on the temperature of an object, microwaves emission is determined by other physical properties such as the atomic composition and the crystalline structure. The crystalline ice lattice reflects much more microwave energy from the sun compared to clouds and liquid waters, therefore, sea ice can be easily distinguished from the open ocean and clouds. A sensor designed to measure the natural (or passive) microwave energy emitted or reflected by an object is called passive sensor. The biggest limitation of measuring passive microwave radiation is that the natural energy emitted by sea ice is relatively low, to collect a proper signal, the sensor must integrate a large area at the expenses of detailed features (i.e cracks or leads) that are not easily detected (Fig.12B). Nevertheless, due to their great versatility, a series of passive sensors (some of them listed in Table 3) have been used for remote sensing applications collecting every day, since 1972, the most complete and reliable long-term record of changes in Arctic sea ice.
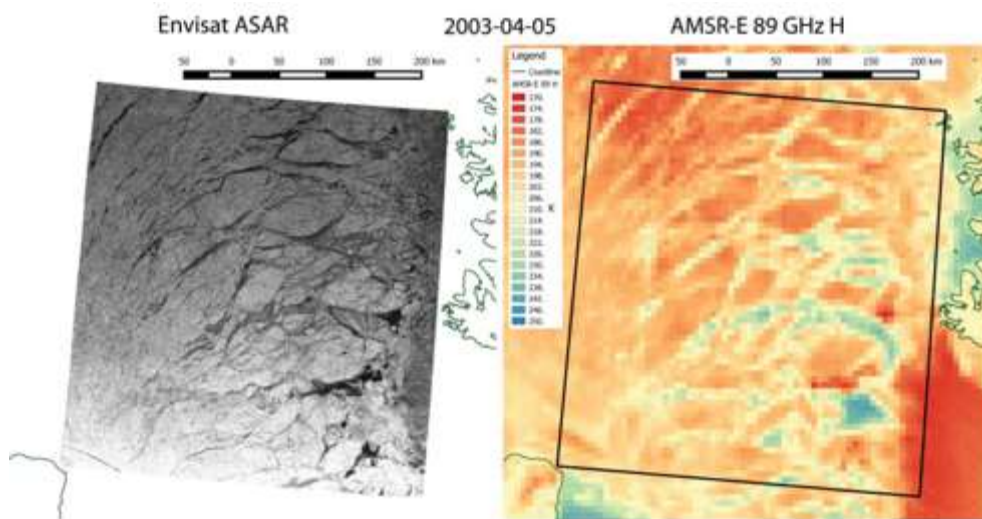
Figure 12: Comparison of (A) a synthetic aperture radar (SAR) image with 150 m spatial resolution (but limited coverage) with (B) the Advanced Microwave Scanning Radiometer – Earth (AMSR-E) radiometer observations at 89 GHz and about 5km resolution on 5 April 2003. Similar features in the ice can be observed but with much different detail.
From: D.Thomas, Sea ice 3°Ed.

Differently from passive microwaves, active sensors provide their own source of energy to illuminate the objects they observe. Similar to radar installed aboard of aircrafts and ships, active sensors (also called radar) send microwave energy from an emitting antenna and measure the amount of radiation reflected or backscattered from the target. For sea ice investigation three type of active sensor are commonly used. The first type is the Synthetic Aperture Radar (SAR), a kind of

imaging radar which is particularly able to distinguish between sea ice types (FYSI vs MYSI) based on their different backscattered radiation. SAR data are also used to detect very detailed features on the ocean such as icebergs, ships and leads on sea ice (Fig. 10 and 12A). Non-imaging radar, or scatterometer, can be another type of active sensor. It is similar to SAR (but with a lower resolution) measures the backscattered radiation from the ocean surface inferring wind direction and sea ice extent. Finally, the last type of active sensors called "Altimetry Sensors", are used to measure the height of sea ice above sea level (from which is possible to infer sea ice thickness) by sending a pulse of energy towards the earth's surface and measuring the time it takes to come back to the satellites. ESA's Cryosat and NASA's Icesat are two example of satellite altimeters operating above polar regions.

Table 1: Overview of active and passive sensors used for sea ice research since 1972. (From NSIDC)

LAUNCH	OPERATING	SENSOR	TYPE	SATELLITE	AGENCY
1972	5 years	Electrically Scanning Microwave Radiometer (ESMR)	Passive	Nimbus-5	NOAA
1978	1 year	Scanning Multichannel Microwave Radiometer (SMMR)	Passive	Seasat 1	NASA
1987	Ongoing	Special Sensor Microwave/Imager (SSM/I)	Passive	DMSP	NASA
1995	17 years	Synthetic Aperture Radar (SAR)	Active: Imaging Radar	Radarsat-1	CSA
1999	10 years	*Seawinds*	Active: Scatterometer	Quikscat	NASA
2002	Ongoing	Advanced Microwave Scanning Radiometer-Earth Observing System (AMSR-E)	Passive	Aqua	NASA
2003	6 years	*ICEsat*	Active: Laser Altimetry	Icesat	ESA
2010	Ongoing	SIRAL (SAR/Interferometric Radar Altimeter)	Active: Radar Altimeter	Cryosat	ESA
2018	Ongoing	*ICEsat-2*	Active: Laser Altimetry	Icesat	ESA

3.1.3 Modern changes of Arctic sea ice concentration and thickness

Considering a satellite-based square grid cell, if the percentage of sea ice concentration within the cell is higher than a low-threshold (usually 15%) the corresponding region will be defined as ice-covered, if lower, it will be considered ice free. The sum of the ice-covered cells gives the total sea ice extent which in the Arctic has been observed to decline constantly since 1979 (-3% decade^{-1} relative to the 1981-2010 average (Cavalieri and Parkinson, 2012). In particular, September sea ice extent (usually the annual minimum in the Artic) might be seen as a crucial indicator of the ongoing sea ice decline in response to the increase of atmospheric temperatures strictly linked with the amount of GHG in the atmosphere (IPCC-AR5). An evidence is that 13 of the lowest sea ice extents recorded in the satellite era have all occurred in the last 13 years (2006-2019). On September 18, 2019, Arctic sea ice extent reached 4.15 million km^2 effectively tied with 2007 and 2016 for second lowest, only behind 2012, which is the record minimum. (Fig 13A). Looking at other sea ice records including operational chart and other written sources it was observed that Arctic sea ice extent has been declining since at least the early 1950ies (Kinnard et al., 2011). Sea ice volume decrease is another sensitive indicator of the current climate change with 75% of the total sea ice volume lost in the last 40 years (Gascard 2019, TC *in discussion*). Consistent with sea ice extent also sea ice thickness in fact have showed a marked decline in the second half of the 20th century. Using submarine data, 1.3 m of difference in sea ice thickness between the 1950s - 1990s was calculated by Rothrock et al. in 1999. A further study examining 42 years of submarine records, from 1958 to 2000, and a 5 years of ICESat records (2003-2008) concluded that the mean Arctic sea ice thickness decreased of 1.75 m between 1980 and 2008, passing from an average of 3.64 m to 1.89 m (Kwok and Rothrock, 2009) (Fig. 13B). To conclude, Laxon et al. (2013), compared sea ice volume between 2003-2008 and 2010-2012. They found that sea ice volume declined by 1,479 km^3 at the end of winter and 4,291 km^3 at the end of summer.
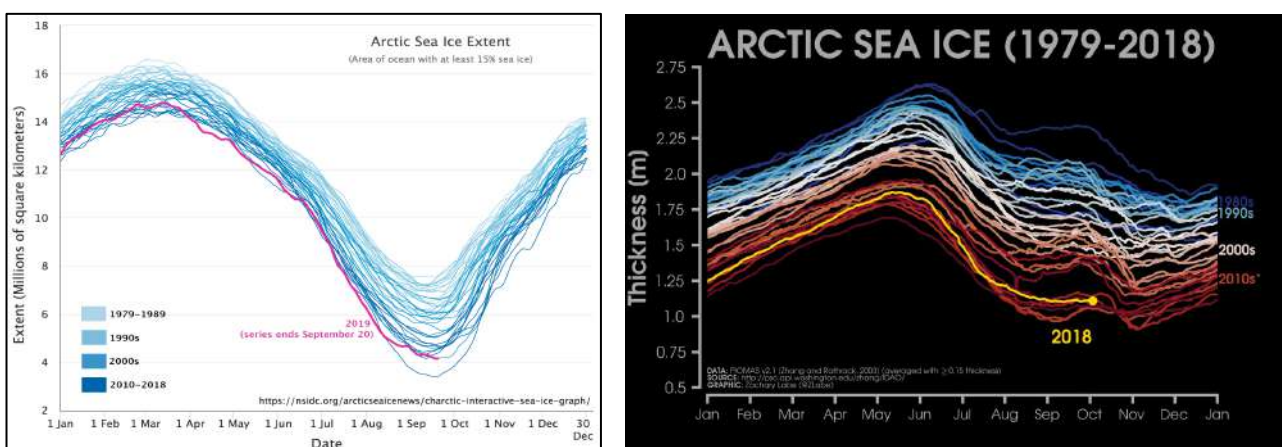

Figure 13: (A): Arctic sea ice decline per decade. The colour scheme moves from lightest to darkest blue, from 1979 to 1989 and 2010 to 2018, respectively. 2019 is shown in magenta. Credit: M.Scott, NSIDC (B)Sea ice thickness change from 1979-2018. Data from the Pan-Arctic Ice-Ocean Modeling and Assimilation System (PIOMAS). Credit: Zachary Labe.

3.1.4 Sea ice Age

During its lifecycle Arctic sea ice is subjected to drift, deformation and fracture. The result of recurrent sea ice dynamics is an overall thickening (through cracking, rifting and ridging) based on its age; the average sea ice thickness, in fact, passes from the 0.3 m of first-year ice up to 5 m or more for aged multiyear sea ice. As mentioned before, the two sea ice types have also different salinity, a feature that make them distinguishable also from remote passive microwave sensors (because of a different EM radiation emitted), thus sea ice age can be used to estimate the thickness.

Since the mid-1980s, consistent with the ice volume reduction, the presence of ≥5 year sea ice in the Arctic basin decreased from the 57% in 1987 to only 7% in 2007. (Maslanik et al, 2007). Since then, due to enhanced summer melting or sea ice export from the Fram Strait, the amount of MYSI in the Arctic continues to decline (Perovich et al., 2014). (Fig.14)

Estimates of sea ice age for the Arctic Ocean derived from remotely sensed sea ice motion and sea ice extent are provided in the the EASE-Grid Sea ice Age, Version 4 released by NASA-National Snow and Ice Data Center (NSIDC). It covers the Northern Hemisphere from 90-27° N with a spatial resolution of 12.5 km x 12.5 km and a temporal resolution of 7 days. The temporal coverage goes from 1984 up to the present. (Tschudi, M. et al., 2019). The method used to estimate sea ice age is based on the combination of two different dataset. One is the satellite sea ice concentration while the other contains weekly gridded sea ice motion vectors. First, sea ice extent (SIE) is computed by considering only the grid cells (12.5 km x 12.5 km) with at least 15% sea ice concentration (SIC). Secondly, a Lagrangian tracking is applied to each cell that moves according to the mean weekly sea ice drift (the new Polar Pathfinder Daily 25 km EASE-Grid Sea ice Motion Vectors, V.4.) (Tschudi et
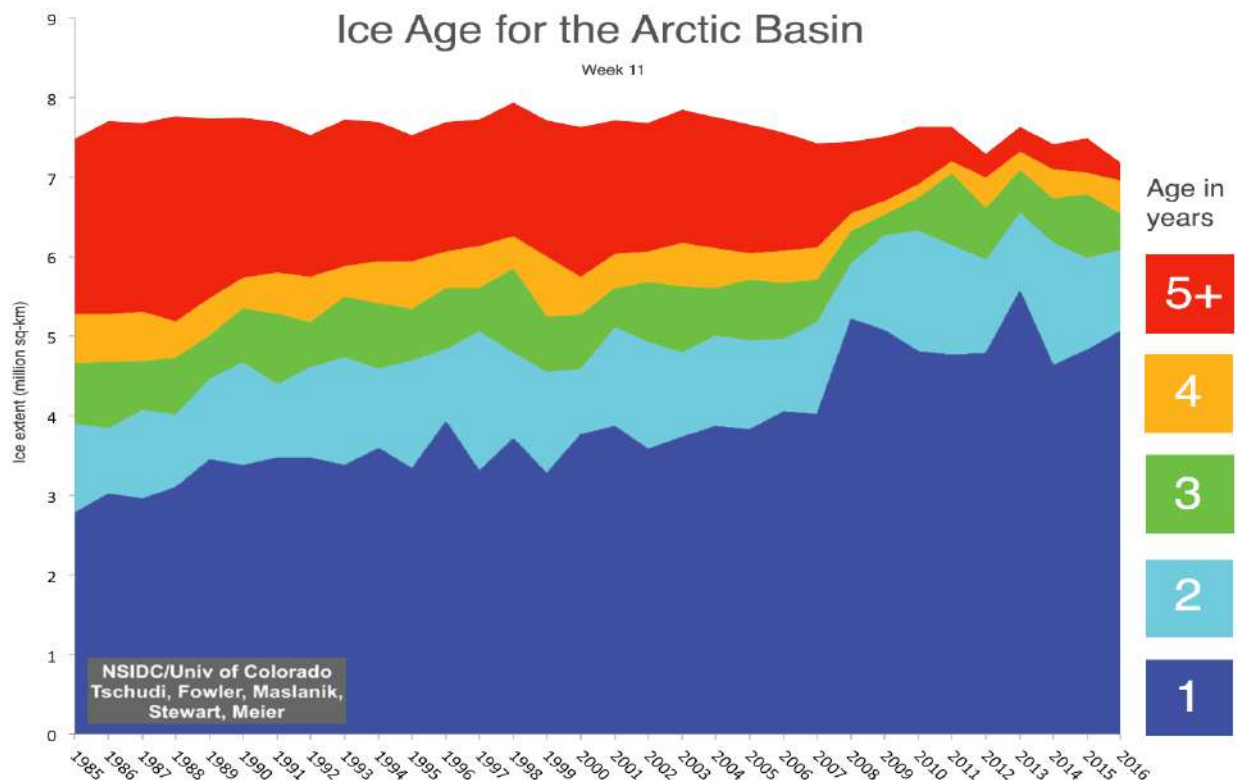
Figure 14: Winter sea ice age distribution in the Arctic basin since 1985.

al., 2019). The cell's position is tracked for every week and, based on the residence time (the sum of the weeks) inside the weekly SIE area, is than possible to calculate its age. If after its translation due to the sea ice drift the particle is located out of the SIE area, then it is assumed that the sea ice within that cell has melted. In contrast, if the cell is still present within the SIE area between week 37 and 38, (when the sea ice start to form in September), its age is rounded up to the successive full year. For example, a grid cell with > 15% of 1°-year ice whose age is 48 weeks it passes to 2°-year ice while a grid cell of the age 2 years and 50 weeks will become 3°-years and so on. When two or more different age parcels coexist in one grid cell, only the age of the older one (with SIC>15%) is accounted for. The physical principle is that younger and thinner sea ice deforms and melts more easily than older sea ice, thus, in case of a cell with 85% of 2°-year ice and 15% of 5°-year ice, the cell will be assigned to 5-year old (Fig.15).
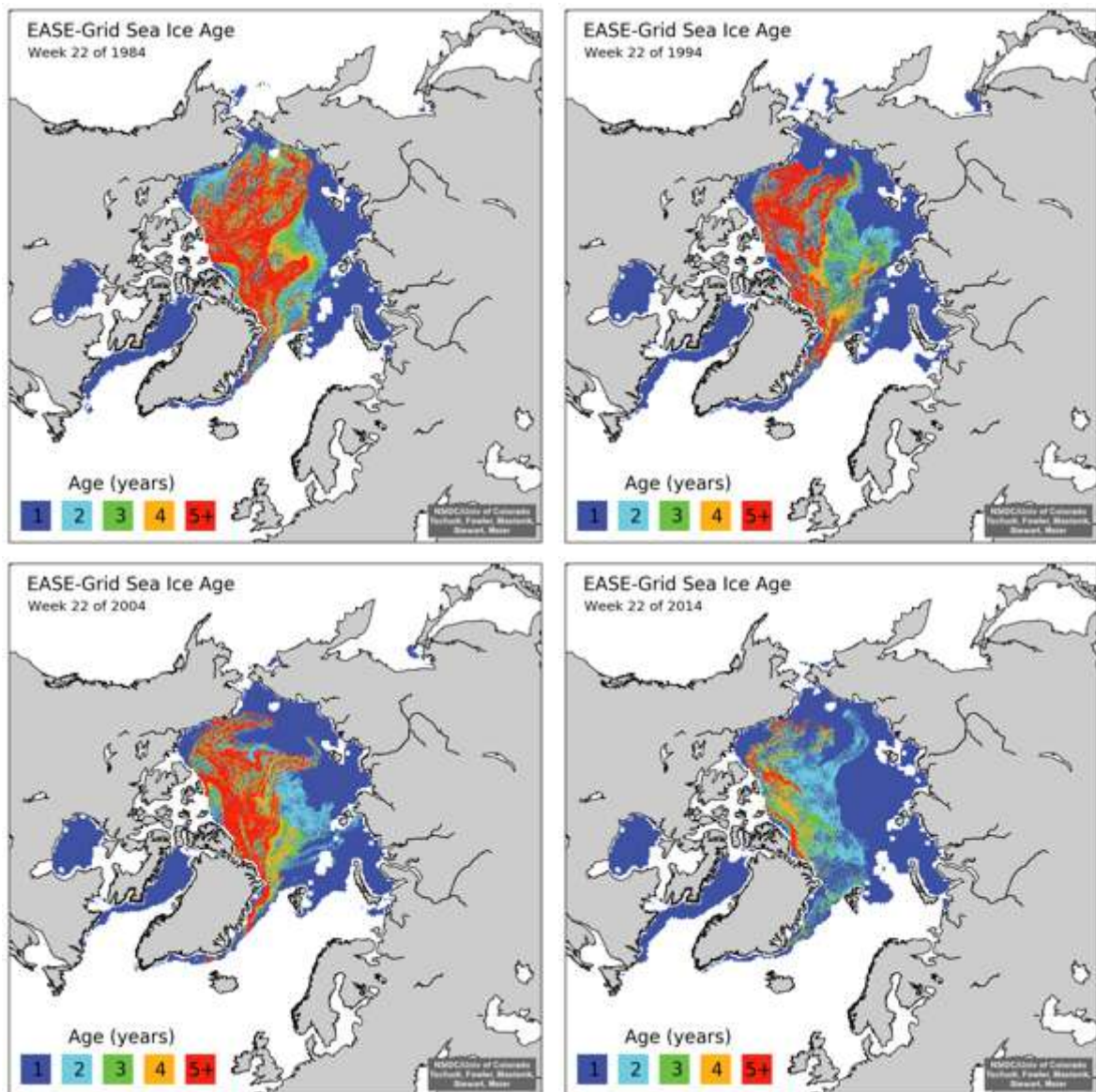
Figure 15: Sea ice age distribution for the Arctic for week 22(end of May) of the years 1984, 1994, 2004, and 2014. Each pixel colour represents a different sea ice age according to the legend.

3.2 Marine and Terrestrial sea ice proxies

As seen in the previous paragraph, the satellite Artic sea ice record covers approximately the last 40 years. Before this period, sporadic photographs, written description or navigational chart can provide local information restricted to the last century. Especially in the perspective of a warming climate, the knowledge of past sea ice evolution result to be crucial to better understand its links with the other components of the Climate system. Therefore, to overcome this limitation, geochemical proxies from both marine core (Belt et al., 2007; Polyak et al., 2010; Cronin et al., 2013; Collins et al., 2013) and terrestrial archives such as ice cores (Abram et al., 2013; ; Spolaor et al., 2013; Levine et al., 2014; Curran et al., 2014; Spolaor et al., 2016) can be used to reconstruct past sea ice conditions.

3.2.1 Marine Archives

Regarding sea-sediment cores, benthic foramifera, ostracodes or on the molecular marker IP_{25} are often used for past sea ice reconstruction. Benthic foraminifera are divided into two main proxy groups based on their ecological preferences. The first group includes taxa that are commonly considered endemic Arctic species (eg. *Bolivina arcticna*) and indicator of perennial sea ice. The other foraminiferal group comprises the so-called "phytodetritus" species (eg. *Epistominella exigua*) which develop in the frontal oceanic zones or at the sea ice edge (Muller et al.,2009). Alike foraminifera, other marine crustaceous, the ostracodes, can be used to study past sea ice conditions (Cronin et al, 2013) by classifying each taxa according to its distribution range. The organic biomarker IP_{25} (Ice Proxy with 25 carbon atoms), a highly branched isoprenoid (HBI), is a novel approach based on long carbon chains produced by diatoms living in association with seasonal sea ice, probably *Haslea* (Belt et al., 2007). The majority of IP_{25} accumulation in Arctic sea ice coincides with the spring sea-ice diatom bloom, thus its occurrence is believed to reflect seasonal sea ice cover rather than ice-free, multi-year or permanent sea ice conditions. The interpretation of the IP_{25} biomarker as a presence/absence indicator of past Arctic sea ice becomes complicated in permanent or non-seasonal sea ice conditions, both of which result in an absence of IP_{25}. In order to distinguish between these two extreme scenarios, Muller et al. (2009) introduced the PIP_{25} index that put together IP_{25} and brassicasterol (BC), a phytoplankton-derived biomarker considered an indicator of ice-free sea surface condition. It is defined as:

$$PIP_{25} = IP_{25} \ / \ (\ IP_{25} + N \ . \ OW)$$

Where OW refers to the brassicasterol (or dinosterol, both proxies for Open Water) and N is a normalization factor that accounts for the marked different scales in concentration between IP_{25} and the OW proxy. Using this ratio, the PIP_{25} can vary from 0 (indicating open water conditions) to 1 (multiyear conditions). Intermediate values indicate marginal sea ice conditions (Müller et al. 2009; Hoff et al. 2016) (Fig.16).
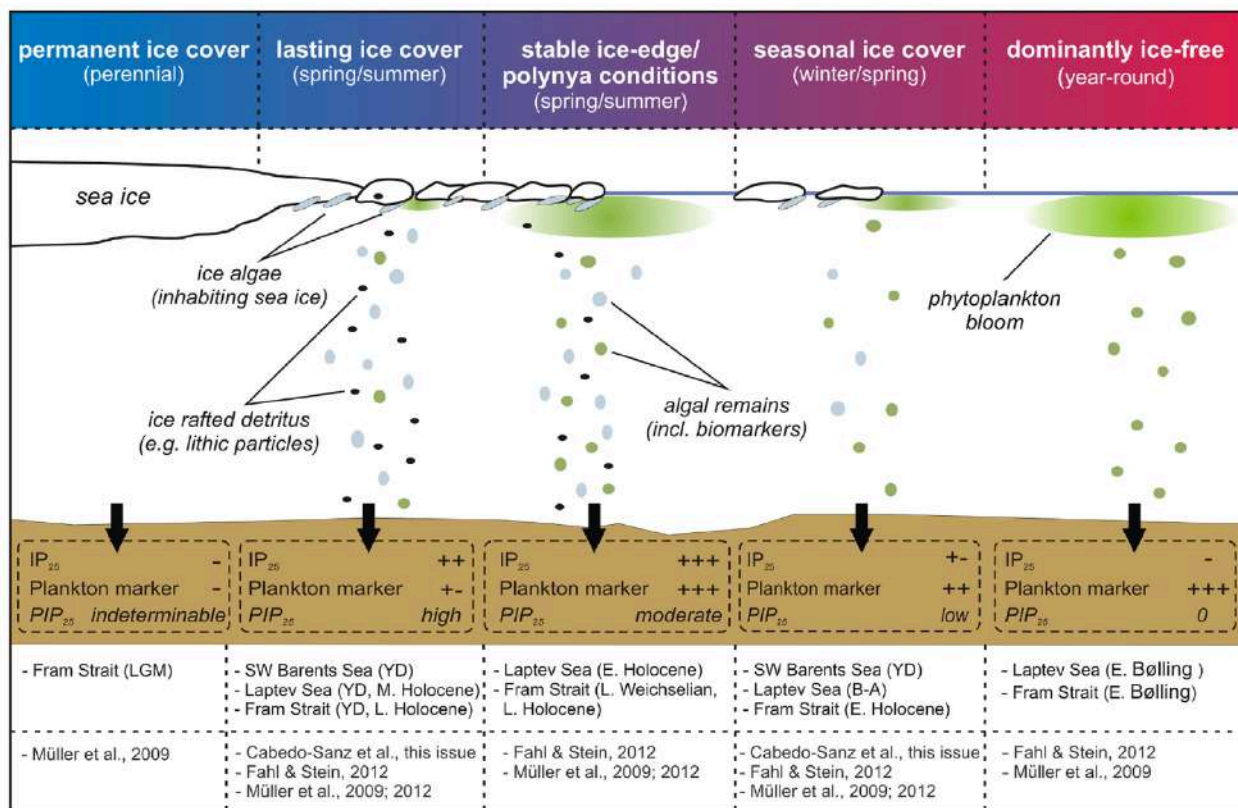
permanent ice cover (perennial)	lasting ice cover (spring/summer)	stable ice-edge/ polynya conditions (spring/summer)	seasonal ice cover (winter/spring)	dominantly ice-free (year-round)

sea ice

ice algae (inhabiting sea ice)

phytoplankton bloom

ice rafted detritus (e.g. lithic particles)

algal remains (incl. biomarkers)

IP_{25}	$-$	IP_{25}	$++$	IP_{25}	$+++$	IP_{25}	$+-$	IP_{25}	$-$
Plankton marker	$-$	Plankton marker	$+-$	Plankton marker	$+++$	Plankton marker	$++$	Plankton marker	$+++$
PIP_{25}	indeterminable	PIP_{25}	high	PIP_{25}	moderate	PIP_{25}	low	PIP_{25}	0

- Fram Strait (LGM)	- SW Barents Sea (YD) - Laptev Sea (YD, M. Holocene) - Fram Strait (YD, L. Holocene)	- Laptev Sea (E. Holocene) - Fram Strait (L. Weichselian, L. Holocene)	- SW Barents Sea (YD) - Laptev Sea (B-A) - Fram Strait (E. Holocene)	- Laptev Sea (E. Bølling) - Fram Strait (E. Bølling)
- Müller et al., 2009	- Cabedo-Sanz et al., this issue - Fahl & Stein, 2012 - Müller et al., 2009; 2012	- Fahl & Stein, 2012 - Müller et al., 2009; 2012	- Cabedo-Sanz et al., this issue - Fahl & Stein, 2012 - Müller et al., 2009; 2012	- Fahl & Stein, 2012 - Müller et al., 2009

Figure16: Schematic representation of different sea ice conditions and respective IP25 and phytoplankton biomarker contents within sediments together with the resulting PIP25 indices (modified from Müller et al., 2011). Examples of recent palaeo application studies where the combinatory biomarker approach has been used for sea ice reconstructions in the Arctic Ocean are also listed. From: Belt and Müller,2013.

3.2.2 Terrestrial Archives

Information of past sea ice conditions can be extracted also from land-based archives. Interestingly, past local sea ice reconstructions have been accomplished based on observations of raised beaches (St- Hilaire-Gravel et al. 2010) or taking into account the frequency of drifted material such as wood or whale bones arriving in the coasts of polar regions (e.g. Häggblom 1982; Funder et al. 2011). However, up to the present, the most reliable sea ice proxies from terrestrial archive comes from geochemical species measured in polar ice cores.

One of them is the Methanesulfonic acid (MSA), an oxidation product of the Dimethyl Sulphide (DMS), which is primarily produced by phytoplankton and, in Southern Ocean, by sea-ice algae. Once sea-ice is melting, it promotes a phytoplanktonic bloom that produces great emissions of DMS into the atmosphere. In Antarctica, the DMS' oxidation product (MSA) exhibited a good correlation (r > 0.5, depending on the considered Southern Ocean sector) with the sea-ice extent on relatively short timescales (Curran et al., 2003; Abram et al., 2010; Thomas and Abram, 2016). Unfortunately, MSA is unstable and it is not preserved over centennial to millennial timescales (Röthlisberger et al., 2010) thus it's not suitable for long-term reconstructions. In addition, MSA is strongly site-depended therefore a network of ice core records and a multiproxy approach are required to produce reliable past sea-ice reconstructions (Abram et al., 2007). Another potential sea ice proxy is Sodium (Na^+)

whose source is still under debate. Actually, if the SO_4/Na in seawater is typically 0.25 (Abram et al., 2013), the one found in aerosol and snowfalls over Antarctica is strongly depleted in SO_4 (Rankin and Wolff, 2003). Some authors proposed that Sodium derived from frost flowers (Douglas et al., 2012), while others from the sublimation of salty blowing snow (Yang et al., 2008). Sea-salt sodium can give reliable information regarding the long-term trend for sea-ice reconstructions based on the fact that it was more concentrated in the glacial periods, when the open ocean was further away. However, on shorter time scale the analytical signal is strongly influenced by meteorological factors and extra contribution from open water (Abram et al., 2013; Levine J. G., et al., 2014).

3.3 Halogens in polar ice cores

Among the sea ice proxies derived from polar ice cores, halogens (bromine and iodine) have been used several times to reconstruct past sea-ice extent both in the Arctic (Spolaor et al., 2013; Spolaor et al., 2016 a,b; Cuevas et al., 2018) and in Antarctica (Vallelonga et al., 2017; Spolaor et al., 2012). The last part of this chapter is dedicated the theoretical background and the use of halogens as proxies for past sea ice conditions.

3.3.1 Sources of halogens in the PBL and evidence of activation

The main source of bromine in the Polar Boundary Layer (PBL) is the sea spray aerosol (SSA) with a ratio of about one bromine atom for every 660 chlorine atoms and 1612 sodium atoms, Millero et al., 2008. However, bromine can also be found condensed in other substrates such as frost flowers, snow pack and sea ice brine (Simpson et al., 2007). In particular, among different sea ice types (i.e.
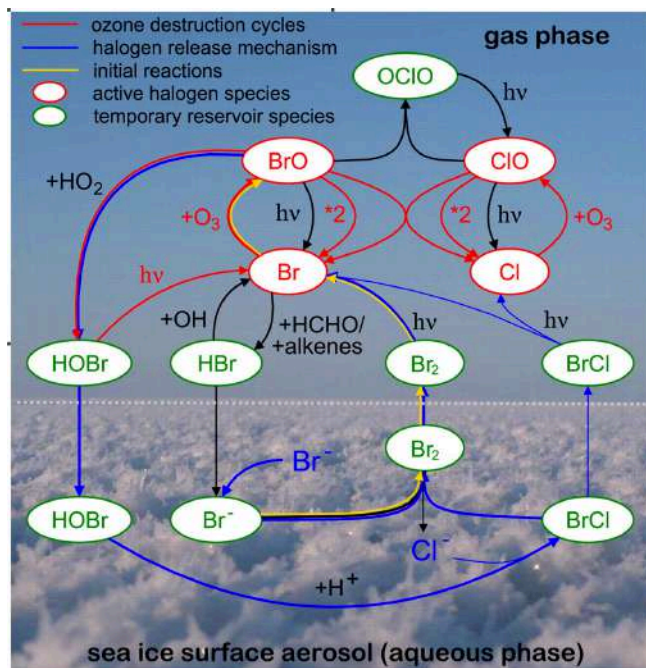
ages) the high salinity brine pockets formed within the ice lattice of seasonal or first-year sea ice (FYSI) make it a greater reservoir of inert halide salt ions (such as Br $^-$) rather than fresher aged or multiyear sea ice (MYSI) (Simpson et al., 2007). During polar springtime, however, a series of autocatalytic reactions favoured by the presence of light, sulphur and nitrogen acid species (Vogt et al., 1996) converts inert Br- into reactive halogen species (such as Br, Br_2 and BrO) which quickly react with tropospheric ozone (O3) depleting it to near zero levels (Abbatt et al.,2012; Simpson et al., 2007) (Fig 17).

Figure 17: A simplified scheme of bromine and chlorine ozone destruction and explosion cycles from sea ice and frost flowers reservoirs of halides. From Pöhler et al. 2010

28

These particular events, widely known as "bromine explosion" (Pratt et al., 2013) are yearly observed by optical spectrometers mounted on polar-orbiting satellites (i.e. the SCIAMACHY or GOME-2) that, during polar springtime, show a simultaneous increase of BrO levels over the sea ice surface concurrently with a decrease in the ozone concentration (also referred to as Ozone Depletion Events, ODEs) (Schonhardt et al., 2012) (Fig.17 and 18).

The highest atmospheric BrO concentrations are usually observed above seasonal sea-ice, while low or no concentration are displayed above multiyear ice (Sihler et al., 2012). The enhancement of BrO concentration has both the effect to alter the oxidative capacity of the atmosphere leading to the removal of many pollutants, including mercury (Schroeder et al., 1998) and, ultimately, to increase the bromine concentration in the atmosphere just above seasonal sea ice and not over the free-ocean surface, multiyear sea ice (MYSI) and lands.
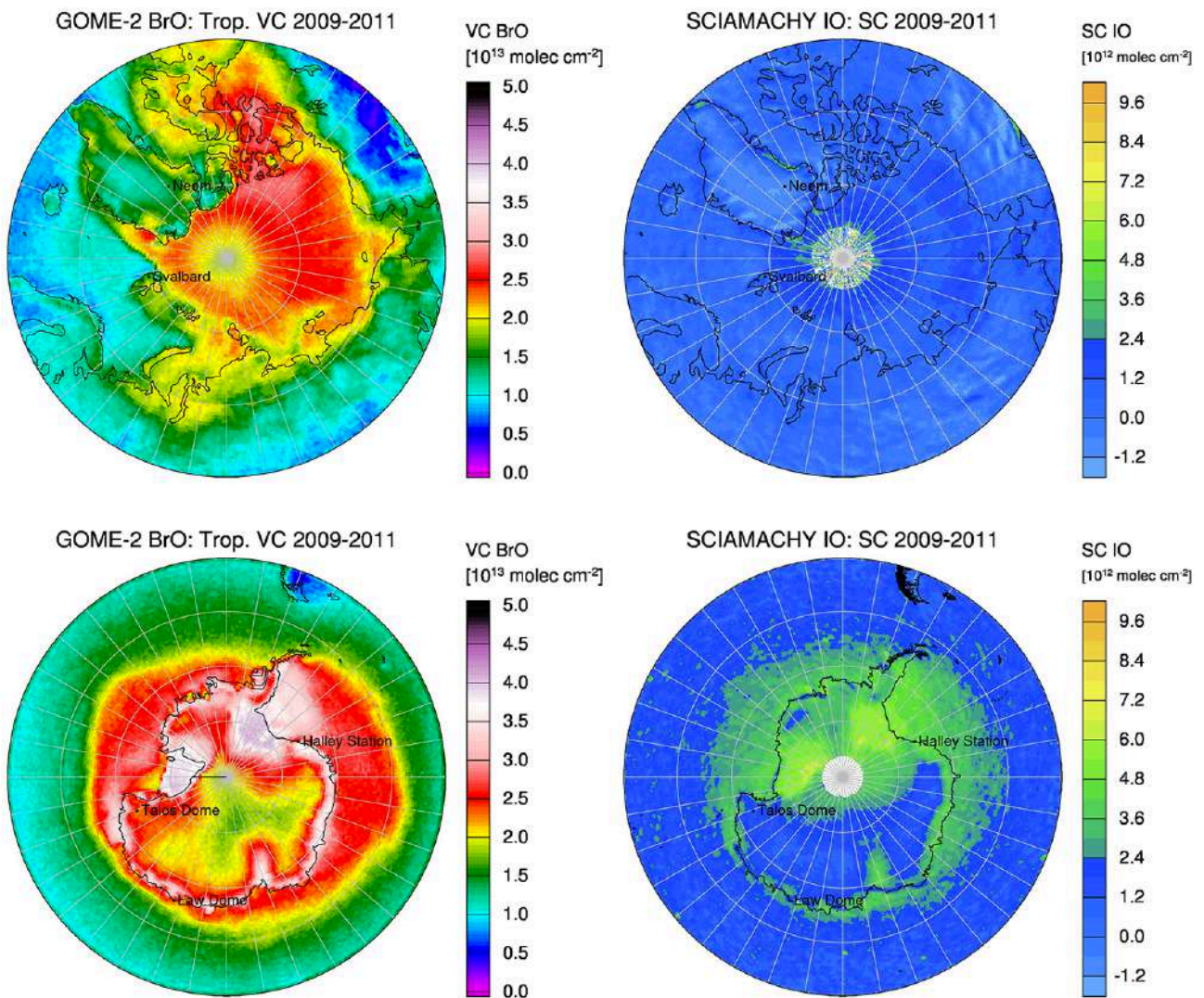

Figure 18: Atmospheric colunns of BrO and IO measured by the SHIAMACHY sensor in Antarctica and the Arctic between 2009 and 2011.From Spolaor et al. 2014.

After emission, the BrO plume is taken in charge by polar atmospheric circulations and, in some cases also by high-latitude cyclones, until it reaches land and falls in the form of bromine enriched snow compared to seawater Br/Na ratio. Bromine enrichment (Br_enr) defined as:

$$Br_{enr} = \frac{\left(\frac{[Br]}{[Na]}\right)_{snow}}{\left(\frac{[Br]}{[Na]}\right)_{sea\,water}}$$

where [Br]/[Na] in seawater is equal to 0.0062 (Millero et al., 2008) can be hence considered as a tool to discriminate the presence or absence of FYSI prior to the instrumental period. For completeness, other bromine contributions in the atmosphere can be due to organobromine species emitted from marine biota and from volcanic eruptions.

Similar to bromine, inorganic iodine in the PBL is mainly emitted from the ocean surface in form of hypoiodous acid (HOI) and molecular iodine (I2) following the deposition of tropospheric ozone (O3) to the surface and the subsequent reaction with iodide (I$^-$) ions (Carpenter et al.,2013; MacDonald et al., 2014). This process is estimated to account for 75% of the total source of atmospheric iodine, with the remainder coming from biological iodine (i.e., CH_3I, CH_2I_2) emissions from micro-algae contained within and underneath sea ice (Saiz-Lopez et al. in 2015; Cuevas et al., 2018). Sea water measurements of organohalogens in the polar regions, in fact, have shown that maximum concentrations of several species are higher during the beginning of the sunlight period throughout summer, in association to algae blooms, and especially near the sea ice edge. Halocarbons can also be produced by algae living within the sea ice matrix and in brine channels: emission in the atmosphere could occur during the sea ice melt season or through diffusion and percolation up to the sea ice surface. Based on these processes, the conceptual idea is that, similarly to bromine enrichment, the iodine enrichment measured in the snow can be calculated as:

$$I_{enr} = \frac{\left(\frac{[I]}{[Na]}\right)_{snow}}{\left(\frac{[I]}{[Na]}\right)_{sea\,water}}$$

where [I]/[Na] in seawater is equal to 0.0000056 (Millero et al., 2008). Excluding all the complex post depositional processes such as iodine reemission from the surface snow, this new proxy is based on the hypothesis that an increment of I/Na ratio recorded in the snow (normalized over sea water ratio) could reflect an increase of biogenic iodine emitted in response to a change in the ocean conditions (i.e. warmer SST) or sea ice thinning (Cuevas et al., 2018) and, by extension , it can be also used to discriminate no-MYSI sea ice conditions.

3.3.2 Use of Bromine and Iodine enrichment factors for sea ice reconstruction

As stated before, bromine and iodine from trace measurements on polar snow and ice cores have been used to reconstruct past sea-ice extents both in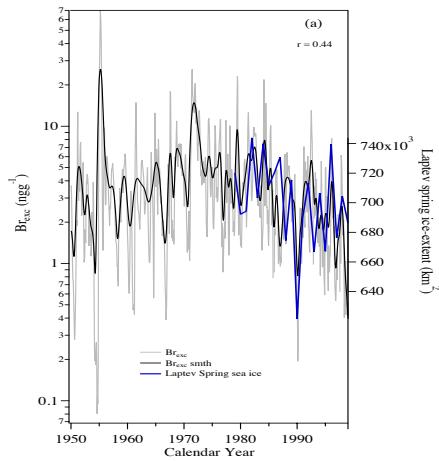 the Arctic (Spolaor et al., 2013; Spolaor et al., 2016b) and in Antarctica (Vallelonga et al., 2017). A good correlation between Br_{enr} and FYSI were found in Svalbard especially with the sea-ice extension in the Arctic Ocean ($r = 0.81$) and the Canadian Archipelago ($r = 0.82$) (Spolaor et al., 2013), in Severnaya Zemlya with the FYSI in the Laptev Sea ($r = 0.44$) (Spolaor et al., 2016b) (Fig. 19) and in Antarctica with the sectors adjacent to Law Dome ($r = 0.35$) (Vallelonga et al., 2017). In this latter situation, a positive correlation with the MSA record (Curran et al., 2014) corroborated the reliability of this proxy for sea ice reconstruction also on short time scales. The first study that used Br_{enr} to long-scale sea ice reconstruction was carried on the NEEM ice core (Northern

Figure 19: Br_{enr} vs Laptev sea ice extent from Spolaor et al., 2016b

Greenland) down to 120,000 years ago (Spolaor et al., 2016a). In this study, presented also in Chapter 5, the authors found that Br_{enr} was positively correlated with temperature ($r^2 = 0.54$) suggesting a connection among warmer temperatures, greater presence of FYSI and enhancement of the bromine explosion phenomenon. The highest values of Br_{enr} were found approximately 9,000 years ago in coincidence with the Holocene Climate Optimum (HCO) while minimum values were found during the colder phases of glacial period (Greenland Stadials, GS). These findings were interpreted with marked different conditions of the NEEM sea ice bromine source (i.e. the Canadian Arctic) that was assumed to be most likely free of sea-ice during summer in the HCO and covered by a thick-MYSI coverage during the glacial stadials. Iodine concentration in polar snow has been also investigated several times as sea ice proxies in the Arctic (Spolaor et al., 2013; 2016b) and in Antarctica (Vallelonga et al., 2017). In particular, Cuevas et al. in 2018 found a link between iodine level measured in eastern Greenland ice (ReCAP ice core) and the Arctic sea ice thinning observed since 1950. Finally,
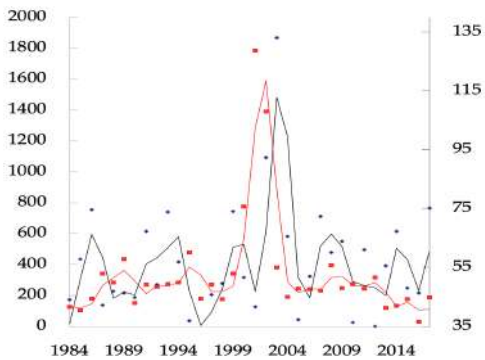
Figure 20: I_{enr} from SIGMA-A ice core (left axes- red line) and summer phytoplanktonic productivity (mgC. m^{-2} d^{-1}) in Baffin Bay (right axes-blue line).

presented as an additional work in Chapter 6, annually-average iodine enrichment values from the SIGMA-A ice core (Northwest Greenland) are compared with outputs from a numerical simulation and observations of the main physical and biological parameters characterizing the Northern Baffin Bay during the satellite era (1980-2018). Positive significant correlation between iodine enrichment, sea ice volume and primary productivity from small ocean phytoplanktonic species might further confirm the use of I_{enr} to discriminate past marine biological activity (Fig 20).

4. Satellite calibration of bromine enrichment in Arctic Ice cores: a novel method for sea ice reconstructions

4.1 Introduction

Since early 1950s, Arctic sea ice is showing a progressive reduction of its summer extent (12.8% decade[-1] relative to 1980-2010) and volume (-2.8x10^3 km^3 decade[-1] for 1978-2010) (Kinnard et al.,2011). This current decline is receiving an increasing interest because it could trigger a series of positive feedbacks contributing to a climate warming. Sea ice surface, in fact, has a high reflective power, defined as albedo, able to reflect from 50 to 80% of the incoming solar radiation. However, the increasing portion of the ocean (whose albedo is smaller than 15%) which is being exposed due
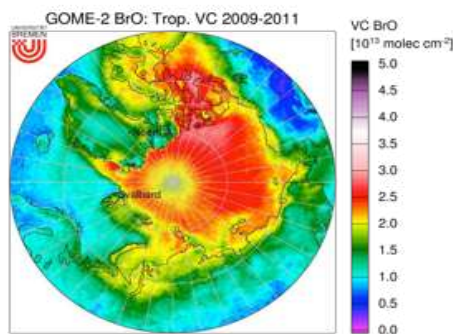

to sea ice is able to absorbs much more energy from the incoming solar radiation. Thus, this mechanism, which plays a central role in the so-called polar amplification, in the next future might also alter the Earth's energy budget. Besides that, sea ice also plays an important role in the production of deep waters affecting in such a way the global oceanic circulation system (Dieckmann and Hellmer, 2010 ; Kinnard et al., 2011).

Figure 21: Bromine explosions detected from GOME-2 sensor.

Sea ice observation for climatic studies and navigational charts spans the last century. Although a consistent amount of data has been acquired from satellite and in-situ observations during this period, still decadal-to-centennial natural fluctuations remain poorly understood. To extend our knowledge of past sea ice conditions paleo-records such as marine sediments and ice cores are frequently used. In particular, several studies on polar ice core records (Spolaor et al., 2013; Saiz Lopez and Von Glasow, 2012) have identified bromine as potential indicator of past sea ice changes. During polar springtime, in fact, the photochemical recycling of bromine is extremely efficient over first-year sea ice (FYSI), resulting in enhanced concentrations of inorganic gas phase bromine (e.g. BrO) compared to the ocean surface, multi-year sea ice or snow-covered land. This process largely investigated because of its ozone depletion capabilities (Simpson et al., 2007), it's referred to as "bromine explosion" and is detected by satellite sensors (Schoenart et al., 2012) and in-situ measurements each year from early March to late May (Fig.21). After emission, the BrO plume is transported in the lower troposphere by high-latitude cyclones until it reaches land and falls in form of bromine-enriched snow compared to seawater Br/Na ratio. Based on this concept, bromine enrichment (Br$_{enr}$) from Arctic and Antarctic

ice have been extensively investigated for semi-quantitative sea ice reconstructions at different temporal scales.

Combining modern ice core trace measurements with satellite and in-situ observations of Arctic sea ice extent this study suggests, for the first time, a quantitively link between bromine enrichment from two Greenland ice cores (ReCAP and SIGMA-A) and higher North Atlantic sea ice evolution since 1984. Although both ice cores sites are located relatively close to the coast, they are thought to sample marked different aerosols source areas. Springtime atmospheric reanalysis calculated for 1984-2014 showed that the main air masses at ReCAP (Renland ice core project) arrive from south-east. This means that before reaching the ice core site the air masses mostly travelled over Greenland Sea, a portion of the Greenland Seas usually (1984-2016) covered by a mixture of seasonal and multiyear ice outflowing from Fram Strait. Differently, at SIGMA-A, the main transport during the same period derived from south-west, suggesting that the air masses passed over the central and northern Baffin Bay, a basin fully covered by seasonal sea ice forming during winter (Fig. 22). To define the potential area responsible of inorganic bromine emission (hereafter Potential Bromine Source Area, PBSA) spring-averaged (MAM) sea ice maps and 3-days back-trajectories have been overlaid. Two distinct areas of the East Greenland (the ReCAP$_{PBSA}$) and Baffin Bay (the SIGMA-A$_{PBSA}$) have been identified. In particular, being covered by different sea ice types (from 1 to >5+ years old), the ReCAP$_{PBSA}$ was also used as a testbed to assess which sea ice type (*age*) might have been responsible for springtime bromine emission detected in the ReCAP ice core. For the SIGMA-A ice core instead, due to a lack of sea ice data over the Canadian Arctic, it was no possible to consider the complete PBSA thus only seasonal Baffin Bay sea ice was considered for the calibration.
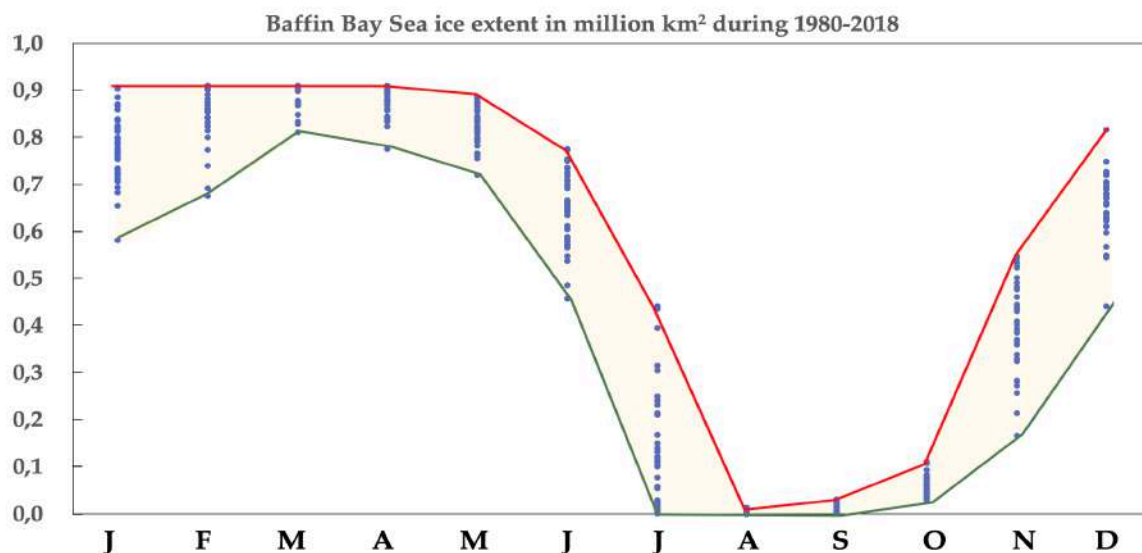

Figure 22: Monthly values of sea ice extent in Baffin Bay over the period 1980-2018. Red line encompasses the maximum extent while green line the minimum For the whole record August is characterized by almost ice free conditions.

4.2 Data and method

4.2.1 ReCAP

The Renland ice CAP (ReCAP) ice core was drilled in May-June 2015 on the Renland ice cap, in coastal East Greenland (71°18'18" N, 26°43'24"W), at an altitude of 2315 meters (Fig.23). The core is
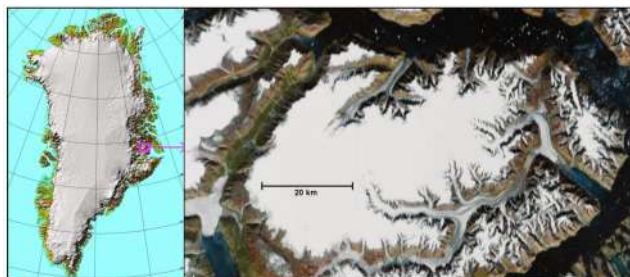

Figure 23: The Renland peninsula where the ReCAP ice core was drilled. Credit:CIC

thought to contain information on oceanic-related chemical species. The present-day ReCAP core sampling region for marine species has been suggested to be the 50-85 °N North Atlantic Ocean, as inferred from a modern (2000-2016) atmospheric circulation reanalysis by Maffezzoli et al., (in discussion) and confirmed

by this study for the period 1984-2012. Iodine records from ReCAP core extending to the last 11.5 kyr BP has been attributed to North Atlantic Ocean processes which include variability in ocean primary productivity, sub-ice phytoplankton production (Corella et al., 2019) and, more recently, to the anthropogenic ozone pollution and related oceanic iodine feedback mechanism (Cuevas et al., 2018). The ReCAP core is speculated to contain information about past North Atlantic sea ice (Maffezzoli et al., in discussion). As showed by NSIDC sea ice age maps (Fig. 15) at present, the ReCAP sampling region is dominated by a mixture of locally-formed sea ice expanding eastwards during winter and older sea ice exported out of the Arctic Ocean by the East Greenland current.

4.2.2 SIGMA-A

The "Snow Impurity and Glacial Microbe effects on abrupt warming in the Arctic" project (hereinafter referred to as SIGMA-A project) was a collaborative Japanese project which aimed to
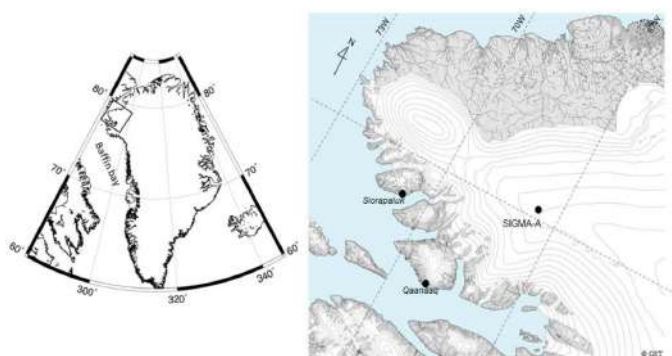
Figure 24: The SIGMA-A ice core drilling site location. From: Matoba et al., 2018

investigates the he processes causing the north-western Greenland Ice Sheet (GrIS) to lose mass (Matoba et al., 2018). During the project four ice cores were drilled and several Automatic Wheatear Station (AWS) installed. In spring 2017, the last ice core (60.06 m long), referred to as SIGMA-A core, was drilled on the Hayes Peninsula

(78°03'06"N, 67° 37'42" W) at an altitude of 1490 m a.s.l (Fig. 24). The drilling site was located approximately 70 km north of the town of Qaanaaq, on a high accumulation area (0.27 m w. eq. y^{-1}

between 1975 and 2010). The climatic information of SIGMA-A extends back to the last 110 years maintaining an extremely high resolution (sub-seasonal) for the whole long record.

4.2.3 Halogen measurements

The ReCAP ice core featured a 98mm diameter and a length to bedrock of 584 meters. The core was processed at the Alfred Wegener Institute (Bremerhaven, Germany), where it was cut and sub sampled for different analyses. 55 cm long ice pieces were dedicated for the Continuous Flow Analyses (CFA). The CFA campaign was carried out at the Centre for Ice and Climate (Copenhagen, Denmark) in autumn 2015. During the melting routine, the meltwater was collected every 55 cm of ice in previously-cleaned polyethylene vials and dedicated to discrete measurements carried out by inductively coupled plasma – mass spectroscopy. In particular, this work makes use of sodium and bromine measurements carried out on N=41 discrete samples, covering the shallow 5 – 28 m depth range and the 2012 – 1984 CE age period. The dating in this depth range is carried out by annual layer counting ($\delta^{18}O$ and δd and other species) and the age uncertainty is estimated to be ± 1 year (Cuevas et al., 2018) .The N=41 ReCAP discrete samples were analysed for bromine and sodium total concentrations by Collision Reaction Cell-Inductively Coupled Plasma-Mass Spectrometry (CRC-ICP-MS, Agilent 7500cx, Agilent, California, USA) in the CNR-ISP laboratories at Ca' Foscari University of Venice. The procedure is further explained in Maffezzoli et al. 2018 (in discussion). Similar to ReCAP also N=564 SIGMA-A discrete samples covering the period 2017-1904 CE were analysed for detecting halogens (Br, I) and impurities (Na, Ca). The first N=240 samples covering the satellite era (1979-2017 CE) were maintained at their original resolution (meltwater from cut of ~7 cm of ice integrating 0.16 year) and analysed) in the CNR-ISP laboratories at Ca' Foscari University of Venice with an Inductively Coupled Plasma Sector Field Mass Spectrometry (ICP-SFMS; Element2, ThermoFischer, Bremen, Germany) equipped with a cyclonic Peltier-cooled spray chamber (ESI, Omaha, US), following the methods of (Gabrielli et al., 2005). The following N=324 samples extending the record back to 1904 were aliquoted doubling the resolution (on average 0.23 years) and analysed subsequently with a quadrupole ICP-MS with a collision cell reaction to complete the long-term record.

The dating of the core was carried out by annual layer counting ($\delta^{18}O$ and δd and other species measured at the University of Hokkaido) and the age uncertainty is estimated to be ≤1 year.

For both cores, the Br_{enr} values in each ice sample are calculated as $Br_{enr} = (Br/Na)/(Br/Na)_{\text{sea water}}$, where Br and Na are the bromine and sodium concentrations in the ice and $(Br/Na)_{\text{sea water}} = 0.0062$ is the bromine-to-sodium mass ratio in sea water (Millero et al., 2008).

4.2.4 NSIDC Sea-ice Age V4.0

The dataset used for satellite calibration of Br_{enr} in ReCAP and SIGMA-A ice cores is the EASE-Grid Sea-ice Age, Version 4 released by NASA National Snow and Ice Data Center (NSIDC). Starting from 1984, it contains weekly estimates of Arctic sea ice age extents from remote sensed and in-situ measurements. Sea-ice age maps are freely available for download in *NetCDF* format. Each file gathers one year of observation (divided in 52 weeks) and is coded as integers in a 722 x 722 gridded subset of the 12.5 km Northern Hemisphere EASE-Grid. (Tschudi, M. Et al. 2019).

Different sea ice ages are represented by different pixel values ranging from 1 for seasonal sea ice to 2 (or higher values) for multiyear sea ice. The springtime (MAM) nature of bromine explosions was taken into account by averaging and normalizing only sea ice age maps between the first week of March to the last week of May (corresponding to bands 9-22 of the NetCDF file (showed in Fig. 25). To isolate the single potential contribution of a given sea ice type (j = 1,2,3,4+ years) to springtime bromine emission, single-type sea ice frequency maps were created averaging only the pixels with equal values (i.e. same age). Thus, after normalization, every pixel value varies from 0 to 1 according to the number of weeks that was covered by a given sea ice type. Pixels equal to zero represent an area where no sea ice was present during spring (0/14 w) such as the open ocean while pixel=1 means that the corresponding area was covered by a specific sea ice type for all the time considered (14/14 w) (Fig. 26). Finally, to pass from sea ice frequencies to sea ice extent every pixel value is multiplied by its area of 156.25 km^2.
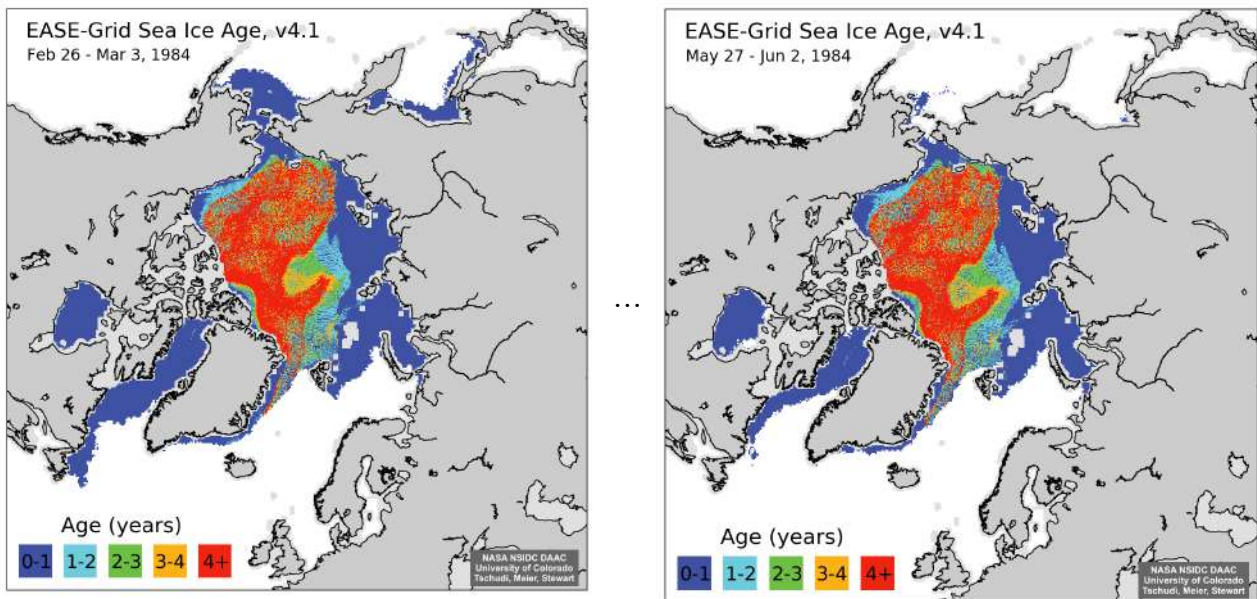

Figure 25: Bands 9 and 22 of NetCDF file ice age_nh_12.5km_19840101_19841231_v4.1.nc" from NSIDC EASE-Grid Sea-ice Age v4.1 dataset. The maps show Arctic sea ice age distribution at the beginning at the end of spring (MAM) of 1984. To create spring averaged sea ice age maps (showed in the next page) all the bands in between 9 and 22 were considered.
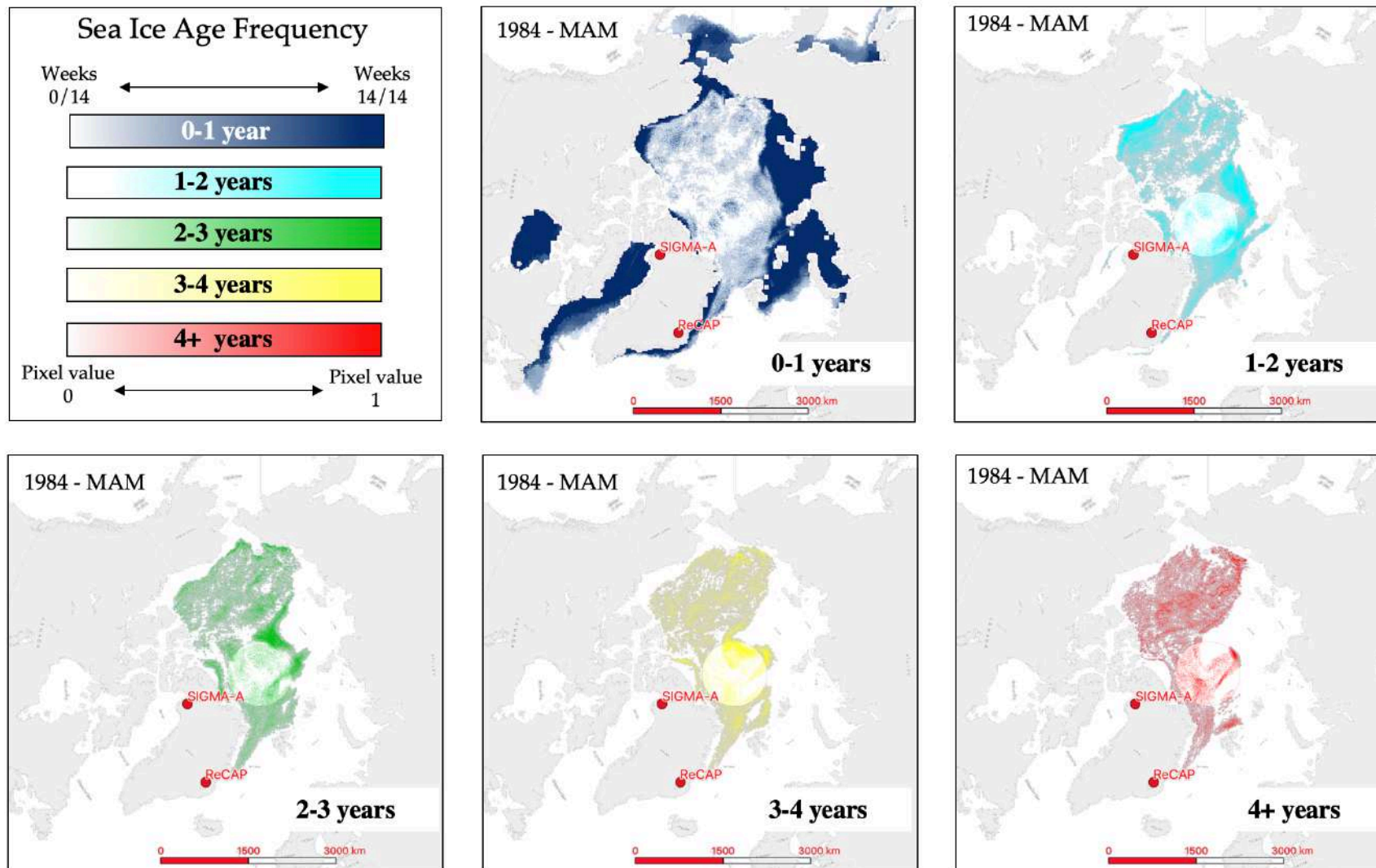
Figure 26: Sea ice frequency maps for spring 1984 divided by sea ice age. Every map was created by averaging bands 9-22 of NetCDF file "iceage_nh_12.5km_19840101_ 19841231_v4.1.nc" and shows the spatial distribution of a given sea ice types between the beginning of March and the end of May (14 weeks). Each pixel's value ranges from 0, where no sea ice was present (i.e ice free ocean), to 1 where the pixel was characterized by the presence of sea ice for the whole period. An example of this last case is clearly showed in the first year sea ice box looking northern Baffin Bay or Hudson Bay which usually are frozen until the end of May.

4.2.5 Back-Trajectories calculations

Spring average air mass frequency plots (Fig.27), were obtained from back-trajectories calculation using the HYSPLIT model (Hybrid Single-Particle Lagrangian Integrated Trajectory, Version 4 – January 2017; Stein et al., 2015). For this the NCEP/NCAR Reanalysis data from the National Weather Service's National Centers for Environmental Prediction provided by the NOAA's Air Resources Laboratory have been used (ftp://arlftp.arlhq.noaa.gov/pub/archives/reanalysis/).
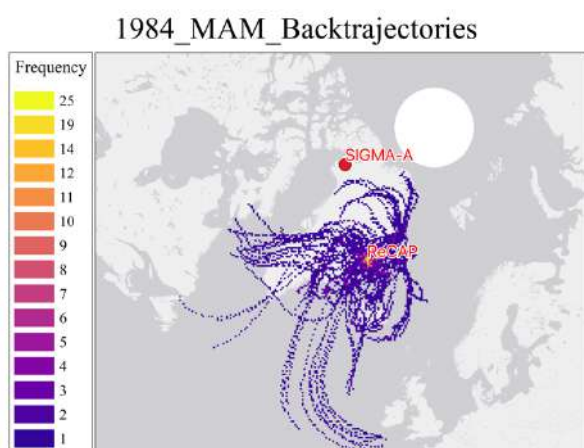

Figure 27: Back-trajectories frequency map for 1984 spring season average (MAM). Each pixel (endpoint) indicates the number of times that was crossed by an air mass travelling to ReCAP.

The three days back-trajectories arriving at ReCAP and SIGMA-A were initiated at 10 m above ground level. Similar to sea ice age maps, the time period considered to run the model was spring (March, April and May) of 1984-2012 for ReCAP, and 1984-2017 for SIGMA-A. Back trajectories that have spent at least 10 hours over the MBL (>900 hpa or <1000 mts a.s.l.) were filtered, in order to ensure the exposure of air masses to marine sources of sea salt aerosols (Maffezzoli et al., 2018).

4.3 Results

4.3.1 Identification of ReCAP and SIGMA-A Potential Bromine Source Areas

The first step of the method here proposed to calibrate the Br_{enr} in ice cores with modern sea ice observation consists to identify the potential sea ice area from which springtime inorganic bromine might have been emitted during the period considered. For shortness, this area is hereafter indicated as the "Potential Bromine Source Area" (PBSA) of an ice core and can be visualised as an irregular box inside which sea ice quantifications are performed. To identify the PBSA of the two Greenland ice cores under analysis, a spring-average sea ice map (i.e. the FYSI map in Fig. 28A) is multiplied
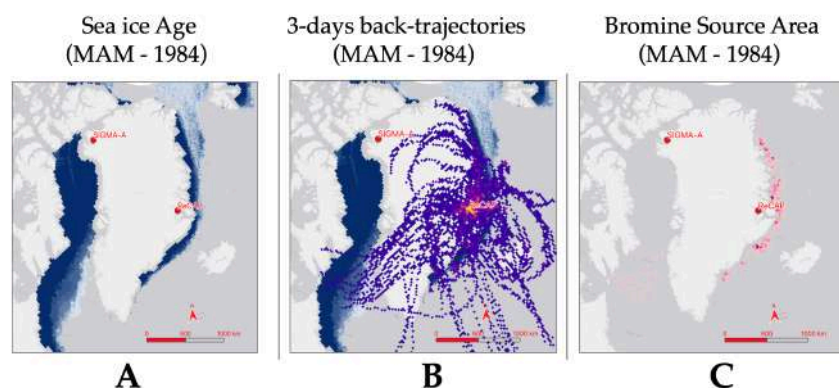

Figure 28:(A) Shadows of blue represent spring First-year sea ice distribution in 1984. (B) In violet, spring averaged back-trajectories arrived in ReCAP during the same period. (C)The potential ReCAP$_{PBSA}$ generated by FYSI during spring 1984. It shows only the pixels of sea ice crossed at least once by a back-trajectory.

with the corresponding air mass frequency map sub-sampled to the same pixel resolution (Fig. 28B), in order to create a new layer showing only the non-zero pixels of the product (Fig. 28C). Physically speaking, the lowest pixel value displayed in this map corresponds to an area (whose size depends on the pixel resolution) covered by sea ice for one week of MAM and above which passed at least once an air mass back-trajectory directed to the ice core site.

Repeating this procedure for all the different sea ice types (from 1° to 5° years old), and overlaying all the bromine source maps simultaneously, the mean PBSA of SIGMA-A (for 1984-2016) and for ReCAP (1984-2012) were identified by contouring of all the bromine source pixels showed (Fig.29 A, B).
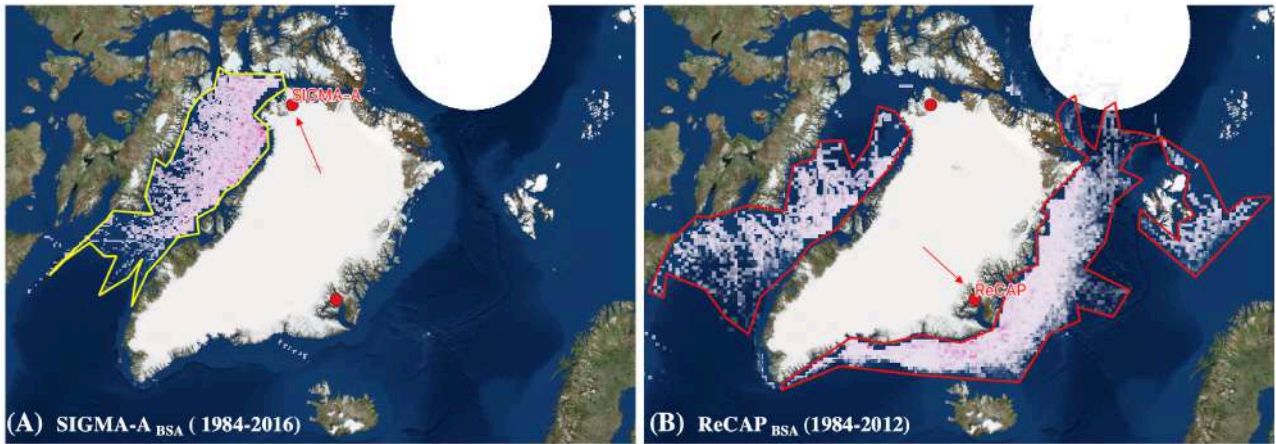
Figure 29: (A) The yellow line delimitates the SIGMA-A_BSA. It is obtained by contouring all the bromine source pixels obtained by the overlay of annual bromine source maps. (B)The red line delimitates the ReCAP_PBSA. Contrarily to SIGMA-A which samples only Baffin Bay sea ice, the ReCAP_PBSA is composed by 3 different sectors including part of Baffin Bay, East Greenland and Svalbard.

4.3.2 Sea ice type quantification and correlation with Br_{enr}

Defined the size of two potential bromine source areas the next step was to quantify the amount of a given sea ice type present within them during the periods considered. Inside the SIGMA-A_PBSA (Fig. 30) only seasonal ice was observed for 1984-2016, thus only FYSI extent was calculated. Within the ReCAP_PBSA, instead, five distinct time series (one for each sea ice type) were obtained from the quantification of the different-year sea ice extents. Considering a single pixel value (P_i) given by:

Figure 30: FYSI present in spring 1984 within the SIGMA-A_PBSA delimited by the yellow line.

$$P_i = \frac{(weeks\ of\ sea\ ice\ presence)}{Total\ period\ (14\ weeks)} \cdot A_i$$

Where the ratio between the number of weeks of sea ice presence over the total period corresponds to the sea ice frequency (i.e. maps showed in Fig. 26) and A_i is the pixel's area (12.5km x12.5 km=156.25 km²). Therefore, the spring sea ice extent (SIE) for a given year (y) and a given age (j) will be:

$$\text{SIE}_{(y,j)} = \sum_{i \in pixel=1}^{n} P_i \qquad \begin{array}{l} y \in year\,[1984 \dots 2016] \\ j \in age[1,2,3,4+] \end{array}$$

In addition to sea ice presence, the equally important role of atmospheric transport has been taken into account by using the bromine source maps (such as Fig. 28C) as new raster layers for sea ice quantification. As said before, they are generated by the product of the sea ice extent with the air mass frequency therefore the sum of all the bromine source pixel values do not correspond anymore to the real sea ice extent, rather, it represents an equivalent value (or Equivalent Bromine Source Area, "EBSA") which equally depends both on sea ice presence and atmospheric transport. In other words, if one pixel of the bromine source map has a value equal to 3, this can be obtained by a pixel fully covered by sea ice area that have been crossed 3 times by the back-trajectories or, equally, by the same pixel just covered by sea ice for half of its area (or time) but crossed for 6 times by the air masses directed to the ice core site (Fig. 31).

Figure 31: For construction, the bromine source pixels that compose the bromine source maps depend equally on sea ice presence and atmospheric transport.

Using bromine source maps, the EBSA have been calculated for each year (y) and each age (j) as describe below:

$$\text{EBSA}_{(y,j)} = \sum_{i \in pixel=1}^{n} \left(P_{(i)} * Air\ mass frequency_{(i)} \right) \qquad \begin{array}{l} Y \in year[1984 \dots 2016] \\ J \in age[1,2,3,4+] \end{array}$$

The final result of the previous calculations were five new time series of sea ice extent (from 1 to 5y) and five equivalent ones considering transport (EBSA) extracted from the ReCAP_PBSA while the SIGMA-A_PBSA provided just one record of FYSI extent and its EBSA due to the absence of MYSI. Focusing on the data retrieved from the ReCAP's study case, Pearson's correlation analysis was performed to evaluate to which extent the bromine record measured in the ice depends on the

variability of a specific sea ice type. A positive significant ($p < 0.05$) correlation (r=0.38) was found between yearly average Br_{enr} (log2) and FYSI sea ice extents within the East Greenland sector of the $ReCAP_{PBSA}$ while there is a negative and low ($p>0.05$) significant correlation when other sea ice ages are considered (Table 2-3). This result confirmed the hypothesis that, differently from older and fresher sea ice, the newly-formed seasonal sea ice might constitute an efficient substrate for springtime bromine emission. It's worthy also to note that the choice to consider logarithmic values of bromine enrichment instead of normal values was made to better represent the exponential nature of the autocatalytic sequence which lead to the release of inorganic bromine (from the photolytic break-up of 1 molecule of bromine gas (Br_2) released from the FYSI surface, the two bromine radicals bonds with tropospheric ozone (O3) forming 2 new molecules of BrO).

Table 2: Correlation coefficients between Br_{enr} (log2) at ReCAP and Sea ice age extent (km^2) within the PBSA divided by sectors. *r* =Pearson's correlation coefficient, Sig.= significance; Sig. < 0.05, highlighted in bold font)

	1°-year sea ice		2°-year sea ice		3°-year sea ice		4°-year sea ice		5°-year sea ice	
SIE	*r*	*Sig.*	*r*	*Sig.*	*r*	*Sig.*	*r*	*Sig.*	*r*	*Sig.*
Baffin Bay	-0.03	0.88	0.31	0.10	-	-	-	-	-	-
East Greenland	**0.38**	**0.04**	-0.15	0.43	-0.29	0.12	-0.04	0.82	0.22	0.24
Svalbard	0.29	0.13	0.01	0.97	0.13	0.50	0.19	0.31	0.21	0.27
Total	0.27	0.16	-0.14	0.48	-0.29	0.17	-0.03	0.87	0.23	0.23

Table 3: Correlation coefficients between ReCAP's Br_{enr} (log2) and Equivalent Bromine Source Area (EBSA) divided by sectors. *r* =Pearson's correlation coefficient, Sig.= significance; Sig. < 0.05, highlighted in bold font)

	1°-year sea ice		2°-year sea ice		3°-year sea ice		4°-year sea ice		5°-year sea ice	
EBSA	*r*	*Sig.*	*r*	*Sig.*	*r*	*Sig.*	*r*	*Sig.*	*r*	*Sig.*
Baffin Bay	0.26	0.88	0.31	0.11	-	-	-	-	-	-
East Greenland	0.32	0.09	-0.06	0.75	-0.30	0.11	-0.11	0.58	0.10	0.62
Svalbard	0.22	0.25	0.31	0.10	0.22	0.26	-	-	-	-
Total	**0.37**	**0.04**	-0.06	0.77	-0.30	0.11	-0.11	0.58	0.10	0.62

Looking at the correlation with the Equivalent Bromine Source Areas (Table 4), the correlation with East Greenland sector decreased (r=0.32) and became not significant (sig=0.09), while a positive and statistically significant correlation was found for the equivalent FYSI present in the whole $ReCAP_{PBSA}$ area (r =0.37; Sig = 0.04) thus including minor contribution of Baffin Bay and Svalbard.

This result seems to suggest that although the Br_{enr} record of the ReCAP ice core was mainly modulated by change of East Greenland FYSI conditions (as found also by Maffezzoli et al,in discussion) it might be also influenced by bromine originally emitted quite far from the Renland Peninsula such as in Baffin Bay (~1500 km west of ReCAP) or Svalbard. This suggests that the

bromine deposition at the ice core site might be a composite signal influenced both by local conditions and medium-range transport.

4.3.3 Satellite calibration of ReCAP's Br_{enr} record (1984-2012)

Sea ice age frequency maps filtered for atmospheric reanalysis revealed a vast area around
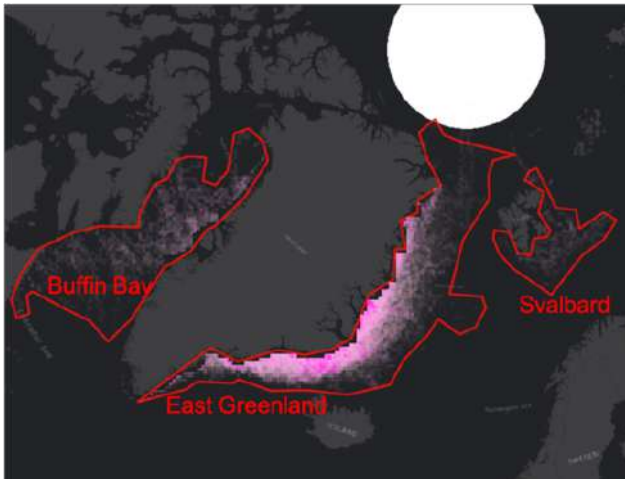
Greenland identified as the potential bromine source area (PBSA) of the ReCAP's ice core (Fig.32). The whole area can be divided in 3 main sub-sectors that, in order of dimension, are: Eastern Greenland Sea (1.152.540 km²), Baffin Bay (905.331km²) and the Eastern Svalbard (254.028 km²). Among the different sea ice types present within the ReCAP$_{PBSA}$ for 1984-2012, only first-year sea ice (FYSI) extent is in agreement with the annual bromine variability showed by the ice core record (r =0.38 p =0,04). From a detailed analysis it also emerged that, during the period

Figure 32: The ReCAP$_{PBSA}$ samples 3 different sectors: Baffin Bay, East Greenland and Svalbard.

considered, the amount of FYSI present within the Eastern Greenland sector was less extended than the constant spring sea ice coverage of Baffin Bay (Fig.33A), however, due to its closeness to the ice core site (hence a higher air mass frequency) it contributed on average to 88% of the total EBSA (Fig 33B). Minor contribution to the total bromine source came from the distant (but prevalently FYSI-covered) Baffin Bay (11% of the EBSA) and from Eastern Svalbard sea ice (1%).
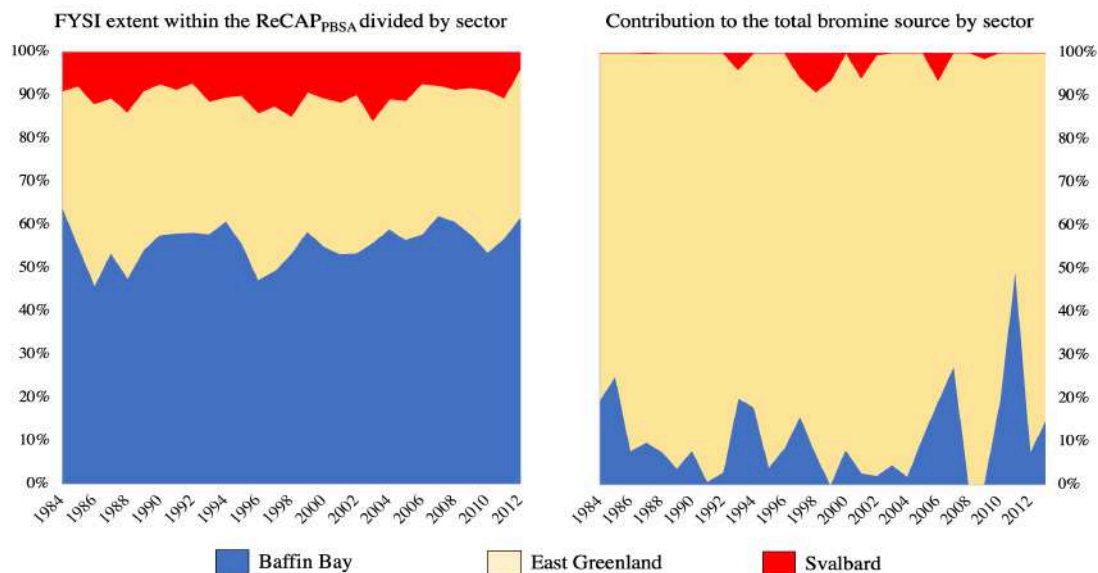
Figure 33: (A)Percentage of FYSI extent measured within the ReCAP$_{PBSA}$ divided by sectors. East Greenland box contains~350.000 km2 of FYSI while Baffin Bay ~560.000 km2, however, due to its closer position to ReCAP ice core (B) it accounted on average for 88% of the total contribution to the bromine source for 1984-2012 while Baffin Bay only 11%.

Table 4: Annual values of FYSI calculated within the ReCAP$_{PBSA}$ and its equivalent values considering the air mass frequency (EBSA). In bold the column that showed a statistically significative correlation(sig.≤0.05) with the ReCAP bromine enrichment record.

YEAR	(log2) Br$_{enr}$	First year sea-ice (km^2)				Equivalent bromine source area (km^2)			
		Baffin Bay	**East GRNL**	**Svalbard**	**Total FYSI**	**Baffin Bay**	**East GRNL**	**Svalbard**	**Total EBSA**
1984	0.96	638181	263817	90446	992444	51239	210100	0	261339
1985	3.99	518248	353237	76105	947589	37511	112009	0	149520
1986	3.12	457857	422902	118929	999687	35257	412958	0	448214
1987	2.44	560871	379230	111842	1051942	37902	349219	625	387746
1988	1.39	550480	445871	161518	1157868	25670	307232	67	332969
1989	3.43	623638	426239	103917	1153795	12277	313136	0	325413
1990	2.16	677946	411127	86217	1175290	25826	300279	0	326105
1991	1.86	648917	373136	97344	1119397	3225	426507	0	429732
1992	2.31	628225	374967	77333	1080525	3125	107020	0	110145
1993	2.87	699766	371808	138549	1210123	64129	245234	12455	321819
1994	2.12	598504	285335	102467	986306	44877	205536	0	250413
1995	0.76	570692	355692	103092	1029475	4018	95982	0	100000
1996	2.63	515312	422288	155033	1092634	32009	339442	0	371451
1997	3.59	524408	404944	133281	1062634	42612	214174	15279	272065
1998	3.46	547779	326752	153817	1028348	34989	405357	44275	484621
1999	1.04	552980	306897	87511	947388	0	230837	15614	246451
2000	3.16	564029	354185	109453	1027667	33694	389007	0	422701
2001	2.02	548917	363437	119074	1031429	10156	356071	22812	389040
2002	2.39	542656	374877	99911	1017444	7109	325413	2132	334654
2003	1.37	531127	269933	150379	951440	10536	221283	0	231819
2004	2.20	487723	249364	89855	826942	3683	187879	0	191562
2005	2.40	454286	259453	90681	804420	31908	251518	0	283426
2006	0.33	463549	279866	58717	802132	22054	84353	7165	113571
2007	2.36	520234	252879	65212	838326	8393	22277	0	30670
2008	1.37	602333	303627	87165	993125	0	187054	0	187054
2009	1.73	590703	347589	85759	1024051	0	215547	2958	218504
2010	1.36	487645	340781	81071	909498	56808	234911	134	291853
2011	2.23	530368	305670	99464	935502	97009	99710	0	196719
2012	1.71	618862	345480	40725	1005067	19587	237455	0	257042

4.3.4 Satellite calibration of SIGMA-A's Br_{enr} record (1984 -2016)

Bromine enrichment record from SIGMA-A core was also calibrated for 1984-2016 with NSIDC Sea-ice Age Maps using the same approach. Similar to the ReCAP study case, a positive significant correlation ($r= 0.40$ $p.= 0,01$) was found by the comparison of yearly-average Br_{enr} and the FYSI extent calculated within the SIGMA-A$_{PBSA}$ (Fig. 30). Unfortunately, due to the lack of sea ice data in some region of the NSIDC Sea-ice Age V4.0 dataset (i.e the Canadian Arctic or the North West Passage) the EBSA for SIGMA-A was not calculated. This might explain why the highest Br_{enr} values observed in 1990 (with a 4-folds increase in respect to the previous year) are not accompanied by any drastic change of the Baffin Bay sea ice extent (Fig.35A).
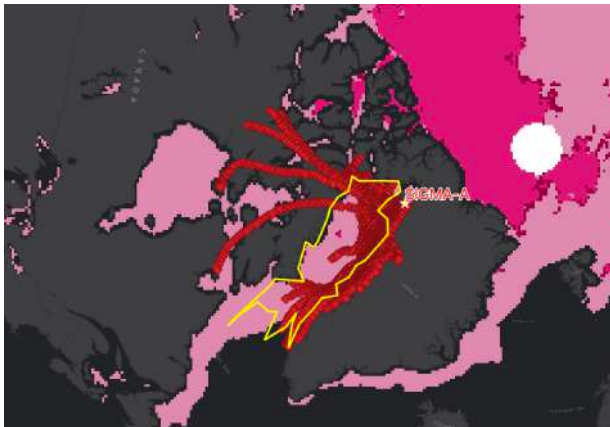

Figure 34: Red square represents the backtrajectories arriving ay SIGMA-A during spring 1990 overlaid over Copernicus sea ice type maps. Pink represents FYSI, purple multiyear one. In 1990, the air masses travelled over the North West Passage (covered by FYSI) that might have contributed to bromine emission over the SIGMA-A$_{PBSA}$ (yellow line).

A possible reason for such high Br_{enr} values, in fact, can be due to an extra source of bromine not included in the PBSA such as the North-west passage which was crossed several times by the back-trajectories in spring 1990 (Fig.34). Thus, based on another sea ice satellite dataset (the *Copernicus Sea ice Edge and Sea ice Type*) it has been observed that North-West Passage was effectively covered by FYSI suggesting that this additional area could have contributed to inorganic bromine emission recorded in SIGMA-A. The amount of extra sea ice source was quantified to be approximately 100,000 km^2 that, added to Baffin Bay FYSI extent in 1990, led to a substantial increase of the correlation with the whole Br_{enr} record ($r=0.70$ $p= 0.03$) (Fig.35B). Although the bromine calibration has been possible by combining sea ice age data from two different datasets, the correct quantification of the SIGMA-A EBSA still remains an open issue for future investigation and more accurate sea ice satellite maps are needed.
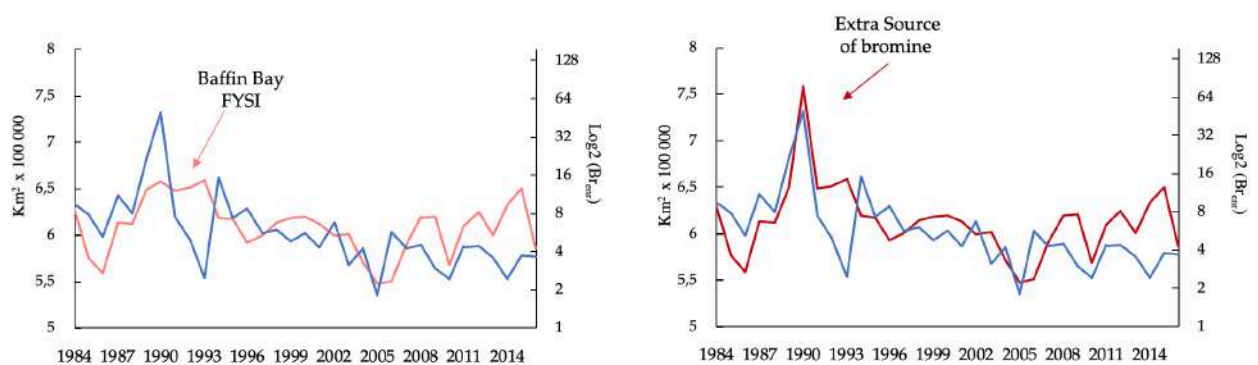

Figure 35: (A) The bromine enrichment record (blue line) vs FYSI extent measured within Baffin Bay (SIGMA$_{PBSA}$) and (B) considering the extra contribution from Canadian Arctic.

4.4 Discussion and Conclusions

Photolytic bromine explosions are observed cyclically from satellite and in-situ measurements both over Arctic and Antarctic sea ice. Newly formed first-year sea ice (FYSI) is supposed to be the main source of non-sea-salt (nss) springtime bromine emission, while, older and fresher sea ice is thought to have minor-or-no contribute to this process. Using this connection, many studies used bromine enrichment in ice cores has as proxy for semi-quantitave sea ice reconstructions in both the polar regions and at different time scales. Comparing the recent bromine enrichment records from two Greenland ice cores (ReCAP and SIGMA-A) with satellite sea ice age maps and atmospheric reanalysis this study provides for the first time a quantitave link between the bromine enrichment in polar ice cores and seasonal sea ice presence. Considering different sea ice ages (from 1 to 5 ys) and spring-average atmospheric circulation, only FYSI resulted to be statistically correlated with the bromine record. (r =0.38 p=0,04 for ReCAP and r= 0.40 p= 0,01 for SIGMA-A).

At ReCAP (Central-East Greenland), the effect of the transport it has been seen to strongly affect annual bromine depositions. Considering 3 and 5-year moving averages of both FYSI extent and EBSA (Fig. 36) the correlation with bromine enrichment data increased notably (up to r=0.84; p=1,84 x 10^{-7} for 5-y average EBSA (Fig. 37A). Two possible explanations are first that dating uncertainties (±1 y) having a great impact on the correlation between annual values were smoothed and/or, more interestingly, that the average-period considered (3-5 years) is compatible with the interannual variability of the North Atlantic Oscillation (NAO) observed since 1984 (Fig. 37B). The moving averages have, in fact, the effect to reduce or eliminate the oscillations that have a period equal to the number of terms involved in the calculation of the moving average itself. Considering 3 or 5-terms moving average means almost detrend the bromine record from the NAO signature supposed to regulate precipitation and temperatures over southern Greenland (Vinther B. M., 2003). Therefore, minimizing the transport variability, the linear regression found for the recent period (1984-2012) between the ReCAP's bromine enrichment and FYSI extent within the East Greenland sector might be applied also to long-term paleoclimatic studies in which the transport still remains a large uncertainty.
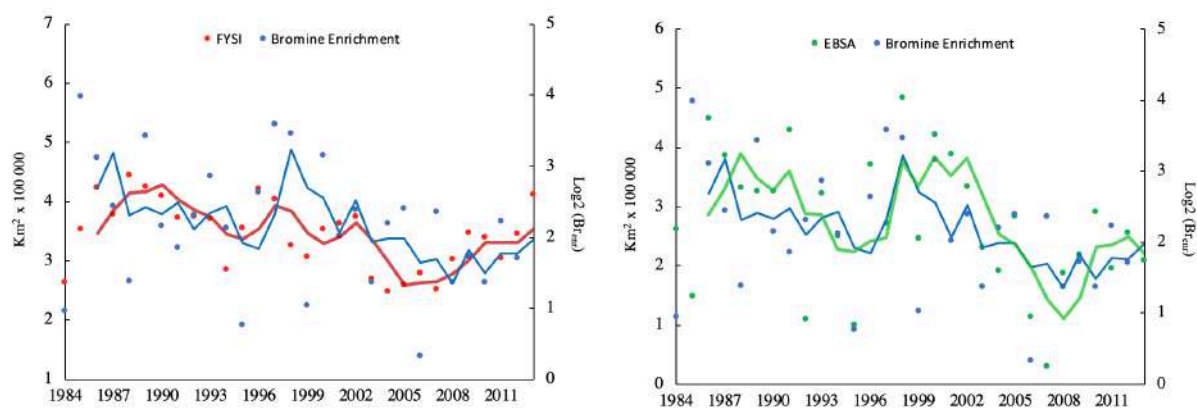

Figure 36: 3-years moving averages of FYSI (red line) and total EBSA (green line) vs Bromine enrichment (blue line) measured at ReCAP for the period 1984-2012. The annual values (dots) are listed in Table 4.
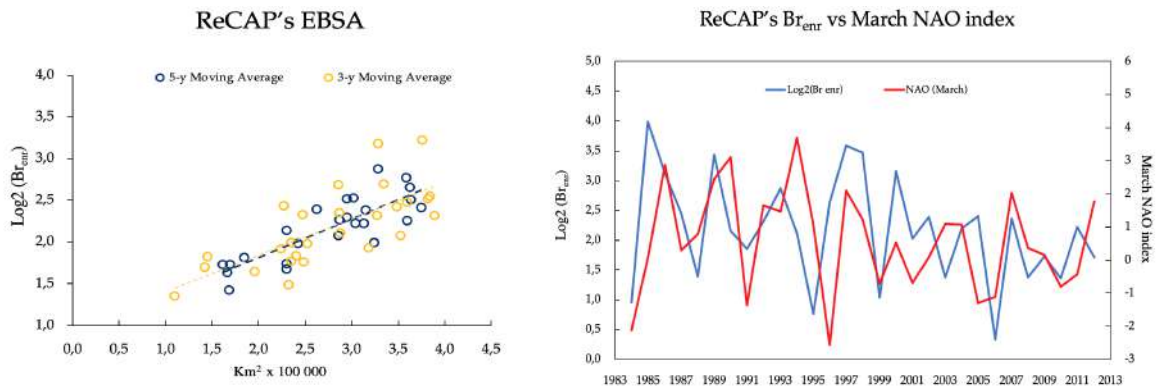
Figure 37: (A) Scatterplot of Log2(Br_{enr}) and Equivalent Bromine Source Area obtained by multiplying the FYSI for the air mass frequency within the ReCAP$_{PBSA}$ (r = 0.84; p = 1,84.10^{-7}). (B) Log2(Br_{enr}) record vs March NAO index since 1984.

Similarly to ReCAP, also the SIGMA-A bromine record is positively correlated with the NAO index for 1985-2014 ($r=0,55$ $p= 0,005$) likely due to its influence on the wind-stress field over Baffin Bay (Kinnard et al., 2006) that modulates the bromine deposition at the ice core site. In addition, from a detailed atmospheric reanalysis, 3-days spring-average air masses trajectories have been considered to explain the highest Br_{enr} values observed in 1990. It was found that during that year Baffin Bay seasonal ice was at its maximum value (~660 000 km^2), however, looking at air mass pathways, a unusual extra-source of inorganic bromine could have contributed to springtime bromine emission recorded at SIGMA-A. Based on the *Copernicus Sea ice Age and Type* dataset, this potential extra source was identified in the Canadian Arctic and North West Passage sea ice, further demonstrating that Br_{enr} in ice cores can yield meaningful information on past Arctic sea-ice conditions and variability at the regional scale. In conclusion, even if this method was focused on the calibration of Br_{enr} with satellite sea ice images, it was showed the importance of transport in modulating the glaciochemical signal of an ice core. The bromine (or in general, an ice core proxy) record depends equally by its source (i.e. FYSI availability) and by a "favourable" transport directed to the ice core site (Fig.38). This means that low values of a given ice core proxy, except for disturbed ice core records, might reflect a decrease of the transport and not only a smaller/lower source. However, when the ice core signal (i.e. the Br_{enr}) is averaged for a similar time-frequency of the main atmospheric pattern which governs its deposition (i.e. the NAO index in North Atlantic) the effect of transport is minimized enhancing the direct effect of the source area conditions. With this concept in mind, the method here proposed could be also applied to identify the potential source area of other proxies (i.e. primary productivity, wildfires etc) from ice cores records.
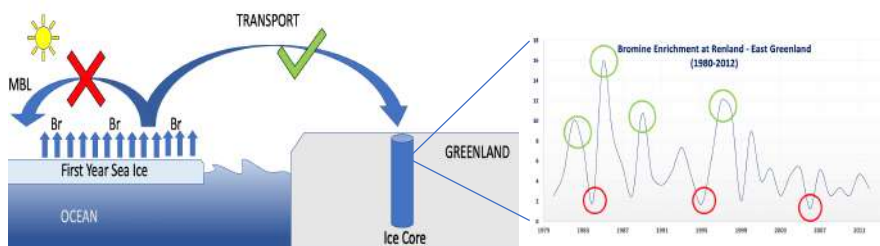

Figure 38: The role of atmospheric transport in modulating the glaciochemical (in this case the bromine enrichment) signal of an ice core. The lowest values of Br_{enr} in this case are due to a relaxation of the atmospheric transport and not to a sea ice reduction.

5. Arctic sea ice evolution during last glacial abrupt climate changes: a focus on Dansgaard-Oeschger events 7 to 10.

Summary

The information obtained from the previous chapter, confirming the connection between Br_{enr} in an ice core record and the presence of FYSI, are here applied to a paleoclimatic study case aiming to investigate the Arctic sea ice response to past abrupt climate changes. Building on a previous study by Spolaor et al. (2016), this chapter presents for the first time a highly-resolved reconstruction of Canadian Arctic glacial sea ice during four selected DO events (DO 7-10) occurred 36-44 kya. Sub-decadal bromine enrichment values obtained by resampling a portion of the NEEM ice core (between 1711 and 1793 m depth) clearly show a shift from predominant multi-year sea ice conditions during colder stadial to increased seasonal sea ice conditions characterizing the warmer interstadials. Finally, the highest bromine enrichment values observed 0.4-0.8 ky after the DO onset have been interpreted as the signature of rapid sea ice expansion. Trough the ice-albedo feedback, the build-up of extended seasonal sea ice could have determined a gradual atmospheric cooling bringing back the climate system from interstadial to stadial conditions.

To evaluate the causality relationship between sea ice collapse and atmospheric warming occurred in North-Western Greenland, two robust statistical methods were applied to the new dataset obtained from halogens measurements on n= 1319 discrete samples.

In conclusion, by providing with an unprecedent detail information about sub-decadal to centennial high Arctic sea ice variability, this study aims to investigate the regional sea ice response to past abrupt climate instabilities in order to better understand future sea-ice conditions in a warming climate.

5.1 Introduction

Using bromine and sodium concentrations measured in the NEEM ice core (North West Greenland), Spolaor et al., (2016) provided a reconstruction of the Canadian Arctic sea ice over the last 130,000 years going back until the Eemian, the previous interglacial (Fig.39A). The study was based on the use of bromine enrichment (Br_{enr}) in ice cores as a chemical marker for first-year sea ice conditions (FYSI). During polar springtime, in fact, the presence of sunlight triggers a series of photolytic reactions over the newly formed sea ice surface, activating an efficient recycling of gas phase inorganic bromine. The end result of this processes is the emission and concentration of non-sea-salt bromine (nssBr) in the marine boundary layer (MLB) as showed also by satellite and in-situ observations (Fig.18). After emission, the BrO resulting from sea ice-related bromine explosion is carried by polar air masses and, eventually, it terminates it cycle in form of bromine enriched snow. Similarly to bromine, also iodine variations in ice cores have been linked with sea ice conditions. Iodine is emitted mainly in form of sea-salt aerosol but, very recently, it has been showed a positive correlation also between organic iodine emissions and enhanced activity of sub-ice phytoplanktonic species (Cuevas et al., 2018; Corrella et al., 2019 *in discussion*) in response to modern period Arctic sea ice recent thinning. Using these two key concepts, we can calculate the enrichments of bromine (Br_{enr}) and iodine (I_{enr}) by normalizing the ratios of (Br/Na) and (I/Na) measured in the snow over their constant sea-water mass ratio equals to 0.0062 for (Br/Na) and 0.0000056 for (I/Na) (Millero et al., 2008). The complex reactions involving halogens species in polar troposphere were implemented in a chemical-transport model (the Tropospheric halogen model, THAMO) developed by the Atmospheric Chemistry group of CSIC in Madrid (Spain) (A. Saiz-Lopez et al., 2008) which confirmed the experimental observations. (Fig. 39B)
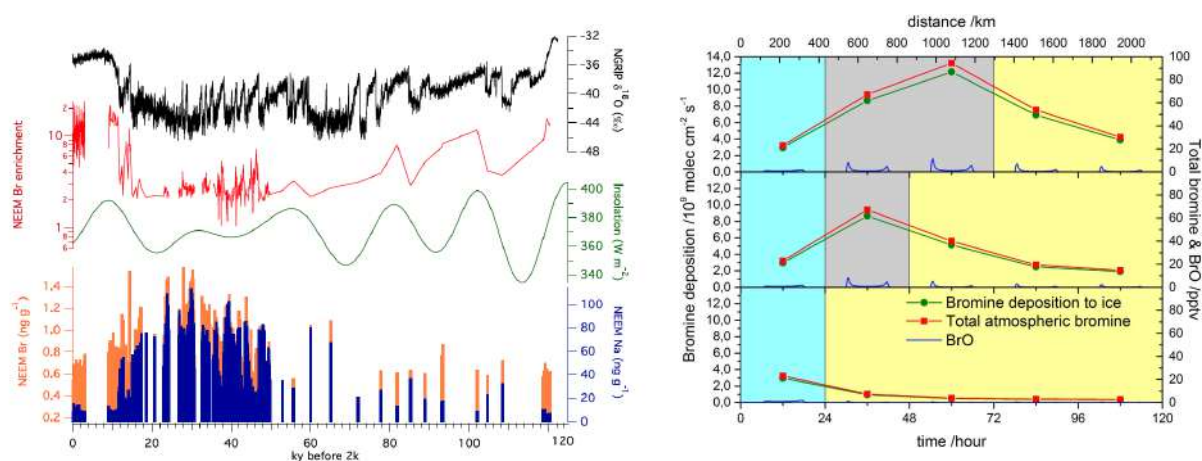
Figure 39 : (A) The complete record of Br_{enr} from the NEEM ice core (credit: Spolaor et al. 2016). Red line indicates the Br_{enr} while black line indicates NGRIP delta oxygen variations. (B) The outputs from the 1-D transport and chemistry model. They show a simulation in which the air mass, starting from the ocean (blue) spends 48 and 24 hours over FYSI (grey) with active bromine recycling on the surface. In the lower panel the simulated air mass travel just on MYSI/land (Yellow).

Going back to the long-term Canadian Arctic sea ice reconstruction, it was found a positive correlation ($r = 0.73$) between water oxygen isotopes from the NGRIP ice core and Br_{enr} from NEEM (Fig.39A-40) suggested a solid connection between atmospheric temperatures and sea ice conditions. The lowest Br_{enr} values are showed during late glacial stadials, with mean $Br_{enr} = 2.21 \pm 0.92$ (1 σ) interpreted with a thick multi-year sea ice (MYSI) coverage of the high Arctic. Contrarily, the highest values are showed throughout the Holocene ($Br_{enr} = 15.6 \pm 3.2$ (1σ) 9–11.5 ky b2k) indicating a more pronounced FYSI conditions which could have led to enhanced heterogeneous recycling of halogens in the polar boundary layer. If on the one hand, this paper provided the first long-term record of Canadian Arctic sea ice based on halogen species from ice cores, on the other hand, the bag mean resolution (1.10 m for each rod of ice melted) did not allowed to resolve in detail the abrupt climate instabilities occurred in the last glacial period known as Dansgaard-Oeschger
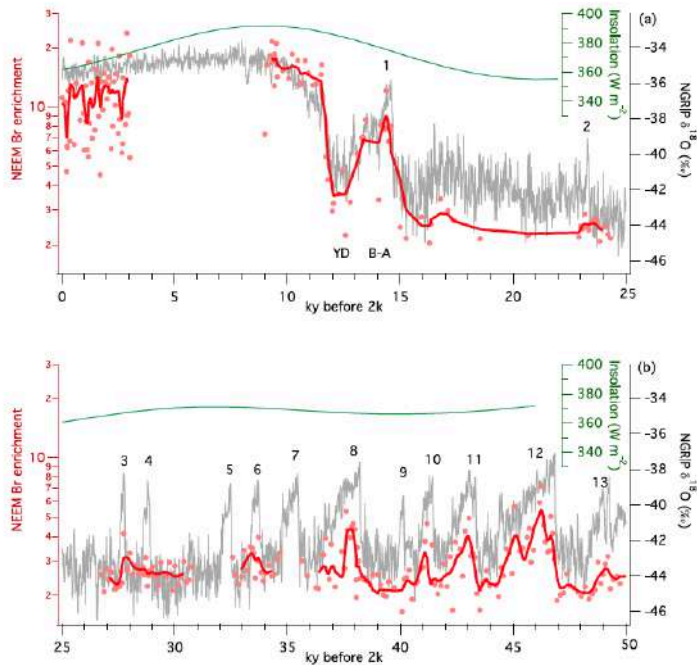

Figure 40: Red line is a 2-points moving average of Br_{enr} from the NEEM in core while grey lines is the oxygen isotopic record from NGRIP. The upper panel show the Holocene, the lower one shows the last part of the glacial period covering DO events 3-13.

event (DO). They are rapid climatic shift characterized by a relatively quick atmospheric warming occurred in few decades followed by a gradual cooling lasting generally for 1-2 kyrs. Due to the ice layers compression, however, discrete bag-mean samples from the glacial period usually integrate between 60 and 120 years, a time interval too large to catch the rapid DO transition. Therefore, to better understand the timing and the mechanisms controlling sea ice dynamics in response to past climate instabilities there is a need for a higher time-resolution (i.e. sub-decadal time scale).

In addition, although there is no evidence of past *DO like* shifts during interglacial periods, the temporal scale of each warming event (20-60 years) is reasonably comparable with the recent anthropogenic global warming, thus, these particular events might provide a unique analogue to predicting future Arctic sea ice evolution. These motivations, together with the need to fill a substantial data gap in the discrete-sampled record (i.e. the GI-7) have led to the resample of glacial interstadials 7 to 10 in order to conduct new detailed (1-2 cm resolution) trace analysis on halogens.

5.2 Data and method

5.2.1 NEEM ice core

The North Greenland Eemian Ice Drilling (NEEM) was an international project taking place in Greenland (camp site: 77.45°N, 51.06° W, altitude 2484 m a.s.l.) between 2008-2012 (Fig. 41). At the
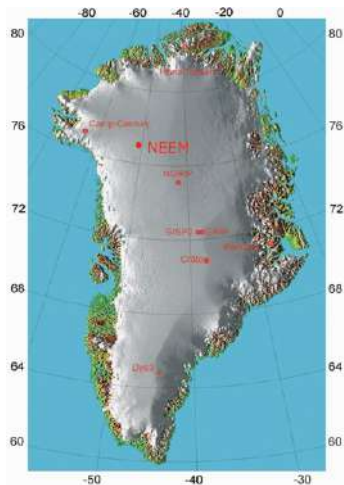

end of the drilling campaign, in 2010, a 2.54 km-long ice core was retrieved. For present time, the mean annual temperature at the ice core site is -29 °C while the accumulation rate is 0.22 ice equivalent/year (NEEM community members, 2013). The core extracted contains an unprecedent climate record of the last 130 000 years. The Holocene is recorded from the top to 1419 m of depth while the glacial period reaches 2206 m. Being undisturbed, this portion of the core was matched to the NGRIP GICC05 extended timescale up to 108 thousand years before present, where 'present' is defined as AD 1950. Below this, ice-penetrating RES images showed a disturbed and folded ice, however the presence of zones with relatively high stable water isotope values indicated that the ice dated back from the last interglacial, the Eemian

Figure 41: The NEEM ice core site relative to other ice cores in Greenland.

(130–115 kyr BP). The dating of the ice core , together with the others deep Greenland ice cores namely NGRIP, GISP2 and GRIP was done according to the Greenland Ice Core Chronology 2005, GICC05 (Vinther et al., 2006; Rasmussen et al., 2006;Andersen et al., 2006; Svensson et al., 2008 based on annual layer counting of several chemical parameters measured continuously on the NGRIP, GRIP and Dye3 ice cores and featuring a clear annual cycle, back to 60 ka before 2000. The Maximum Counting Error (MCE), which can be regarded as a 2error estimate (Rasmussen et al., 2006) is 1439 a at 38 ka b2k. The transfer of the GICC05 to the NEEM ice core was done by matching peaks of electrical conductivity measurements and dielectrical properties, measured continuously on the others ice cores. The timescale obtained for NEEM is called GICC05-NEEM (S. O. Rasmussen et al., 2013).

Based on 5-days back-trajectory reanalysis, it was found that the majority of air masses reaching the NEEM site follow a westerly circulation pattern and transport toward northwest Greenland (Zhao

et al.,2015). In particular, along their path they progressively entrain both terrestrial aerosols from long-range transport associated with dust emission from northern North America and Asian deserts (Shüpback et al., 2018) and marine spray from the Canadian Archipelago, Hudson Bay and Baffin Bay. Since the first satellite observations, these regions (hereafter referred to as the Canadian Arctic) are covered by prevalent seasonal sea ice conditions, thus, they have been indicated as the dominant sources of bromine emissions recorded at NEEM site. (Fig. 42).

Figure 42: The NEEM aerosols entrainment area.

5.2.2 New high-resolution halogens measurements

Low resolution meltwater samples (1.10 m rod of ice melted) were collected from the Continuous Flow Analysis (CFA) system operated by the University of Bern at the NEEM ice core drilling site. When the CFA approached to melt the glacial ice, between 34 and 42 ky BP, additional n=1319 discrete samples were collected every 2-3 cm of ice melted into acid-cleaned polyethylene bottle and immediately frozen. The frozen samples were sent to the University of Venice where they were kept frozen and shielded from light until the analysis carried at CNR-ISP laboratories.
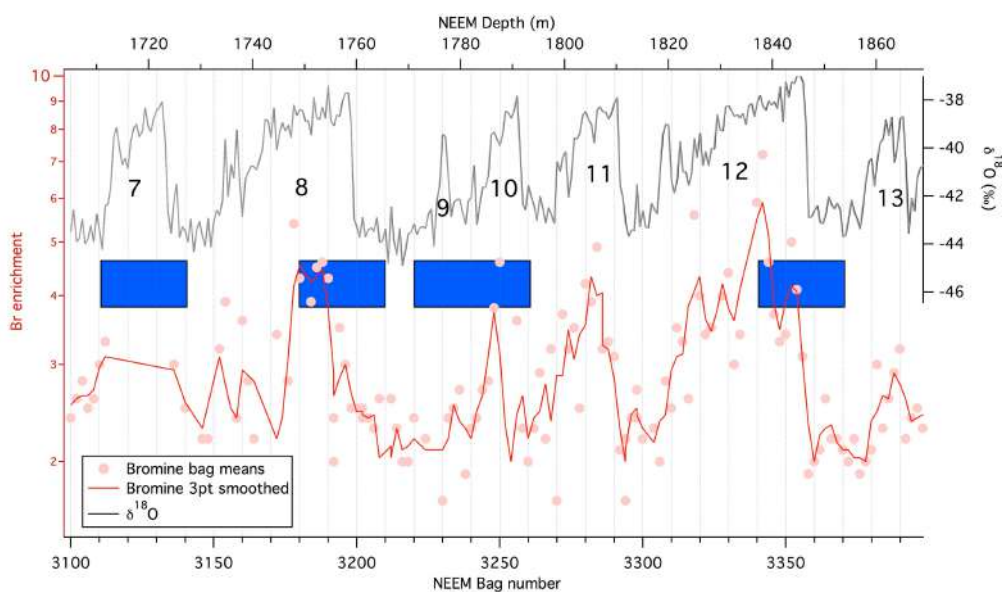

Figure 43: Bag-mean (1.10 m rod of ice melted) bromine enrichment data (red points) showed in the previous study by Spolaor et al., 2016. Blue boxes include the requested sections for high-resolution analysis (this study). Note that DO-12 was not included.

The portion of the NEEM core resampled includes three sections extracted between 1711 and 1793 m depth corresponding to DO events 7, 8, 9, 10 (Fig. 43). The new measurements were conducted strictly following the procedure described in the previous study by Spolaor et al. 2016. Concentrations of Br and Na were determined by Inductively Coupled Plasma Sector Field Mass Spectrometry (ICP-SFMS; Element 2, Thermofischer, Bremen, Germany) equipped with a cyclonic Peltier-cooled spray chamber (ESI, Omaha, USA). The sample flow was maintained at 0.4 ml min^{-1}. Detection limits, calculated as three times the standard deviation of the blank, were 52 pg g^{-1} 79Br. Reproducibility was evaluated by repeating measurements of selected samples characterized by different concentration values (between 400 and 600 pg g^{-1} for Br). The residual standard deviation (RSD) was low for both halogens and ranged between 2–11%. The analytical system was cleaned for 24 h prior to each analysis session, consisting of alternating 180 s washes of 5% ammonium solution (Traceselect® NH4OH, Sigma Aldrich), then 2% HNO3 acid (trace metal grade, Romil, UK), with 30 s of MQ water between reagents. Between each analysis a single cleaning cycle was run to return the background to within 1% of the initial background level. Bromine was calibrated by external calibration using standards of 10 to 4,000 pg g^{-1}, prepared by diluting a 1,000 mg L^{-1} standard solution (Tracecert® purity grade, Sigma Aldrich, MO, USA) in MQ water. All calibration curves showed correlation coefficients greater than 0.99 (df = 4, $p = 0.05$).
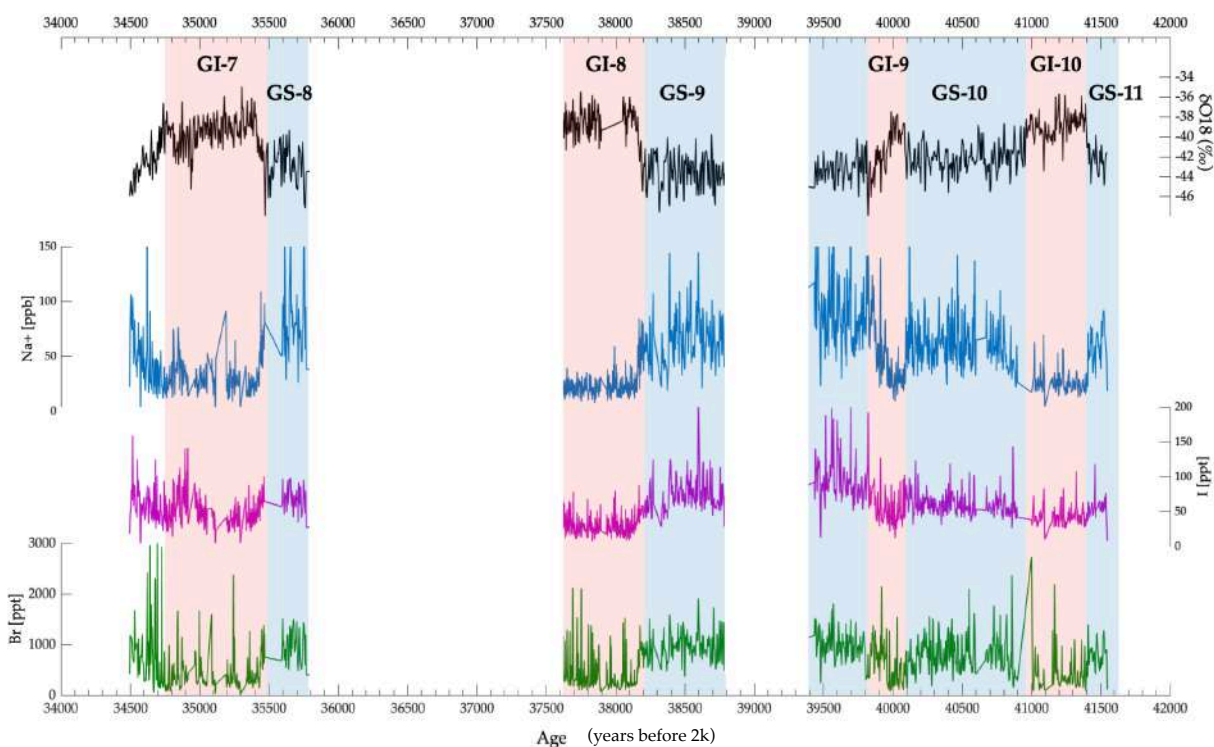
5.3 Results

5.3.1 Halogen concentration and fluxes

Figure 44: High resolution δO18 variations (black line) kindly provided by V. Gikinis (CIC) with sodium (blue), iodine (purple) and bromine (green) concentrations from this study. Light blue bands indicate the Greenland stadials (GSs) while reddish bands indicate Greenland interstadials (GI).

Sodium, bromine and iodine concentrations and fluxes show a similar trend with generally higher values during colder stadial (GS) and lower values during warmer interstadials (GI). In particular, the lowest sodium concentrations are observed during GI-8 (Na=23 ppb ± 11 ppb (1σ)) while the highest during GS-8 (Na=79 ppb ± 31 ppb (1σ) followed by GS-9 and GS-10 (Na=61 ppb ± 19 ppb (1σ)) (Fig.44). To assess the reliability of the new trace analysis performed, sodium concentrations were compared with CFA measurements conducted by Shüpbach et al., (2018) on the NEEM ice core, showing a general good agreement between the two independent records. (Fig. 45). As said before, also iodine and bromine show a sharp decrease passing from stadial conditions (with an average concentration of I=66 ppt ± 22 ppt (1σ) and Br=857 ppt ± 382 ppt (1σ)) to warmer interstadials (I= 44 ppt ± 31 ppt (1σ) and Br=425 ppt ± 353 ppt (1σ)). It's important to note that the GS-GI transition involved but atmospheric temperature and precipitation change, with a doubling snow accumulation passing from dryer GSs to wetter GIs. For
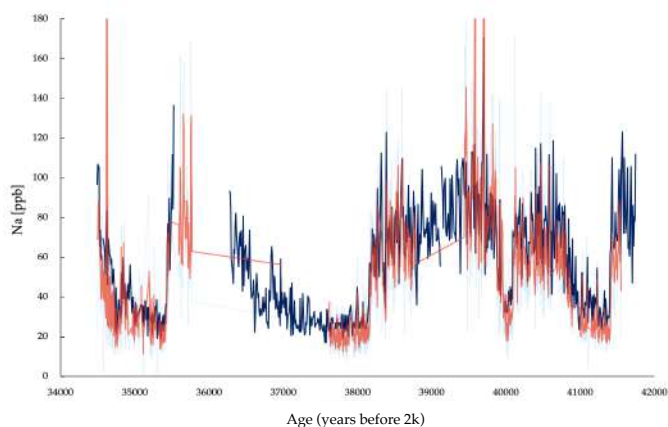

Figure 45: Discrete Sodium concentrations obtained from this study (red curve) compared with CFA measurements by Shüpbach et al. 2018 (blue curve).

this reason, sodium and halogens deposition fluxes were also calculated considering Na, I, Br concentrations [ng/mL] and the NEEM site Accumulation Rate [m.y^{-1} i.e.]) displaying not substantial differences with just the concentration trends. (Fig 46)
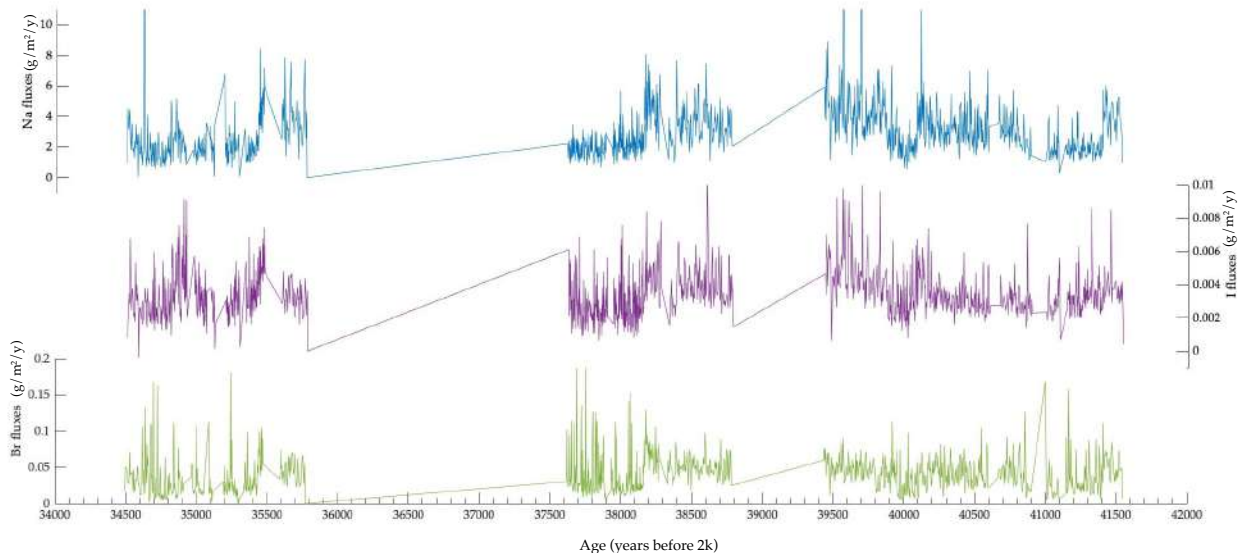

Figure 46: Sodium (blue), Iodine (purple) and Bromine (green) deposition fluxes.

5.3.2 Bromine and iodine enrichment

Bromine enrichment has been used to quantify the excess of bromine resulting from sea ice-related bromine explosion events. In line with the long-record from Spolaor et al, passing from stadials (GSs) to interstadial (GIs) conditions, both Br_{enr} mean value and its variance increases in phase with water oxygen isotopes ($r = 0.46$) (Fig. 47). The highest Br_{enr} increase (GI-GS) occurred during DO-8 (+ 56%) followed by DO-10 (+45%); DO-9 (+18%) and DO-7 (+17%) (Fig.48 and Table5). Likewise the idea of an enrichment of bromine in polar snow, considering the average (I/Na) in sea-water equal to I/Na = 0.0000056 (Millero et al., 2008), it's also possible to calculate the enrichment of non-sea-salt iodine (I_{enr}) thought to reflect major changes of past marine primary productivity (Cuevas et at., 2018). This potential geochemical marker is based on the hypothesis that an increment of I/Na ratio in snow (normalized over sea water ratio) could reflect an increase of biogenic iodine (CH_3I, CH_2I_2) emitted due to a change in the ocean conditions (i.e. warmer SST). Although both sodium and iodine decrease in phase with warmer interstadials (Fig. 46), the latter declines more gently making their ratio increasing consistent with the water oxygen isotopes (i.e. atmospheric temperatures). Differently from bromine enrichment, the highest increase (GI-GS) in I_{enr} occurred during DO-7 (+94 %), followed by DO-10 (+77%) and DO-9 (+61%) while only a slight increase occurred during DO-8 (+20%) (Fig.47 and Table 5).
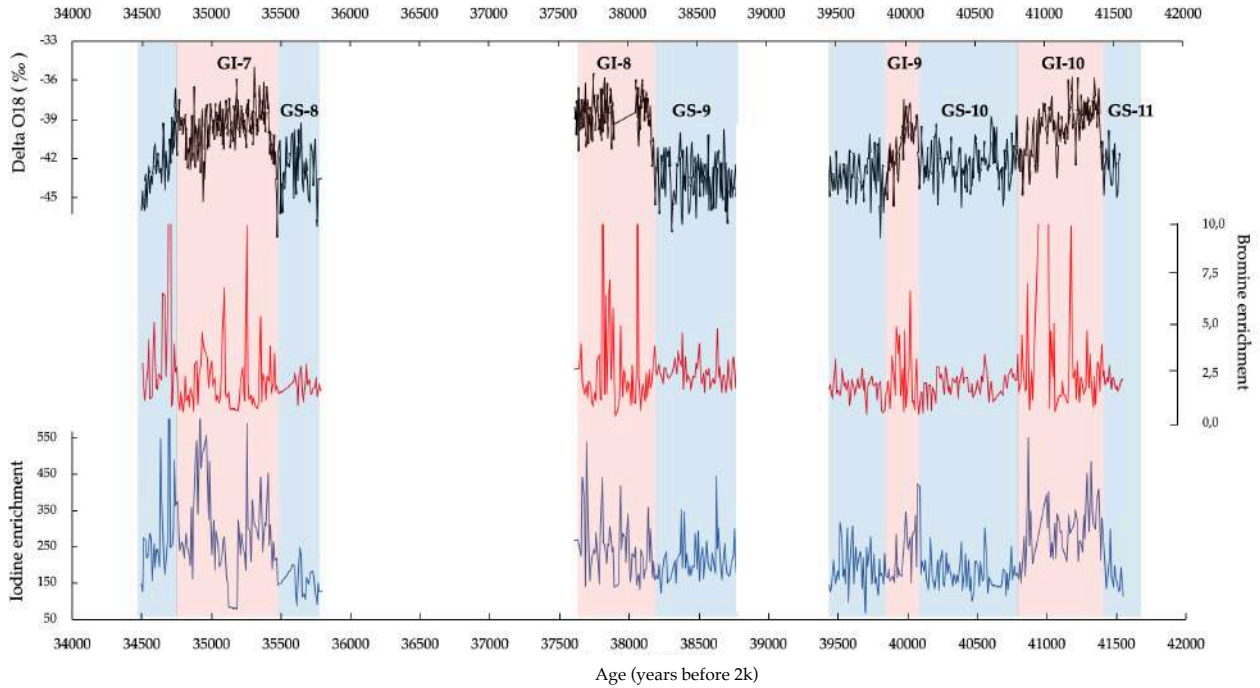
Figure 47: High resolution δO18 variations (black line) kindly provided by V. Gikinis (CIC), bromine enrichment (red line) and iodine enrichment (light blue line) over DO-7 to 10. Light blue bands indicate Greenland stadials (GSs) while reddish bands indicate Greenland interstadials (GI).

Both halogens proxies showed a positively correlation with water oxygen isotopes which are commonly used as proxies for atmospheric temperature and evaporation at the source. It worth noting that, being a ratio between Br and I over Na concentrations, bromine and iodine enrichment result to be no-dimensional values, thus they are not affected by accumulation change during the GS-GI transitions even though they might be affected by different aerosols deposition en route (Shüpback et al., 2018). Finally, to better understand the halogens variability showed during the observed DO, stable oxygen and nitrogen isotopes can be used for temperature and accumulation reconstructions In particular, we know that during DO events, the NEEM site experienced dramatic physical changes with the highest temperature increase occurred during DO-8 (+8.85 °C) followed by DO-10 (+7.72 °C) and DO-9 (+6.02 °C) (Guillevic et al., 2013). (Table 5).

Table 5: DO increase (GI-GS) in δ18O(‰), temperature(°C), accumulation (mm.i.e.a−1) reconstructed at NEEM from Guillevic et al., 2013. Bromine and iodine enrichment increase from this study.

	DO - 7	DO - 8	DO - 9	DO - 10
Stadial δ18O	-	-43.52	−42.66	-42.65
Δ δ18O	-	5.57	3.09	4.32
ΔT	-	8.85	6.02	7.72
Stadial Acc.	-	47	46	53
Δ Acc.	-	58	14	36
Δ Br $_{enr}$	17%	56%	18%	45%
Δ I $_{enr}$	94%	20%	61%	77%

5.3.3 Statistical analysis

As showed in Fig. 47, each DO transition is marked by an increase of both Br_{enr} and I_{enr} variability that can be partly attributed to a higher accumulation rate during GI, but also it might reflect the signature of less stable sea ice conditions of the NEEM aerosols source area. 10-year average Br_{enr} and I_{enr} data, in fact, show a constant fluctuation around low mean values during GSs (with Br_{enr} =2.21 ± 0.92 (1 σ) and I_{enr} =196 ± 76 (1 σ)) while, during GIs, the signals rapidly oscillates from almost no enrichment to the maximum values recorded (Br_{enr}=2.87 ± 3.34 (1 σ) and I_{enr} =281 ± 105 (1 σ)). This is particularly true for Br_{enr} with an observed σ_{Gs} always constrained below 39% while σ_{GI} in same cases arrived up to 140% (GI-8) (Fig.48).
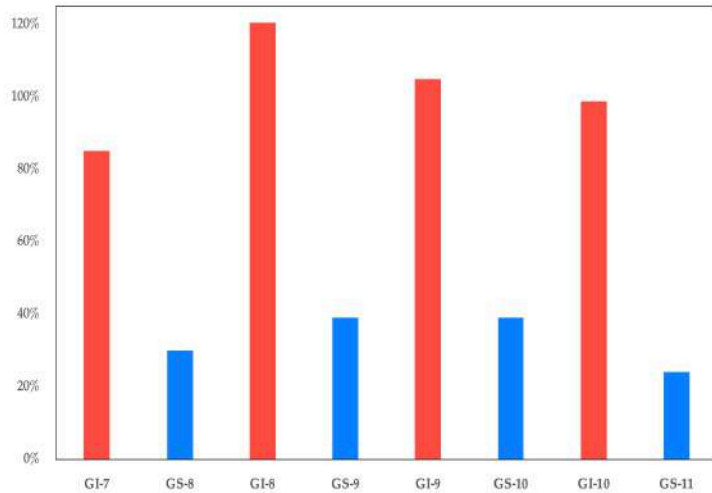

Figure 48: Bromine enrichment Standard Deviation during GIs and GSs

In addition to descriptive statistic, two others robust statistical methods (with 95% of significance) have been applied to calculate the Br_{enr} and I_{enr} variance in order to assess the causality relation and the timing between sea ice change (i.e. Br_{enr}, I_{enr}) and abrupt atmospheric warming (i.e. $\delta^{18}O$ per mill). The first method, called moving variance (Fig. 50), is a weighted variance of the observations in a window centred at a particular time. The lengths of the windows are different for each DO event and they are equal to the time taken by $\delta^{18}O$ to change from stadial to interstadial values. (Fig.49) The weights are distributed according to the gaussian distribution.

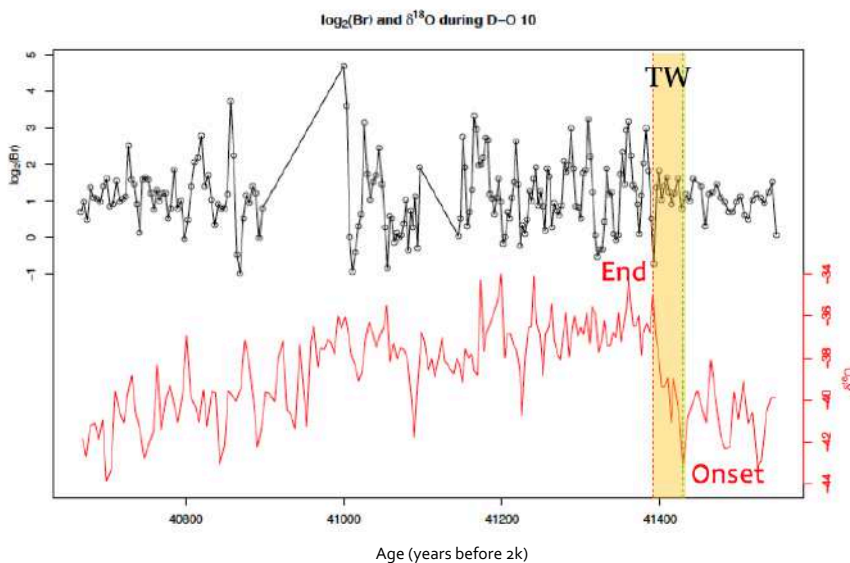*Figure 49: The time window selected to run the moving variance on a single DO event considers the time between the onset and the end of atmospheric warming (red curve). Once that the time window is set for each event, it is applied to the bromine enrichment series. The example showed is taken from DO-10 whose Time Window of 38 years was applied to calculate the moving average of bromine and iodine enrichment data.*
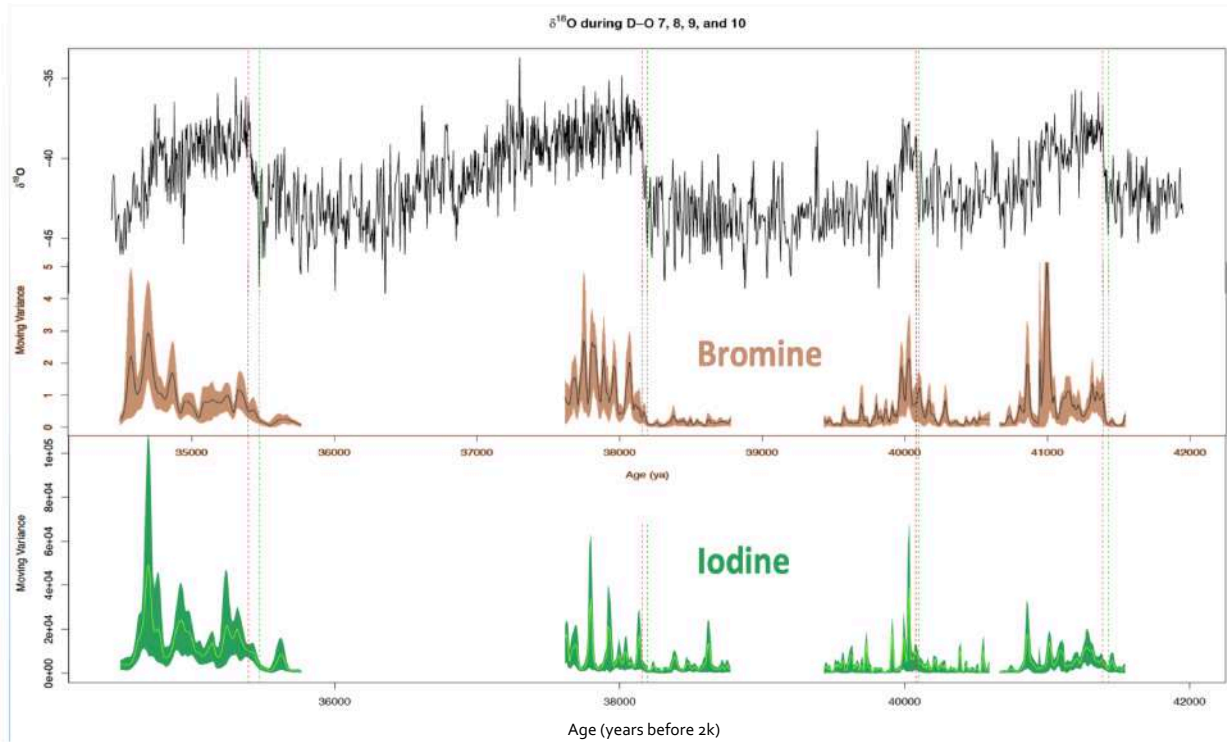
Figure 50:The Moving variance of Br_{enr} (brown) with 95% of significance (black line) and I_{enr} (green) with 95% of significance (light green). Dashed green and red vertical lines indicate the duration of each warming event which is used as time window to run a separate moving average on each event. The centennial time scale variability of both Br_{enr} and I_{enr} showed has been interpreted as natural long-term sea ice variability.

The second statistical method instead, is called smoothed variance, and aims at identifying the first time of occurrence of a statistically significant increase of the variance of the Br_{enr} and I_{enr} series during the interstadial phases. The Br_{enr} series is represented in logarithm scale in order to better reproduce the exponential nature of bromine explosions. The series of $\log_2(Br_{enr})$ and I_{enr} were split in subseries for each DO event given the absence of data between the DO events. For each subseries, a smoothed estimate of the variance of $\log_2(Br)$ during the interstadial phases was computed using penalized regression splines (Wood, 2017) applied to the squared deviations of $\log_2(Br_{enr})$ from its average value. The corresponding 95% confidence band was calculated using the bootstrap method (Efron and Tibshirani, 1993). The first time of occurrence of a statistically significant increase of the variance during the interstadial phases was declared as the first point in the $\log_2(Br_{enr})$ series at which the lower limit of the 95% confidence band exceeds the variance level of the stadial phase for each DO event considered. Computations were carried out with the R (R Core Team, 2019) package mgcv (Wood, 2017). Sensitivity test of the statistical methods have been performed by imposing different fixed time windows that however did not change significantly the results obtained.
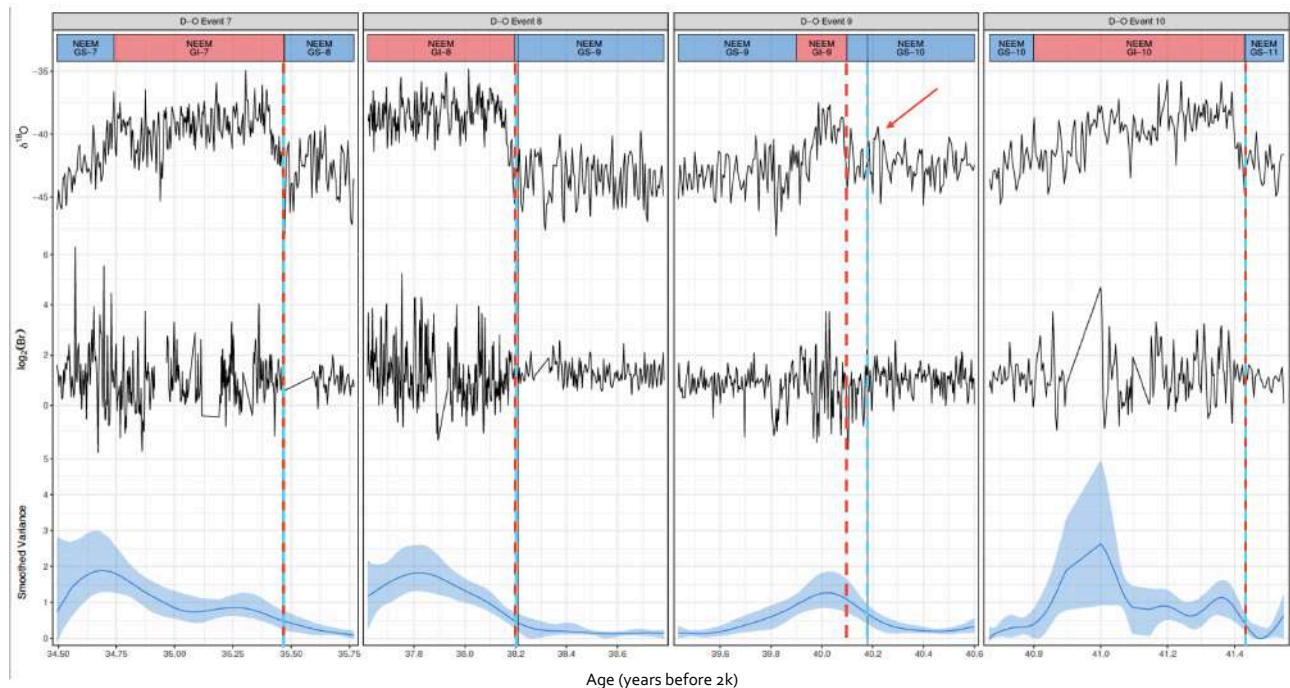
Figure 51: The first row shows high resolution oxygen isotopes (provided from V.Gkinis). The second row is the log2(Br$_{enr}$) record while the last row is the smoothed variance of Bromine enrichment data. Dashed red lines indicates the onset of each DO event, light blue dashed lines mark the first occurrence of a significative increase of the smoothed variance when its lower bound of the 95% confidence interval is greater than the bromine's variance during the stadial phase. Blue bands indicate 95% of significance.

The results of moving and smoothed variance agree on a synchronous change of Br$_{enr}$ and I$_{enr}$ in concomitance with the onset of each GS-GI cycle. This is true for larger events considered such as DO-7 and 10 ($\pm$3 ys) and DO-8 (-15 ys) while, for the shorter and smaller in amplitude DO-9 both sea ice proxies started to oscillate around 80 years before (Fig.50 and Table 6). For larger events, Br$_{enr}$ smoothed variance increased from a smoothed variance (SV)=0.5 during GSs up to SV=2 during GIs. Finally, the sea ice response time to reach the max of its variability was calculated as the time interval between the first occurrence of a statistically significant increase of Br$_{enr}$ and I$_{enr}$ variance and the maximum values obtained for each event. For DO-7 the max of variance change occurred +777 ys after the onset of GI-7, +447 ys for DO-8 and +432 ys for DO-10. As said before, opposite to larger warming events, during the DO-9 the change of the moving variance for both halogen enrichments is asynchronous in respect to the δ18O shift, showing a lead of about 320 years before the onset of GI-9.(Fig 51). Interestingly, for the all events investigated the moving/smoothed variance change could be linked with a threshold of δ^{18}O around -41‰. Above this threshold, the variance starts to increase, below it decreases. This information might indicate that when at the NEEM site (2484 m a.s.l at present day) the reconstructed surface temperature was above -36 °C (Guillevic et al., 2013), its aerosol entrainment area (i.e. Baffin Bay sea ice) was already experiencing a change. Consistent

with this hypothesis, the $\delta^{18}O$ values at ~40.3 kya, which are above the threshold and closer to interstadial ones, might explain why the halogens variance anticipated of ~80 years the main atmospheric warming occurred one century later (red arrow in Fig. 51 and Table 6).

DO event	First year of Significative Br_{enr} change	Time difference (yr) with DO-onset
7	35470	+2
8	38210	-15
9	40178	-79
10	41432	-3

Table 6: The first year of significative change of Br_{enr} variance, the time difference with the DO-onset and the time response to reach the maximum of variance.

5.4 Discussion and conclusions

Stable water isotopes from multiple Greenland ice cores have been used to reconstruct the climate of last glacial period characterized by at least 25 abrupt climate instabilities known as the Dansgaard-Oeschger (DO) events. Each event was marked by a rapid atmospheric warming of few decades (up to +8.8 ± 0.6 °C for DO-8 at NEEM site, Guillevic et al., 2013) followed by a slow gradual cooling lasting for 1-2 ky years preceding the next warmer period. Although many evidences from Arctic ice cores and marine records indicate a sharp shift from a colder and dryer climate (the so-called Greenland Stadials, GS) to relatively warmer and wetter conditions (Greenland Interstadial, GI), the mechanisms and the triggers which led to a reorganization of the global atmospheric and oceanic circulation are still not fully understood. Among the leading theories, abrupt Arctic sea ice demise caused by a strengthening in the Atlantic Meridional Overturning Circulation (AMOC) and deep-water formation is considered the main factor governing the abrupt temperature increase registered in Northern Greenland. In this sense, a recent
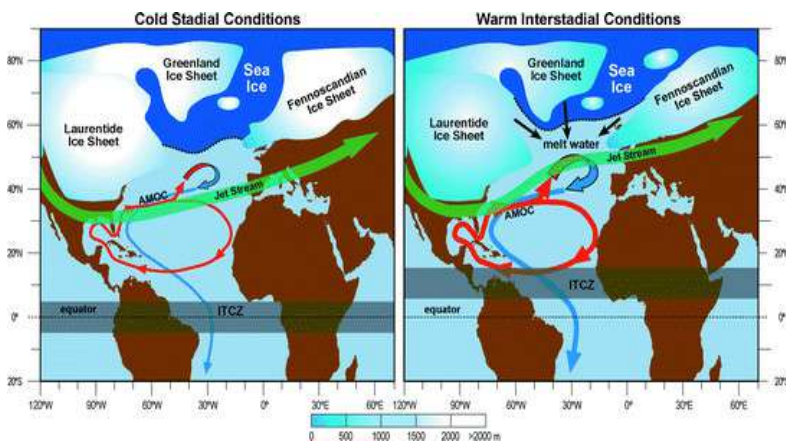
Figure 52: Stadial and Interstadial conditions of Northern Hemisphere from Rosa H. Compagnucci., 1994.

study based on sea ice biomarkers and model data comparison by Sadatzki et al., (2019) showed an offset of 0-250 year between Norwegian Seas sea ice demise and North Greenland temperatures increase (from the NGRIP ice core) occurred during glacial DO-5 to 9 (32-40 kya). The main process which, according to the authors, could have determined the sea ice shrink is a northward advection of warmer Atlantic surface water linked with a series of factors such as stochastic atmospheric

forcing affecting the subpolar gyre circulation, wind-driven advection of saline surface waters from the tropical North Atlantic, and/or an early AMOC strengthening (Sadatzki et al., 2019). Although the paper investigates sea ice evolution of the Norwegian Sea, which is about 3.000 km east of the Canadian Arctic and Baffin Bay, (the NEEM aerosols sampling area) the temporal overlap of 6 ky (34-40 ky BP) could provide a useful complementary information to evaluate the large-scale spatial variability of Arctic sea ice over a series of DO events, in particular DO-7, 8 and 9. Comparing sub decadal bromine and iodine enrichment data (sea ice proxies) with stable water isotopes (proxies for atmospheric temperature and moisture availability) measured along the NEEM ice core, one of the goal of this study is to clarify which is the connection and the timing (whether synchrony or asynchrony) between Canadian Arctic sea ice change and the repeated atmospheric warmings occurred in northern Greenland during the last glacial period.

5.4.1 Sea ice evolution during DO 7 to 10

The sub-decadal Br_{enr} and I_{enr} measurements obtained from this work provided, with an unprecedent detail, a reconstruction of Canadian Arctic sea ice change observed over a series of DO events. Both sea ice proxies vary according to water isotopes changes during glacial DO events, with higher values during longer-lasting interstadials (GI-8, 10,) and lower values showed for interstadials of less than 1000 years of duration (GI- 7, 9). In contrast with high mean bromine enrichment values ($Br_{enr} \approx 15$) of the early Holocene (9-11.5 kya) that have been interpreted with summertime ice free conditions and only FYSI during spring and winter (Spolaor et al., 2016), the last glacial period is characterized by relatively low mean values ($Br_{enr} \approx 2.5$) suggesting a widespread Multi Year Sea ice (MYSI) coverage over the Canadian Arctic with the sea ice bromine source located farther away (i.e. Labrador Seas) from the NEEM site. More specifically, according with different palaeoceanography and models reconstructions, (Sime et al., 2019; Peltier., 1994;) we know that during last glacial period extensive ice sheets extended over North America (Laurentide ice sheet), Greenland, Northern Europe and Siberia (Fennoscandinavian ice sheet) but not over Baffin Bay and Hudson Bay that were assumed to be covered by a thick sea ice (Peltier., 1994) (Fig.52). Furthermore, dealing with aerosols emission and deposition, it is also important to consider the winds change occurred during DO cycles. Little is known about past wind changes, however a work by Schüpbach., et al., (2018), suggests that during GS-GI transitions, the magnitude of regional wind speed changes was on the order of 10%, while the expansion of the continental ice sheets and sea ice was very large, suppressing a huge part of recent continental and open ocean source areas in the glacial. They also found that large part of the sea salt aerosol in Greenland during modern times comes from the open North Atlantic. However, the sea ice, especially in Baffin Bay, represents a significant additional winter source (up to 50%). Thus, sea ice contribution is expected to become relatively more important in glacial times, when sea ice largely expanded (Schüpbach., et al., 2018). Indeed, if on the one hand, stable low-mean values of Br_{enr} and I_{enr} suggest permanent MYSI conditions during colder GSs (Fig.54, stage 1), on the other hand a slight increase of Br_{enr} values (up to +30%) observed in

phase with the onset of GIs might indicate a loss of the prevalent MYSI coverage partially replaced by enhanced FYSI conditions. The sea ice type substitution from fresher MYSI to saltier FYSI could have allowed more inorganic bromine recycling during springtime with subsequently deposition of more bromine enriched snow at NEEM site (Fig. 54, stage 2).. Furthermore, looking at Br_{enr} and I_{enr} trends, the highest values observed about 0.4-0.8 ky after the DO onset (with peaks of $Br_{enr} > 25$) can be the signature of a rapid FYSI expansion towards lower latitudes as showed also by modelled reconstruction of the sea ice edge positions during GS-GI transitions (Sime et al., 2019) (Fig. 53A and 54, stage 3). An explanation for repeated FYSI expansions could be the injections of freshwater from the North America ice sheet into the Labrador seas due to the increase of atmospheric temperatures which could eventually also prevented deep-water formation and weakening of the thermohaline circulation (Dansgaard, et al., 1993; Broecker et al., 1990). In this sense, through the ice-albedo feedback, the rapid build-up of an extended seasonal (and then MY) sea ice could be a very efficient way to cool down the temperatures and shift the climate system to a cold stadial conditions.
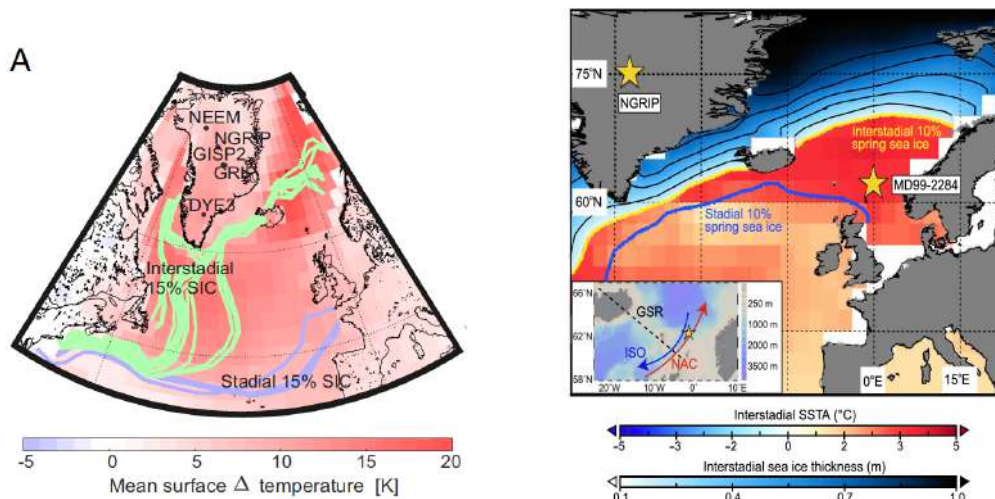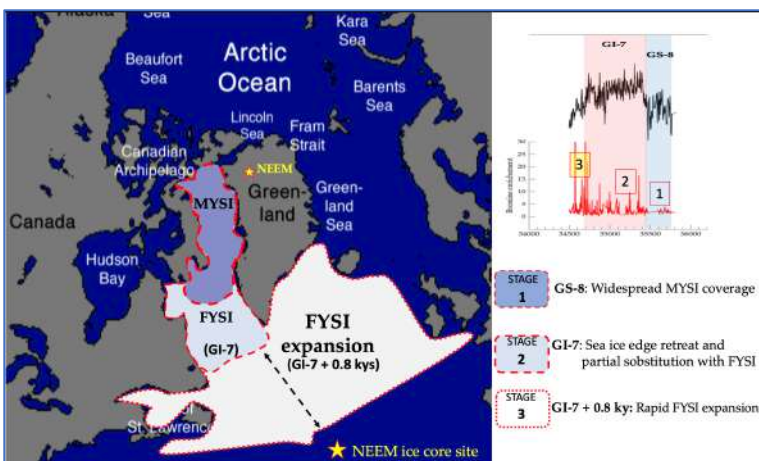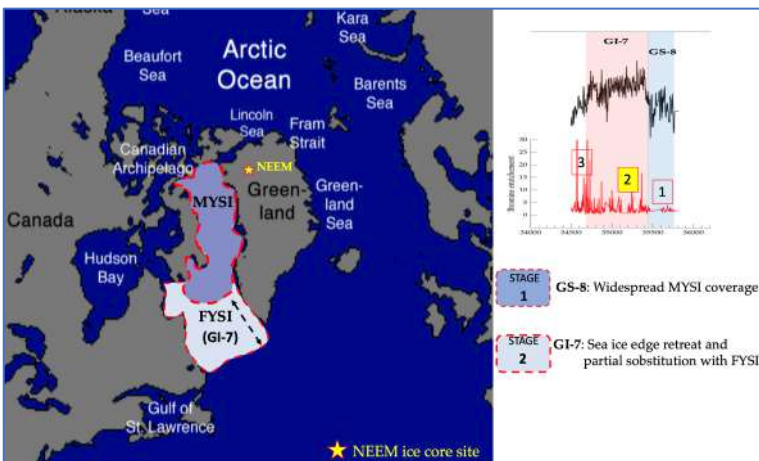

Figure 53: (A) Mean surface temperature change from simulated stadial to interstadial climates. Averages are from 15 simulations with significant (+2.0‰) DO rises in d18O Lines show the standard 0.15 mean annual sea ice concentration (SIC) contour for this subset of stadials (blue) and interstadials (green) from Sime et al., 2019. (B) Annual mean sea surface temperature anomaly (SSTA) and 10% spring sea ice extent for interstadials (yellow line) compared to stadials (blue line) as well as interstadial sea ice thickness derived from the LOVECLIM MIS3 hindcast simulation From Sadatzki et al., 2019.

To summarize, the almost synchronous increase of Br_{enr} and I_{enr} variance in phase with the onset of GI-7,8, 10 suggests that, for larger events the loss of MYSI over Baffin Bay and Hudson Bay did not anticipated significantly the temperature increase recorded at NEEM (as found also by Erhardt et al., 2019) differently from the Nordic Seas sea ice which showed a slight offset up to 250 years (Sadatzki et al., 2019). Combining the data obtained from this work with numerical simulations of sea ice conditions during GS-GI transitions (Sime et al., 2019) it is reasonable that major sea ice type substitution (from MY to FY sea ice) occurred especially in the southern sector of Baffin Bay and in the Labrador Seas (Fig.53A and 54, stage 2). Contrarily to Early Holocene, overall low mean bromine values instead indicates a more stable northern part of Baffin Bay (closer to the NEEM site) that is supposed to remain more isolated from the partial sea ice substitution. Finally, between 0.4 and 0.8

ky after the onset of longer GIs, the maximum increase of Br_{enr} and I_{enr} suggest a rapid sea ice build-up that, expanding the sea ice coverage towards lower latitudes might have repeatedly determined the shift from warmer (GIs) to colder (GS) climate conditions. (Fig.54, stage 3). To complete the spatial evolution of DO warming events it is likely that they originated in the Nordic Seas (Sadatzki et al., 2019) (Fig. 53B) and sub sequentially propagated towards eastern and southern Greenland sea ice provoking the MYSI sea ice edge to retreat and regional atmospheric temperatures over Greenland to increase. This theory is supported by the increase of I_{enr} moving variance (less sharp than Br_{enr}) that however can be interpreted as an enhanced marine biological activity associated with MYSI thinning. The final sea ice expansion is also suggested by the maximum increase of I_{enr} even though a marine bio-proxies comparison is needed to more robust conclusions.
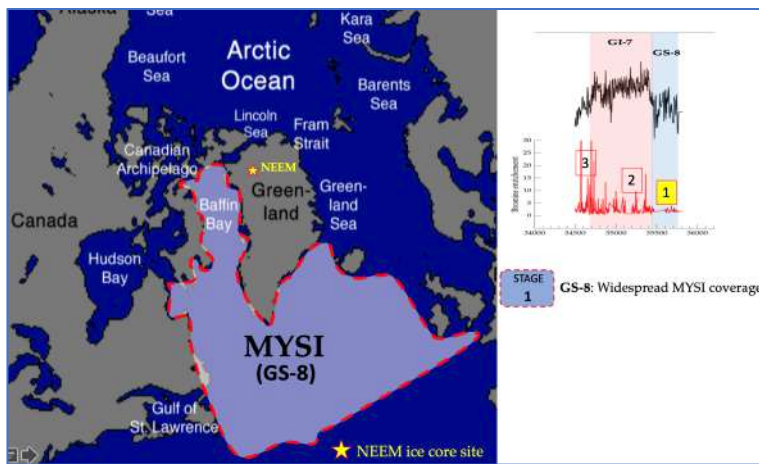
Figure 54: Sea ice reconstruction of Baffin Bay during DO-7. Looking at Bromine enrichment (red curve), 3 distinct stages can be identified. S-1: During GS-8 a widespread multiyear sea ice covers Baffin Bay until Labrador Seas (dashed line). S2: Few decades after the onset of GI-7, the MYSI edge retreats notably and it's partially substituted by enhanced FYSI conditions. S3: After ~0.8 ky from the onset of GI-7 due to the availability of freshwater delivered from the melting of the Laurentide ice sheet, FYSI can rapidly expand towards southern latitudes eventually determining the gradual atmospheric cooling bringing back the climate system to a new stadial period (i.e. GS-6).

6. Additional Works

This Chapter has been thought to present the preliminary results from two additional works carried out during the course of the PhD and still under investigation. Based on analytical measurements conducted on surface snow from a traverse linking two deep ice core drilling sites of the central and eastern Greenland ice sheet (respectively NEEM and EastGRIP) the first work is focused on understanding the role of transport on halogens deposition.

The second work, instead, presents 110-year record of sodium, calcium and halogens (bromine and iodine) measured from the SIGMA-A ice core drilled in 2017 on the North West Greenland Ice Sheet. Due to its location (<100 km from the North-western Greenland coast) the SIGMA-A is thought to register the major changes occurred to the North Water Polynya (NOW), an area of Baffin Bay characterized high biological productivity. Therefore, combining high-resolution halogen measurements at a sub-seasonal time scale with outputs from a numerical simulation and observations of the main physical and biological parameters (for 1980-2018), this study aims to provide new insight about the use of iodine enrichment as an indicator of past phytoplanktonic activity.

6.1 Bromine, Iodine and Sodium in surface snow collected during the NEEM to EastGRIP 2015 traverse (Greenland).

6.1.1 Introduction

In May 2015, n=89 surface snow samples (5 cm) were collected during a traverse linking the NEEM

Figure 55: The NEEM to EastGRIP traverse of Spring 2015. Image from Google Earth

ice core drilling site (77.45°N, 51.06° W, 2484 m a.s.l.) with the East Greenland Ice-core Project site (EastGRIP, 75.38°N, 35.99° W, 2720 m a.s.l.) (Fig.55). The main scientific goal of the traverse was to investigate the halogens (Br, I) and sodium (Na) spatial distribution over central and eastern Greenland, a crucial information which might shed some light about the role of transport on aerosol deposition velocities.

On December 2017, the snow samples have been analysed at Ca' Foscari University of Venice with an Inductively Coupled Plasma Sector Field Mass Spectrometry (ICP-SFMS; Element2, ThermoFischer, Bremen, Germany) equipped with a cyclonic Peltier-cooled spray chamber (ESI, Omaha, US) in order to detect bromine, iodine and sodium concentrations.

6.1.2 Analytical results
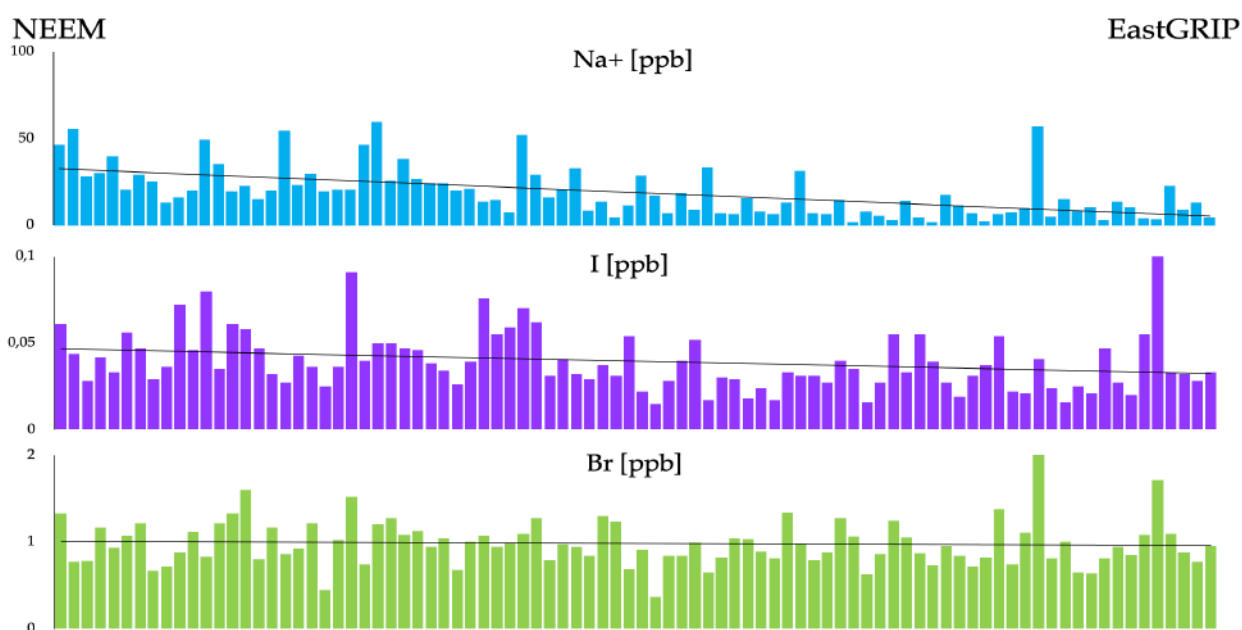
Figure 56: Sodium(light blue), iodine(purple) and bromine(green) concentrations from trace analysis on surface snow samples collected from NEEM (left side) to EastGRIP (right side)ice cores sites in 2015.The black lines indicate the linear fit of all the data .

The analytical results showed different trends for sodium and halogens. Overall concentrations decrease going from north-west (the NEEM site 77.45°N, 51.06° W) to south-east (EastGRIP, 75.38°N, 35.99°), however, once crossed the ice divide (corresponding to sample n=31), mean sodium concentrations decrease greatly from 30 ppb to 13 ppb (-55%). Interestingly, halogens do not change much in concentration across the ice dived with the iodine passing from a mean value of 46 ppt to 36 ppt (-21%) and bromine from 1070 ppt to 970 ppt (-9%) (Fig. 57).
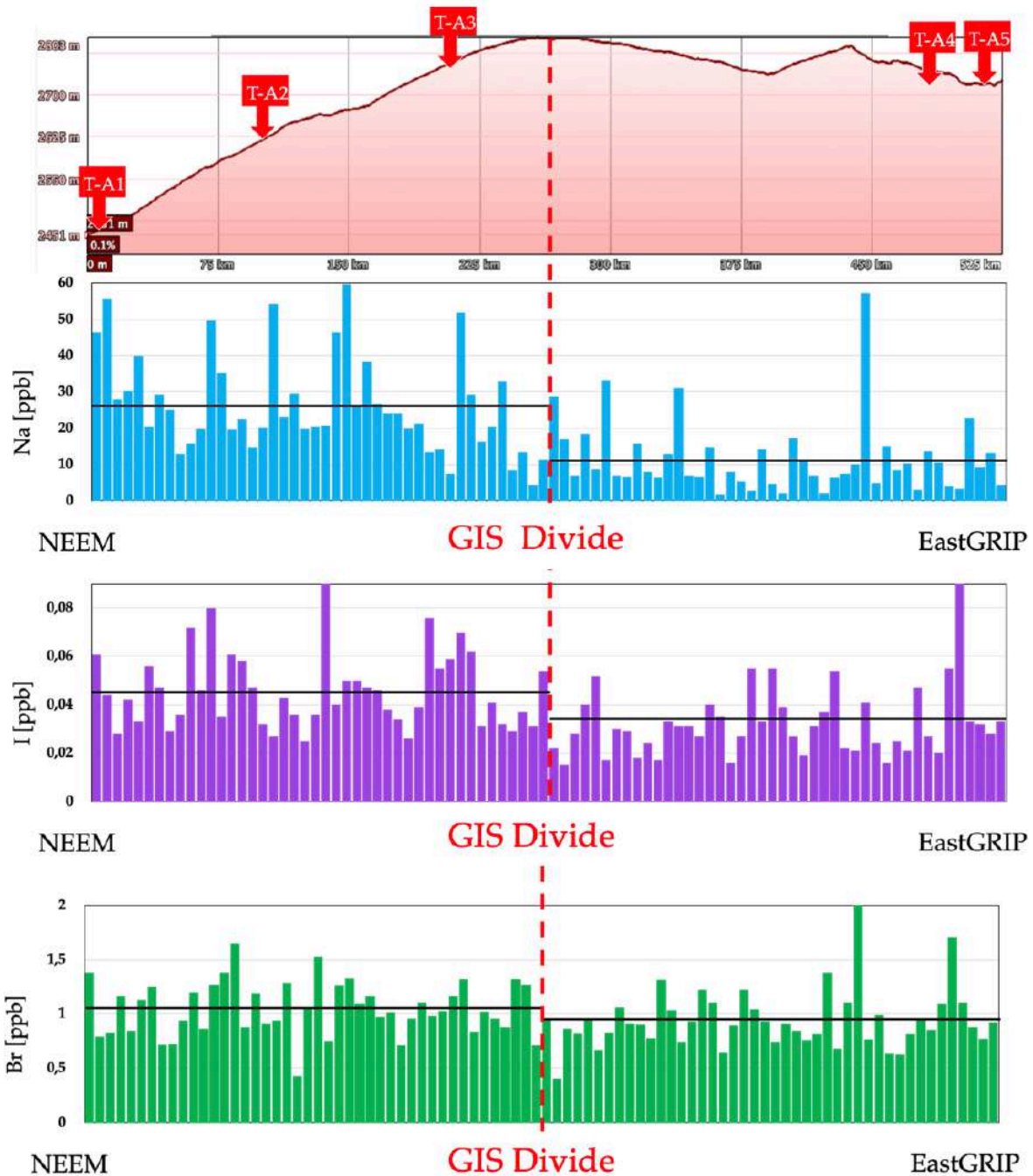
Figure 57: The elevation profile of the traverse and sodium concentration (light blue), iodine (purple) and bromine (green). The black line is the average concentration between samples n=1-32 and samples n=33-89. The dashed red line indicates the Greenland Ice Sheet ice divide. Red arrows indicate the firn cores locations described in Table 7.

Table 7: Description of the firn cores used to extract accumulation rates along the traverse

| Firn core ID	Coordinates N	Coordinates W	Altitude m a.s.l	Core (Time span)	$A_m \pm 1\sigma$ [m w.eq. a^{-1}]	$A_m \pm 1\sigma$ [m snow.eq. a^{-1}]
2015 T-A1 (NEEM)	77.45°	51.06°	2484	(17 yrs)	0.235 ± 0.061	0,67 ± 0,17
2015 T-A2	77.029°	47.479°	2620	(27 yrs)	0.198 ± 0.046	0,57 ± 0,13
2015 T-A3	76.448°	44.771°	2771	(27 yrs)	0.182 ± 0.033	0,52 ± 0,09
2015 T-A4	75.7094°	36.2742°	2701	(35 yrs)	0.144 ± 0.03	0,41 ± 0,09
2015 T-A5 (EGRIP)	75.6299°	35.9867°	2708	(54 yrs)	0.134 ± 0.035	0,38 ± 0,10

Different accumulation rates extracted from 6 firn cores (Table 7) retrieved between NEEM and EastGRIP were also accounted to calculate sodium and halogen depositional fluxes confirming the same trends found for the concentrations with higher fluxes of sodium on the western side of Greenland in respect to the eastern one, and constant halogens fluxes along the traverse. (Fig.58)
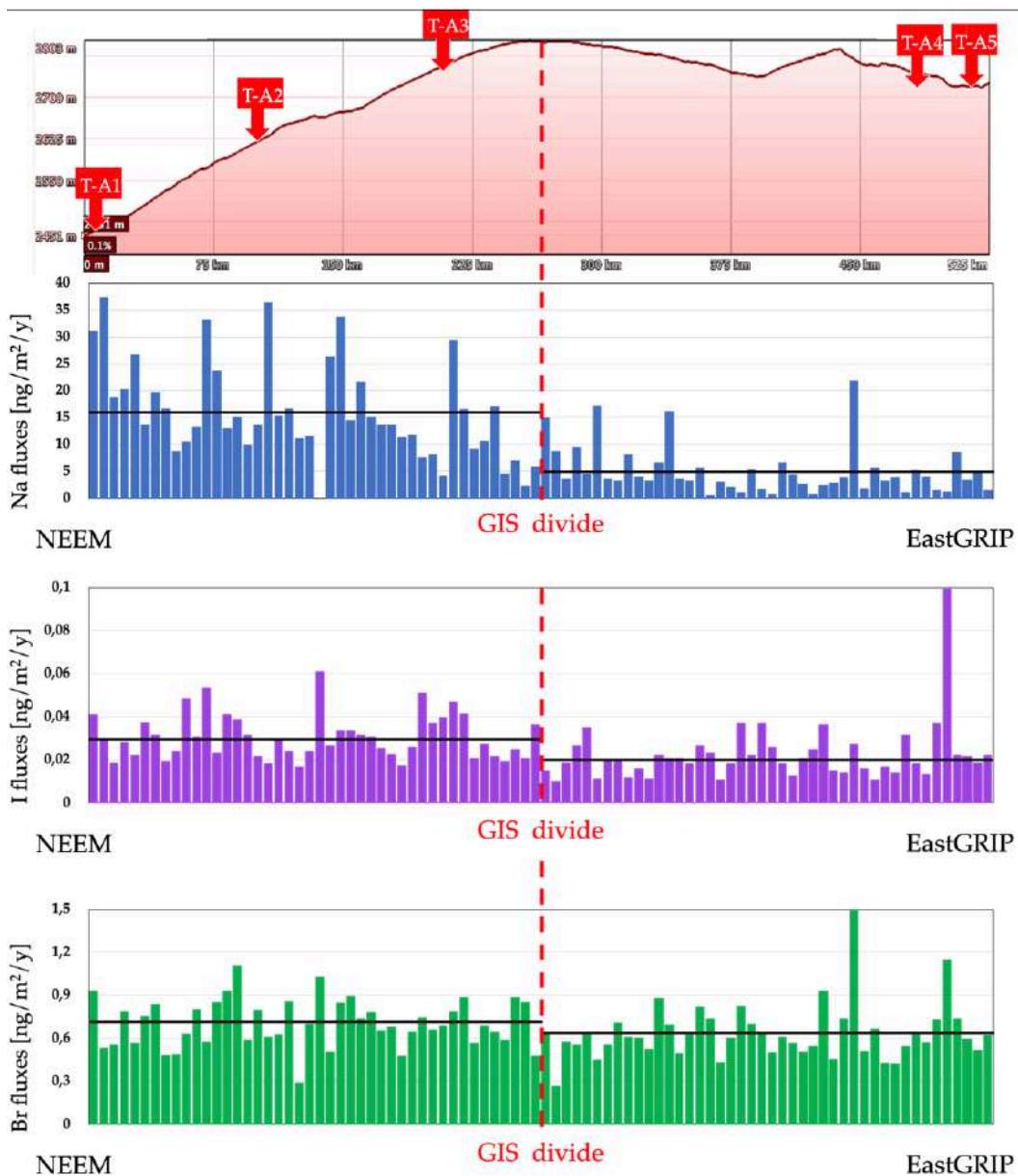
Figure 58: Depositional fluxes (ng/m2/yr) of sodium, iodine and bromine calculated along the NEEM to EGRIP traverse.

6.1.3 Bromine and Iodine enrichments

Similarly to the study cases showed before, bromine and iodine enrichments (Br_{enr} and I_{enr}) have been calculated from relative concentrations of Br/Na and I/Na found in the snow normalized over their sea-water constant ratio (respectively 0.0062 and 0.0000056, Millero et al., 2008). As expected, passing from the western side to the eastern side of Greenland also Br_{enr} and I_{enr} display a drastic change with a 3-fold increase. Br_{enr} changed from a mean value equal to 7 to 21, while I_{enr} varied from an average of 326 to 952 (Fig.59).
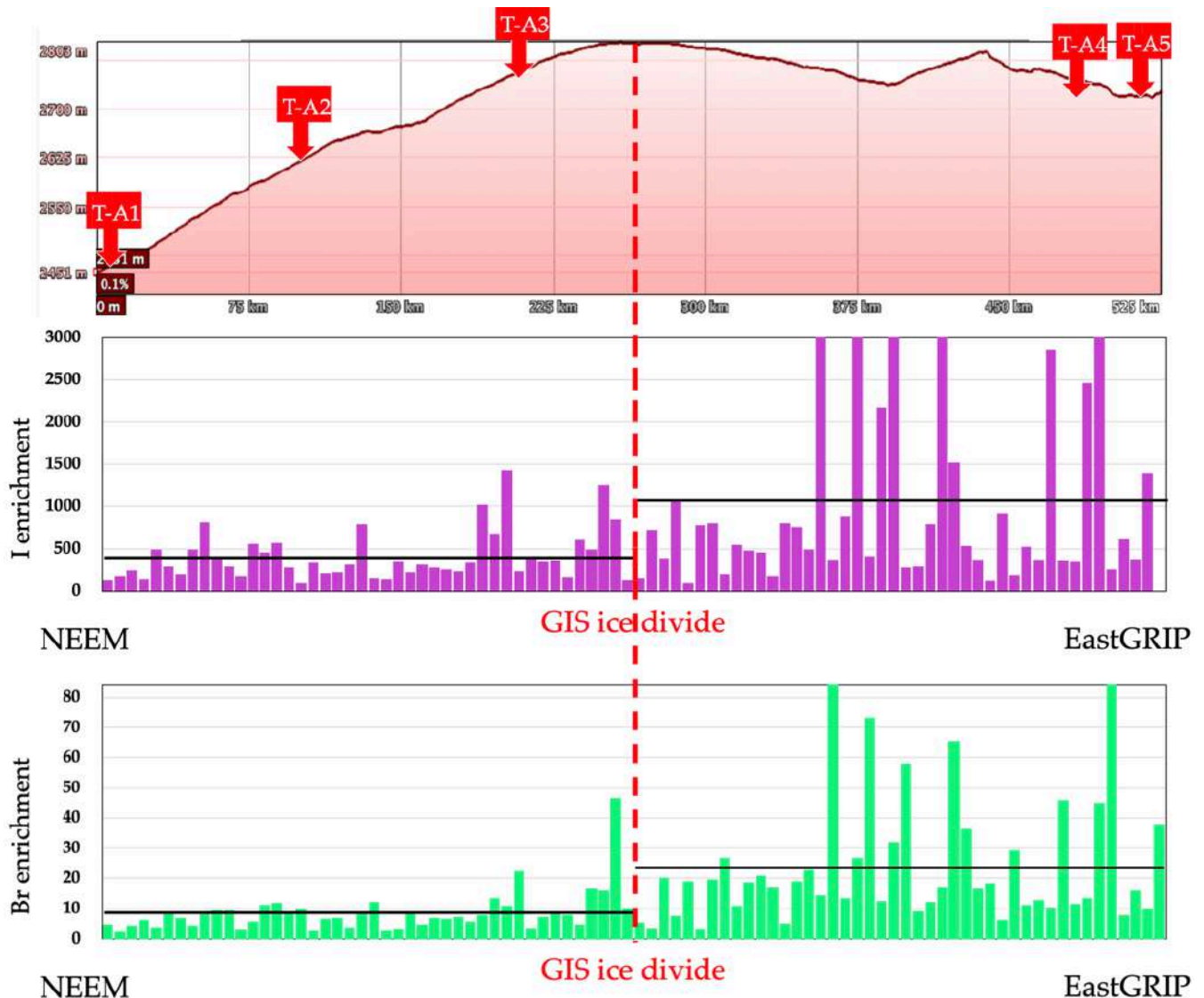
Figure 59: Iodine and bromine enrichments moving from NEEM to EastGRIP drilling sites. Both halogens enrichments show a 3-fold increase passing from the western side to the eastern side of Greenland.

6.1.4 Discussion and Conclusion

As described in Chapter 3, Br_{enr} and I_{enr} have been extensively used to reconstruct past sea ice conditions. The first one depends on springtime bromine explosions occurring over the newly-

formed sea ice (FYSI) while organic iodine has been linked with enhanced sea ice-related biological activity which release, as end product, biogenic iodine species in the polar boundary layer.

To better identify the provenance of the aerosols arriving at NEEM and EastGRIP, 3-days path back-trajectory were calculated using the HYSPLIT model (Hybrid Single-Particle Lagrangian Integrated Trajectory, Version 4 – January 2017; Stein et al., 2015) and averaged for spring (MAM) 2015 to consider both the springtime nature of bromine explosions and the annual snow accumulation rate. Furthermore, weekly NSIDC sea ice age maps (Fig.60) were used to assess the sea ice distribution when the snow sampling traverse was carried (between 18-26 May 2015).
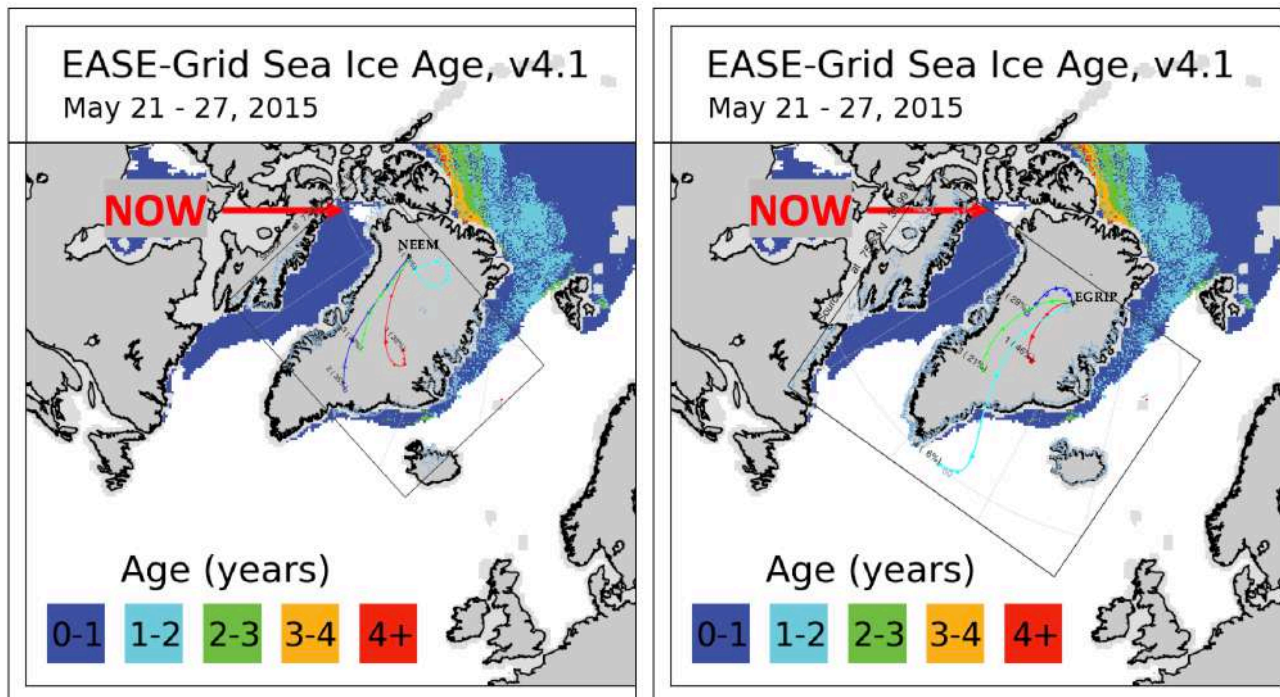
Figure 60: Sea ice Age distribution between May 21-27 and spring average (MAM) back-trajectories arriving at NEEM(left) and EastGRIP (right). The red arrow indicates the NOW. Credit: NSIDC
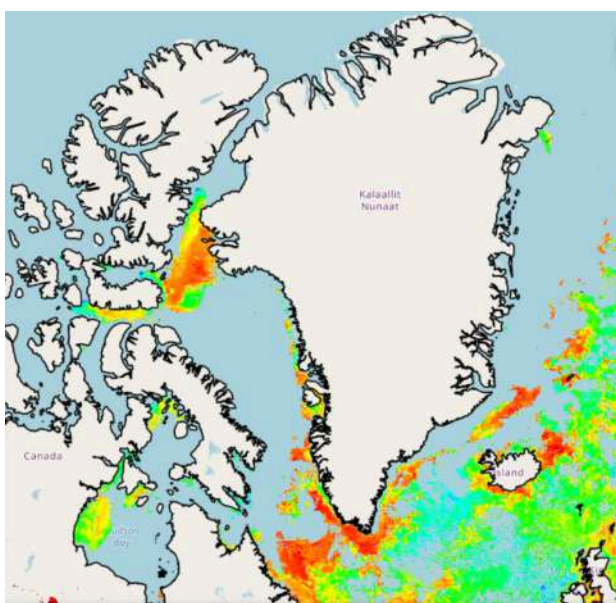
Figure 61: Chlorophyll-A concentrations during May 2015 from ocean colour - Plymouth Marine Laboratory. (blue color =0.005 mg/m3; red color=16 mg/m3).

The atmospheric reanalysis showed that the totality of air masses arrived at NEEM in spring 2015 mainly came from the inland (southern and central Greenland). The same is observed at EastGRIP site where, however, there is a small component (6%) of air masses that before arriving crossed an area of south-east Greenland Sea partially covered by FYSI (Fig.60). Satellite monthly average Chlorophyll-A maps have been also considered to assess marine biological activity in May 2015 (Fig.61). As first guess, quasi-constant values of bromine and iodine fluxes maintained at both sides of the Greenland ice divide might reflect an equal regional-scale distribution around Greenland of both FYSI and marine primary productivity during spring 2015. If all the sample collected during the traverse belong to the same wet precipitation event, the

analytical results suggest a differential deposition for halogens and sodium. While Na is stable and present in the aerosol phase in fact, I and Br could be transported in the gas phase and be less affect by the gravitational deposition. The consequence is a wider and more homogeneous distribution of these elements as showed also by satellite observations over Greenland. Excluded crustal contribution, higher values of sodium found in western Greenland can be attributed to wet deposition of both sea-salt-sodium (ssNa) emitted from the opening of North Water Polynya (NOW) and/or sea ice sea salt (siss) contribution from Baffin Bay (peaking in winter).

Following an east-west elevation profile retracing in part the traverse, a gentler slope characterizes the way up to the ice divide while coming from the eastern coast the slope is way steeper. The NEEM drilling site is located on the western flank of the GrIS about 250 m below of the main ice divide. From there, a very gentle slope (0.1%) led to the EastGRIP site which is located on the plateau. (Fig.62). This difference might bring to think that air masses from western Greenland gradually fractionate sea-salt-aerosols (ssa) along the ascend to the ice divide reaching the maximum of sodium depletion over the GrIS plateau (>2700 m a.s.l.). A similar process might also occur for air masses arriving from the eastern coast, with enhanced ssa loss due to physical barrier encountered, even though, only an additional east-west traverse of Greenland could confirm or deny this hypothesis. Finally, another possibility is that the traverse sampled different snow layer formed during different precipitation events. Although the accumulation is low in both site and a 5-cm of sampling depth might represent a snow accumulation of 2 months, it could be also possible that the upper 5 cm of snow sampled are affected by different deposition events which have delivered on the snow surface a substantial different amount of Br, I and Na.
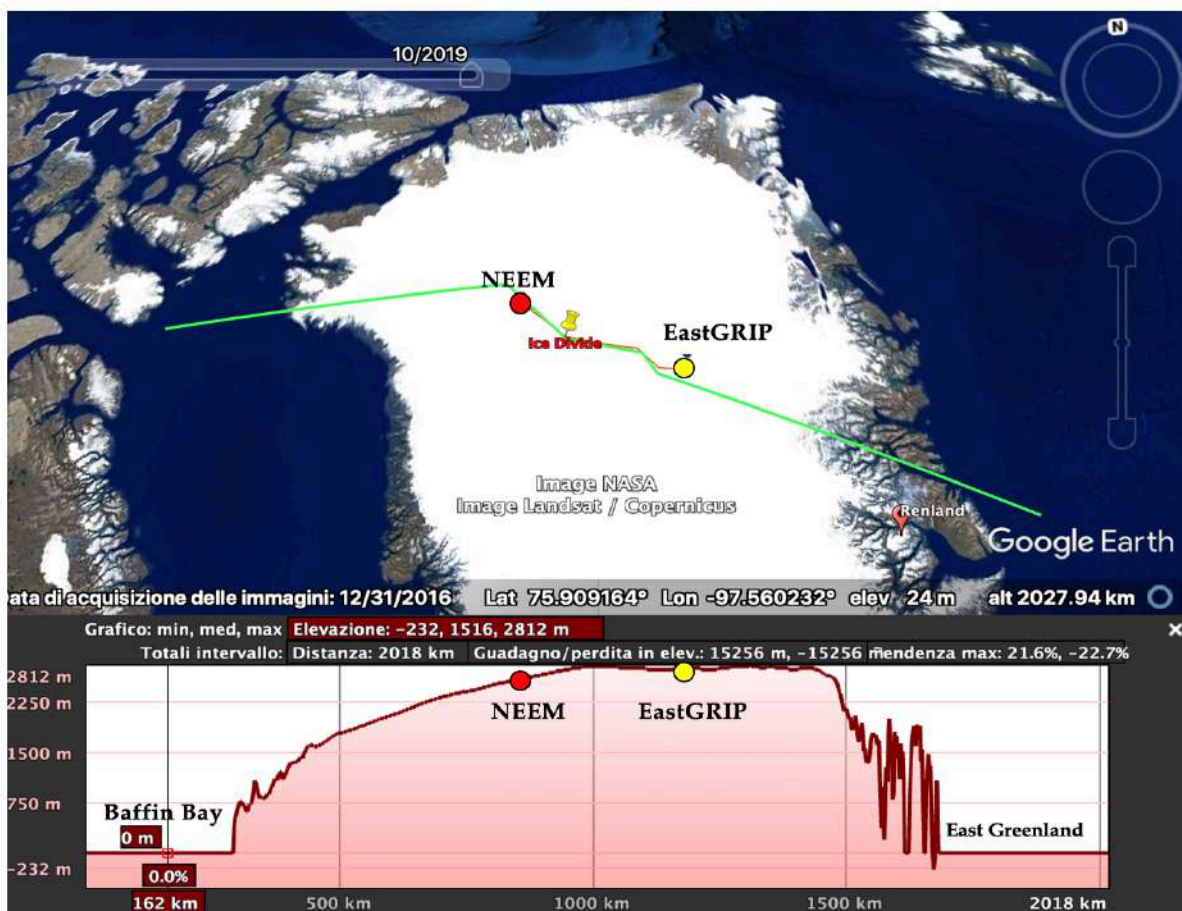

Figure 62: Elevation profile along the green line passing along the NEEM to EastGRIP traverse. The air masses from northern Baffin Bay ascending to the ice divide find a gentler slope than the air masses arriving from Greenland Sea. This can explain differential sodium fractionation (fluxes) between NEEM and EastGRIP surrounds. Credit: Google Earth

6.2 110-year record of Bromine, Iodine and Sodium from SIGMA-A ice core.

6.2.1 Introduction

As already presented in Chapter 4 (section 4.2.2), the SIGMA-A core is a 60.06 m long ice core drilled on the North West Greenland Ice Sheet between May 23-28 of 2017. It is located on the Hayes Peninsula (78°03′06″N, 67° 37′42″ W) at an altitude of 1490 m a.s.l. (Fig.63) and its climatic record extends back to 1904 (113 ys).
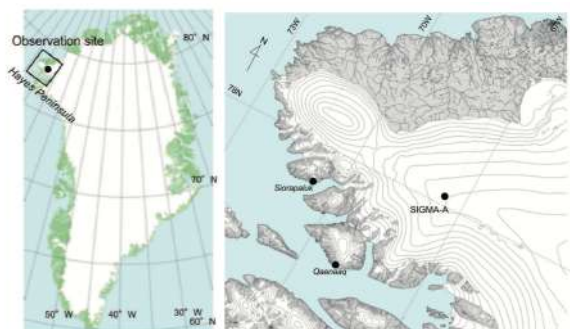
The ice-core samples were placed in polyethylene bags and packed into insulated boxes without any cutting processes. They were then kept frozen

Figure 63: Location of the SIGMA-A site.

during shipment to the Institute of Low Temperature Science in Japan. From there n=564 discrete aliquots were sent to University of Venice for determining halogens (Br, I) and impurities (Na, Ca) analytical concentrations. Starting from the most recent one, the first n=240 samples (covering the period 1979-2017 CE) were analysed with an Inductively Coupled Plasma Sector Field Mass Spectrometry (ICP-SFMS; Element2, ThermoFischer, Bremen, Germany) equipped with a cyclonic Peltier-cooled spray chamber (ESI, Omaha, US) while, to complete the long-term record, the following n=324 samples (from 1979 to 1904) were analysed with a quadrupole ICP-MS with a collision cell.

6.2.2 Analytical Results

Due to high accumulation rate at the ice core site (0.27 m w. eq. y^{-1} between 1975 and 2010) and high sampling resolution (~7 cm/sample) of the core, the analytical measurements conducted in Venice were able to show the annual and sub annual variations of major ions (Na, Ca) and halogens (Br, I). During the long record (113 ys), sodium concentration is very noisy ([Na]=0-1000 ppb) and does not show any particular long-term trend. Differently, calcium varied more sharply from lower concentrations (<100 ppb) during 1910-40 and 1970-90 to higher concentrations (>100 ppb) in between (1940-70 and 1990-2017). Since 1910, halogens concentrations gradually increase showing their maximum values around 1980 for bromine ([Br > 5 ppb]) and in 2003 for iodine ([I > 0.35 ppb]) (Fig. 64). Bromine and iodine enrichment (Br_{enr}; I_{enr}) were also calculated displaying more distinct courses (Fig. 65) somewhat linked also with calcium variation. In particular, during 1910-1950 Br_{enr} progressively decreases (with a 10-y cyclicity observed) to increase again until the end of the record. Two almost symmetric peaks (with Br_{enr} = 25) are showed in 1980 and 1990 when calcium was at its minimum concentrations. Iodine enrichment factors oscillate between 0 and 200 untill the end of

70ies. After that, it show a more pronounced variation with a peak of $I_{enr} > 600$ in 1980 and 2001(Fig.65).
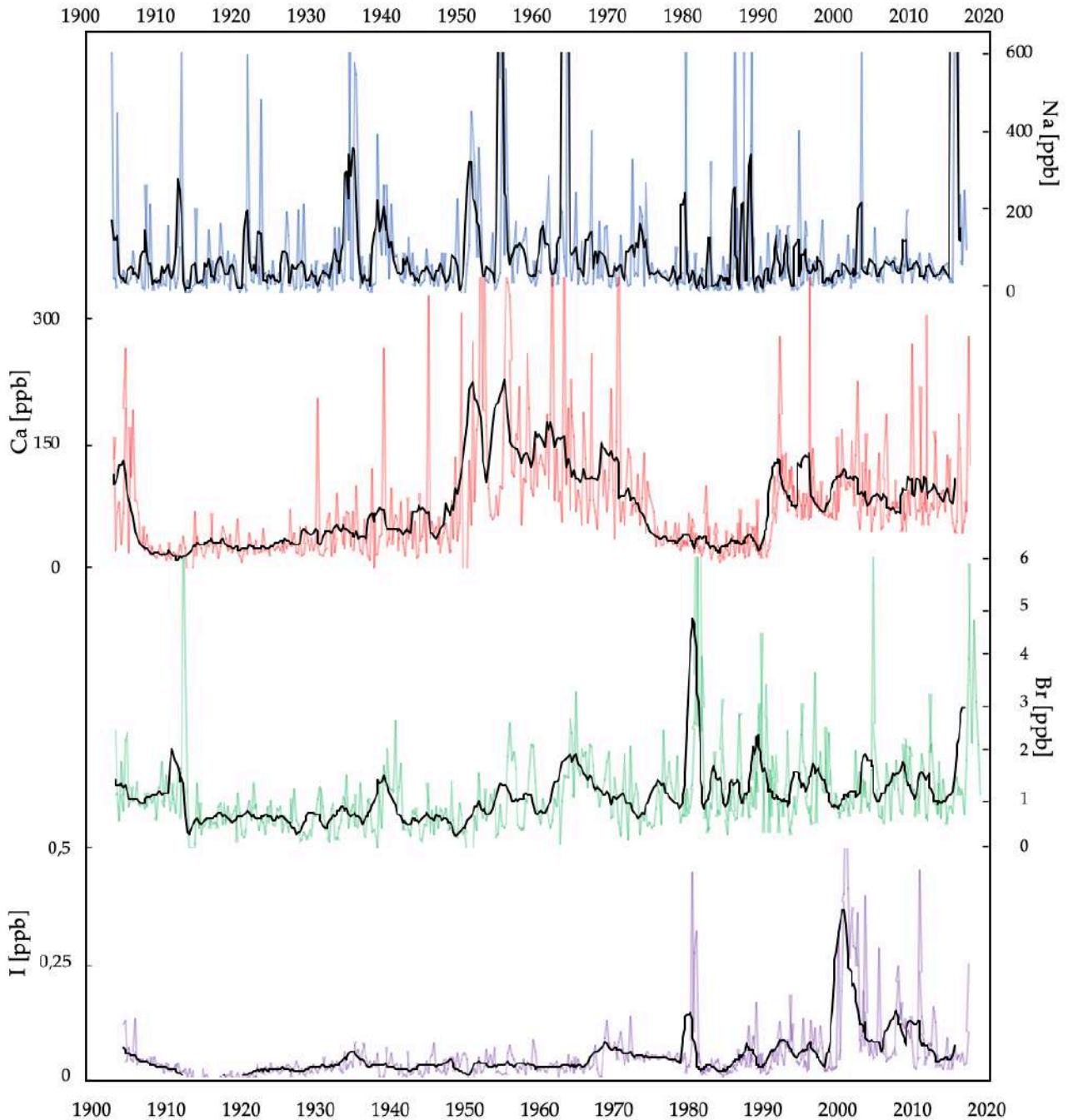
Figure 64: Sodium(blue), Calcium (red), Bromine(green) and iodine (violet) concentrations. Black line is 10-points moving average (about 2 ys smooth)
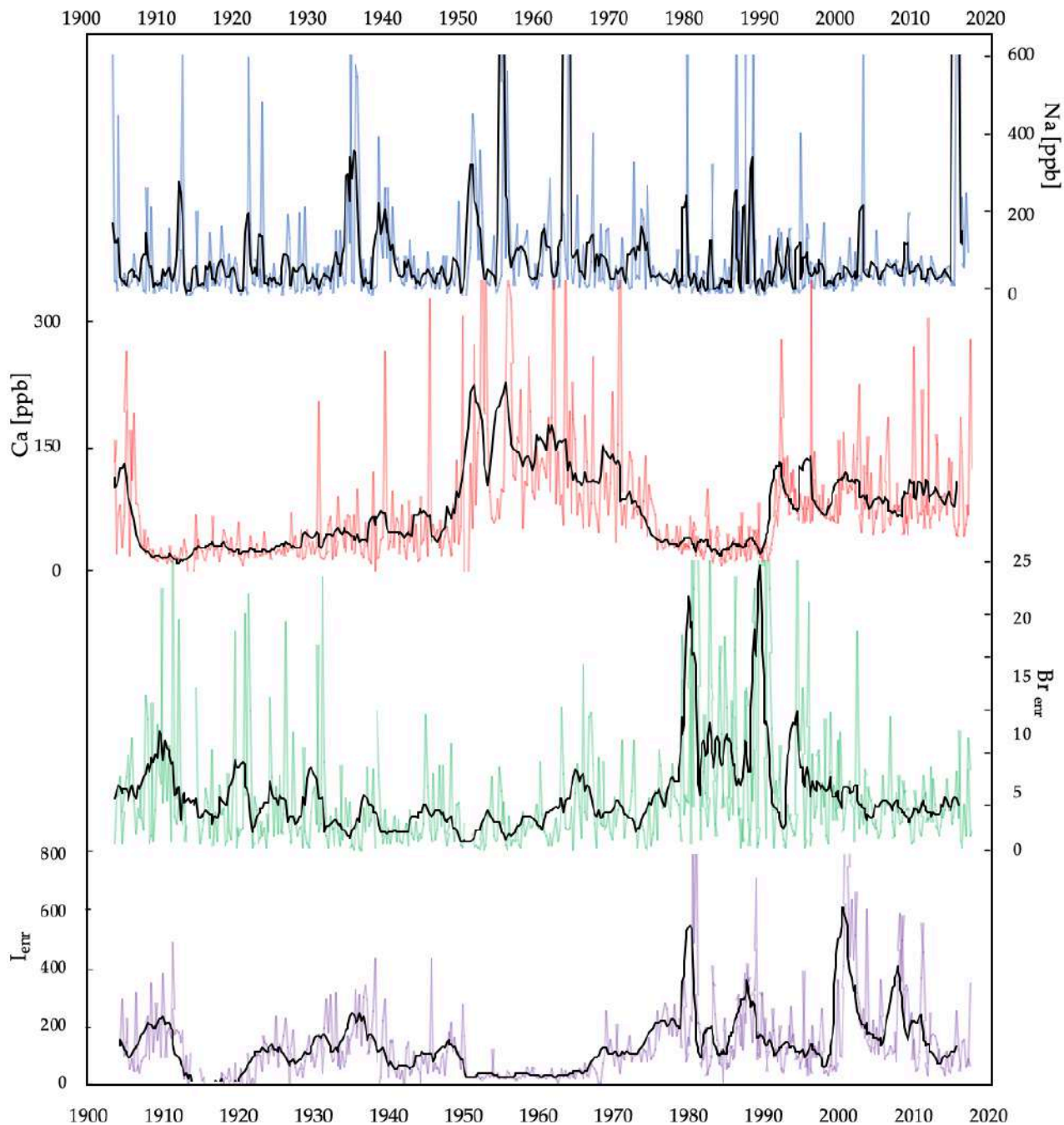
Figure 65:Sodium(blue) and Calcium (red) concentrations with bromine (green) and iodine (violet) enrichments. Black line is 10-points moving average (about 2 ys smooth)

6.2.2 Discussion and future perspectives

The SIGMA-A ice core site is relatively close (<100 km) to the North-western Greenland coast thus it is thought to contain information about the sea ice conditions of Canadian Archipelago and northern Baffin Bay. The main feature of this area is the presence of the North Water Polynya (NOW), an area of year-round open water surrounded by sea ice which forms between Greenland and Canada. With an extent of 85,000 km² it is the largest Arctic polynya and one of the most biologically productive marine areas in the Arctic Ocean (Lewis et al. 1996). Combining high-resolution halogens measurements from the SIGMA-A ice core with multi-physical-and-

biogeochemical parameters provided by the high-resolution Regional Arctic System Model (RASM), for the period 1980-2018, this study aims to test and validate the use of iodine enrichment (I_{enr}) as a potential indicator of past marine productivity.

Although the work is still under investigation some interesting link between I_{enr}, sea ice volume and the primary productivity from small ocean phytoplanktonic species was found. Here are reported the main preliminary findings.
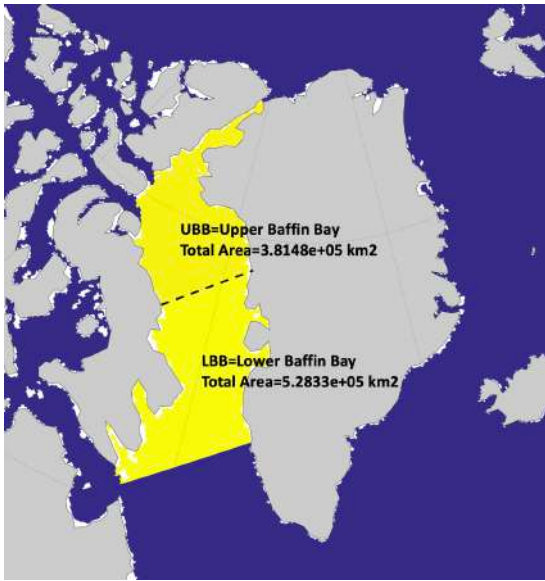
Figure 66: The two sectors of Baffin Bay where the numerical simulation was run.

Table 8: A description of the parameters obtained from the RASM model kindly provided by Younjoo Lee (Naval Postgraduate School). The model performs numerical simulation and synthesis with in-situ and satellite observations, providing monthly values of the parameters listed below.

VARIABLE	NAME	UNIT	INFO
Sea-ice	EXTENT	km^2	sea ice covered region where sea ice concentration is greater than 15%
Sea-ice	VOLUME	km^3	total-integrated sea ice volume over a region
Ocean	SST	deg. C	spatially-averaged sea surface temperature
Ocean	SSS	ppt	spatially-averaged sea surface salinity
Ocean	MLD	m	spatially-averaged mixed layer depth
Sea-ice Algae	NPP	$mgC/m^2/d$	spatially-averaged sea ice algae net primary production
Ocean Diatom	CHL-A	mg/m^2	spatially-averaged diatom chlorophyll-a concentration (depth-integrated)
Ocean Diatom	PP	$mgC/m^2/d$	spatially-averaged diatom primary production (depth-integrated carbon fixation)
Ocean Small-phytoplankton	CHL-A	mg/m^2	spatially-averaged small-phytoplankton chlorophyll-a concentration (depth-integrated)
Ocean Small-phytoplankton	PP	$mgC/m^2/d$	spatially-averaged small-phytoplankton primary production (depth-integrated carbon fixation)
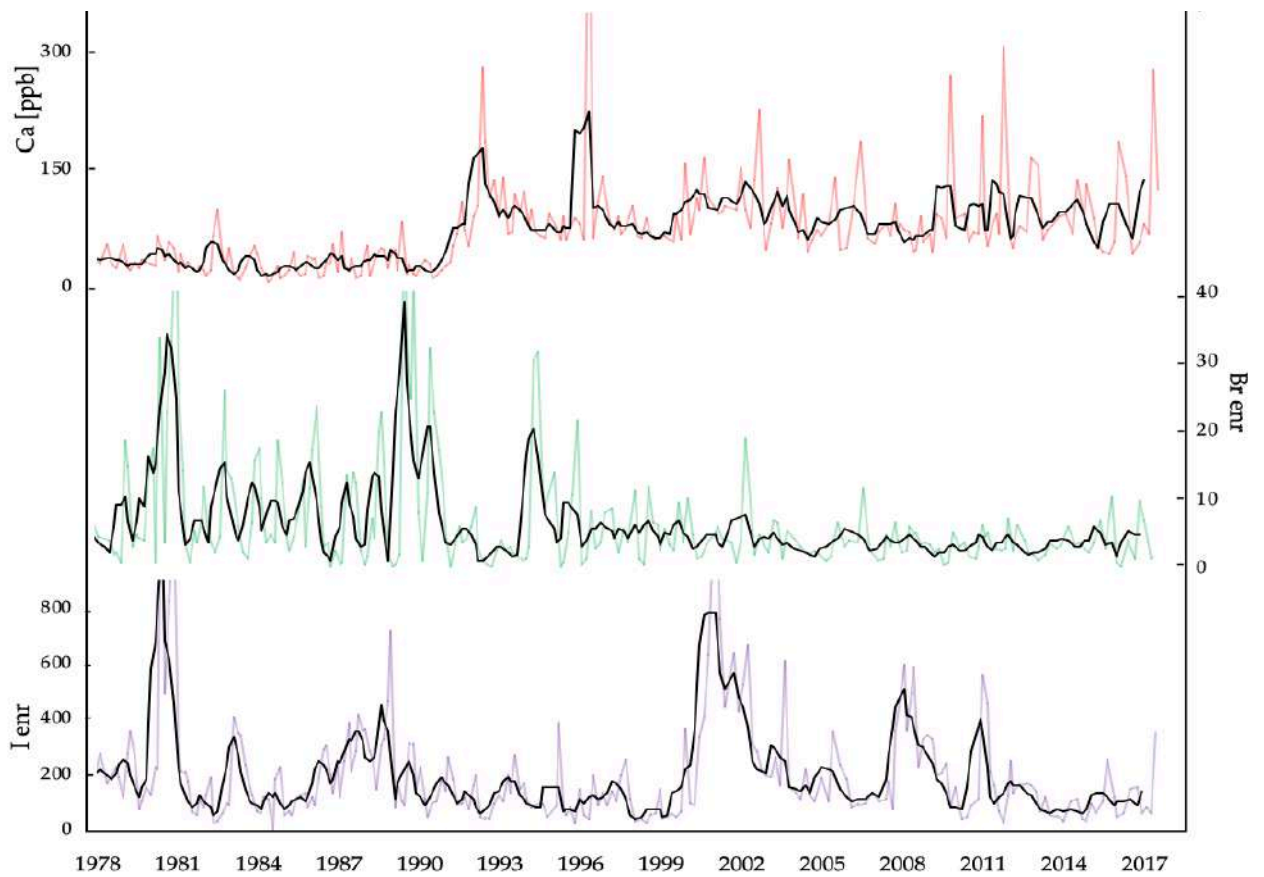
Figure 67: Calcium (red) Bromine (green) and iodine(violet) enrichments during the satellite era (1978-2017). Black line is 4-points moving average (about 1-y smoothing).

Table 9: Pearson's coefficients between annual-average elemental concentration and enrichments from the SIGMA-A ice core and the RASM physical and biogeochemical parameters of upper Baffin Bay for 1980-2018. Model parameters are averaged over May-June-July (MJJ) to consider summertime phytoplanktonic blooms of the NOW polynya.

	[Na]	[Ca]	[Br]	[I]	Br_enr	I_enr
EXTENT	0,17	0,15	-0,19	-0,34	-0,09	-0,37
VOLUME	0,20	0,16	-0,17	-0,34	-0,11	**-0,42**
SST	-0,11	-0,17	0,16	0,28	0,01	**0,38**
SSS	-0,09	-0,34	0,01	0,19	0,17	0,21
MLD	-0,15	-0,37	-0,04	0,07	0,15	0,27
NPP	-0,11	-0,12	-0,22	-0,36	0,19	-0,39
CHL-A	-0,21	0,03	-0,16	0,23	-0,20	0,03
PP	-0,16	0,03	-0,12	0,23	-0,18	0,03
CHL-A	0,06	-0,22	0,43	0,13	0,35	0,21
PP	0,03	-0,27	0,39	0,23	0,23	**0,38**

<div align="right">

C_{HAPTER} 7

</div>

7. Conclusion And Outlooks

7.1 Conclusion and future perspective

In 2016, using bromine and sodium concentrations from the NEEM ice core (North West Greenland) it was provided a reconstruction of the Canadian Arctic sea ice evolution over the last 130,000 years. The study was based on the use of bromine enrichment in ice cores as a chemical marker for first-year sea ice conditions (FYSI). Higher Br_{enr} values indicate enhanced seasonal sea ice conditions while lower values may be attributed both to ice-free conditions or multiyear sea ice (MYSI). Using this concept, the authors were able to distinguish the different phases of the Canadian Arctic sea evolution which has at its extremities two distinct periods: the Holocene Climate Optimum (HCO) and the glacial period. Highest Br_{enr} values recorded about 9,000 years ago during the HCO have been interpreted with the maximum extension of FYSI in Canadian Archipelago, Baffin Bay and Hudson Bay while lowest Br_{enr} values of the glacial period were attributed to a thick developed MYSI sea ice coverage and minimum FYSI conditions. The last glacial period, however, was characterized also by a series of rapid climate instabilities known as Dansgaard-Oeschger event, or more commonly, the DO-events. From stable water isotopes we know that these particular climatic events led to a substantial climate warming of the Artic that, in few decades, passed from a colder and dryer climate (the so-called Greenland Stadials, GS) to warmer and wetter conditions (the Greenland Interstadials, GI). Although several theories have been proposed, the mechanisms behind these climate shifts are still under debate. Some studies indicated Arctic sea ice demise as a potential trigger for DO warmings, however, due to the multidecadal-to-centennial resolution of the samples, the long-term NEEM sea ice record was not able to resolve accurately the rapid GS-GI transition. Thus, one of the main goals of this PhD thesis was to reanalyse a portion of the NEEM ice core (resampled at sub-decadal resolution) looking in detail for sea ice evolution over a series of selected DO events (DO-7 to 10), trying to figure out the causality relation between sea ice change and atmospheric warming. Differently from other studies, for larger DO events (>1 ky), the new sub-decadal measurements did not show any statistically significant lead of the sea ice proxies in respect to atmospheric warming (NEEM oxygen isotopes). This result suggested that the Canadian Arctic sea ice could not have been the trigger for DO but, more likely, it only adjusted to the climate warming. Interestingly, about 400-800 years after the DO-onset, Br_{enr} values show the maximum of

<div align="right">

74

</div>

variance interpreted with a rapid sea ice expansion towards lower latitudes that, consistent with other studies, might have determined the shift to stadial conditions.

The second part of this PhD was focused on the comparison between Br_{enr} from two Greenland ice cores (ReCAP and SIGMA-A) with satellite sea ice images since 1984. Considering sea ice age maps and atmospheric reanalysis it was numerically proved that only FYSI constitutes the main substrate for heterogeneous bromine recycling recorded by the ReCAP and SIGMA-A ice cores. In addition, a positive correlation between Br_{enr} and the NAO index highlighted the role of transport in modulating the glaciochemical signal of an ice core. By minimizing the NAO variability (through the use of 3-5 years moving averages) two linear regressions were found for the recent period between the ReCAP's Br_{enr} and FYSI extent within the East Greenland sector (1984-2012) and between SIGMA-A's Br_{enr} and Baffin Bay sea ice (1984-2016). This new finding can be extremely useful for long-term paleoclimatic sea ice reconstructions using Br_{enr}, since it allows to partially remove/exclude the effects of atmospheric transport noise which still have a high degree of uncertainty for ice cores studies.

Finally, two additional works were presented in the last part of the thesis. The first analyse the critical roles of transport on aerosol and gas phase halogens concluding that, together with depositional and post-depositional processes, there are still some aspects which require further investigation. The second work, instead, presents 110-years record of sodium, calcium and halogens from the SIGMA-A ice core. The preliminary results show some interesting correlations between iodine enrichment and sea ice volume, but also with SST and with the amount of small phytoplanktonic species which populates the North Water Polynya (NOW) in Baffin Bay. These results might validate the use of iodine enrichment to discriminate "warmer" sea ice conditions, excluding the presence of thick MYSI conditions and finally resolving the issue of interpreting low values of bromine enrichment.

Altogether, the following points can be summarized from this research:

- Since 1984, FYSI turned out to be the main efficient substrate responsible for the extra-source of bromine recorded by the ReCAP and SIGMA-A ice cores.

- By averaging Br_{enr} values for the periodicity of the main atmospheric variability (3-5 ys for the NAO index since 1980) the effect of the transport noise was minimized, highlighting the positive connection between FYSI and Br_{enr} in ice cores.

- The sub-decadal halogen enrichments measurements did not show any statistically significant lead of the sea ice proxies in respect to atmospheric warming (NEEM oxygen isotopes) suggesting that the Canadian Arctic sea ice could not have been the trigger for DO but, more likely, it only adjusted to the climate warming.

- Between 0.4-0.8 ky after the onset of the largest DOs, Br_{enr} values show the maximum of variance interpreted with a rapid sea ice expansion towards lower latitudes that, consistent with other studies, might have determined the climate shift back to stadial conditions.

7.2 Summary of the activities

7.2.1 Periods abroad

Period	Institution	Country	Supervisor	Activities
03-05/2019	Norwegian Polar Institute	Svalbard	A. Spolaor	Field Activities
02-03/2019	University of Bern	Switzerland	H.Fisher	Ice core melting (CFA)
03-07 /2018	CSIC-Madrid	Spain	A. Saiz-Lopez	Sea ice-satellite calibration

7.2.2 Projects

Project	Role	Location
Biological Iodine Measurements on Svalbard Snow **(BIOMASS)** **A**rctic **F**ield **G**rant (7.200 €)	Principal Investigator	Ny-Ålesund (Svalbard)
EGRIP CFA Campaign	Participant	University of Bern (Switzerland)
Ice Memory	Participant	Mt.Grand Combin (Switzerland)

7.2.3 Summer School

Date	Title	Location
09/2019	SIOS Training Course: Marine Remote Sensing in Svalbard	UNIS Longyearbyen (Svalbard)
11/2017	Intensive Course: Glaciology (Past, Present and Future)	OGS -Trieste (Italy)
09/2017	Ice Cores Analysis and Techniques (ICAT) Summer School	Centre for Ice and Climate Copenhagen (Denmark)

7.2.4 Scientific Communications

Date	Type	Conference	Location
07/2019	Oral	International Union for Quaternary Research (**INQUA**)	Dublin (Ireland)
07/2019	Oral	International Union of Geodesy and Geophysics (**IUGG**)	Montreal (Canada)
10/2018	Oral	Società Italiana di Scienze del Clima (**SISC**)	Venezia (Italy)
10/2016	Oral	Società Italiana di Scienze del Clima (**SISC**)	Bologna (Italy)
09/2019	Poster	International Conference on Mercury as Global Pollutant (**ICMGP**)	Krocow (Poland)
04/2019	Poster	European Geosciences Union (**EGU**)	Vienna (Austria)
04/2018	Poster	European Geosciences Union (**EGU**)	Vienna (Austria)

7.2.5 Seminars and Conferences

Date	Activity	Location
06/2019	Public Seminar	Venice (Italy)
10/2017	Public Seminar	Catania (Italy)

7.2.6 Other Activities

Date	Activity	Location
07/2019	Tutor of *"Earth's Climate Course"* held by Prof. Barbante at Ca' Foscari-Harvard S.S.	Venice (Italy)
10/2018	Local Organizing Committee SISC 2019	Venice (Italy)

7.2.7 Publications

- (2017) Co-Author of the Chapter 19: "Ice Caves in Italy" of the book "Ice Caves - 1st Edition" published by ELSEVIER. PERSOIU, Aurel; LAURITZEN, Stein-Erik. Ice Caves - 1st Edition. Elsevier, 2017. ISBN: 9780128117392, DOI 10.1016/ C2016-0-01961-7

Acknowledgements

If I were to give an overall opinion about the last three years this would certainly be extremely positive. Overall, I'm really satisfied with the experience gained and, in particular, for the working/friendship relationships that were born in this period.

Naturally, along my path I encountered many difficulties, however, thanks to the people around me I could go always ahead, facing -step by step- all the obstacles. As Galileo said, "behind every problem there is an opportunity!" and I realized that this is particularly true during your PhD. It' always fascinating to push your limit higher and higher!

In these years I had many great opportunities such as to ride the snowmobile across pristine glaciers in Svalbard but also to lose myself in the streets of *Little Italy* in Montreal. I particularly enjoyed the *Movida* of Madrid (also Bologna is not bad! ;-)), cycling in Copenhagen, having several celebratory shots of rum (with thousands of years-old ice inside) in Bern and eating the delicious *Schnitzel* in Vienna accompanied with some interesting *Guinness* in Temple Bar (Dublin).

However, maybe the best part of this period has been offered to me by the people I have dealt with both in Venice and abroad. I think it's impossible to thanks all of them, but someone really deserves a special acknowledge. I had the pleasure to have as supervisor Prof. Carlo Barbante and as co-supervisor Andrea Spolaor. They were both essential to foster my scientific and personal growth together with Alfonso Saiz-Lopez and Paul Vallelonga that constantly helped me during these years. Niccolo Maffezzoli, Carlos Cuevas, Vasileos Gkinis, Clara Turetta, Cristiano Varin and Alessandro Gagliardi were also fundamental for the fulfilment of this work.

Last but not least I would like to thank my family and Ari, my beloved, and all my friends. A particular thank goes to my crazy flatmates (Frank, Nicco EM and Fury) who strongly supported me especially in the last period feeding me and always making "the point".

References

Abram N. J., et al.(2007) Ice core records as sea ice proxies: an evaluation from the Weddell Sea region of Antarctica. *Journal of Geophysical Research: Atmospheres*. 112.D15.

Abram N. J., et al. (2010) Ice core evidence for a 20th century decline of sea ice in the Bellingshausen Sea, Antarctica. *Journal of Geophysical Research: Atmospheres*. 115.D23.

Abram N. J., Wolff E. W., Curran M. AJ. (2013) A review of sea ice proxy information from polar ice cores. *Quaternary Science Reviews* 79: 168-183.

Arrigo, K. R., and van Dijken, G. L.: Secular trends in Arctic Ocean net primary production, *Journal of Geophysical Research*: Oceans, 116, 10.1029/2011JC007151, 2011.

Barrie, L. A., J. W. Bottenheim, R. C. Schnell, P. J. Crutzen and R. A. Rasmussen (1988). "Ozone destruction and photochemical reactions at polar sunrise in the lower Arctic atmosphere." *Nature* 334(6178): 138--141.

Belt S.T. , Massé G., Rowland S.J., Poulin M., Michel C., and LeBlanc B.(2007) A novel chemical fossil of paleo sea ice: Ip25. *Organic Geochemistry* 38(1):16 -27.

Carpenter, L. J. et al. Atmospheric iodine levels influenced by sea surface emissions of inorganic iodine. *Nat. Geosci.* 6, 108–111 (2013).

Cavalieri D. J., Gloersen P., and Campbell W. J. (1984) Determination of Sea Ice Parameters with the NIMBUS-7 SMMR. *Journal of Geophysical Research* 89(D4):5355-5369.

Cavalieri D, Parkinson C, DiGirolamo N, Ivanoff A. (2012) Intersensor Calibration Between F13 SSMI and F17 SSMIS for Global Sea Ice Data Records. *Geoscience and Remote Sensing Letters*, IEEE. 2012;9 (2):233-236.

Collins L. G., et al. (2013) Evaluating highly branched isoprenoid (HBI) biomarkers as a novel Antarctic sea-ice proxy in deep ocean glacial age sediments. *Quaternary Science Reviews*. 79: 87-98.

Corella J. P., Maffezzoli N., Cuevas C. A., Vallelonga P., Spolaor A., Cozzi G., Müller J., Vinther B., Barbante C., Kjaer H. A., Edwards R., and Saiz-Lopez A. (2019) Holocene atmospheric iodine evolution over the North Atlantic, *Clim. Past Discuss*.

Cronin T. M., et al. (2013) A 600-ka Arctic sea-ice record from Mendeleev Ridge based on ostracodes. *Quaternary Science Reviews*. 79: 157-167.

Cuevas C. A., Maffezzoli N., Corella J. P., Spolaor A., Vallelonga P., Kjær H. A. & Fernandez R. P. (2018). Rapid increase in atmospheric iodine levels in the North Atlantic since the mid-20th century. *Nature communications*, 9(1), 1452.

Curran M. A. J., et al. (2003) Ice core evidence for Antarctic sea ice decline since the 1950s. *Science*. 302.5648: 1203-1206.

Curran M. A. J., et al. (2014) Ice core proxy of Antarctic sea-ice extent. *International Symposium on Sea Ice in a Changing Environment*. 69-799.

Dansgaard, W. (1973). Stable isotope glaciology. *Meddelelser om Grønland*. C. A. Reitzel.

Douglas T. A., et al. (2012) Frost flowers growing in the Arctic ocean-atmosphere–sea ice–snow interface: 1. Chemical composition. *Journal of Geophysical Research: Atmospheres*. 117.D14.

Efron B. and Tibshirani R.J. (1993) *An Introduction to the Bootstrap*. Chapman & Hall, New York, London.

Fowler C. W. ,Emery J., and J. Maslanik (2004) Satellite-derived evolution of Arctic sea ice Age: October 1978 to March 2003. *Geoscience and Remote Sensing Letters,* IEEE, 1(2), 71-74.

Funder S., Goosse H.,Jepsen H.,Kaas E.,Kjær K.H., Korsgaard N.J. ,Larsen N.K., Linderson H.,Lyså A., Möller P., et al.(2011). A 10,000-year record of arctic ocean sea ice variability—view from the beach. *Science*,333(6043):747–750.

Gascard J.C., Zhang J., and Rafizadeh M. (2019) Rapid decline of Arctic sea ice volume: Causes and consequences. *The Cryosphere Discuss.*

Gfeller G., Fischer H., Bigler M., Schüpbach S., Leuenberger D., and Mini O.(2014). Representativeness and seasonality of major ion records derived from Neem firn cores. *The Cryosphere*,8(5):1855–1870.

Guillevic M. et al(2014).: Ice-core-based evidence of a three-phase sequence during HS 4. *Clim. Past,* 10, 2115–2133, 2014

Häggblom A. (1982) Drift wood in svalbard as an indicator of sea ice conditions. *Geografiska Annaler*. SeriA. Physical Geography, pages81–94.

Hoff U.,Rasmussen T.L., Stein R., Ezat M.M., and Fahl K.(2016). Sea ice and millennial-scale climate variability in the Nordic seas 90 [thinsp] kyrago to present. *NatureCommunications*,7.

Kinnard C., Zdanowicz C. and Fisher D. (2011) Reconstructed changes in Arctic sea ice over the past 1,450 years. *Nature.*

Kwok R., Rothrock D. A. (2009) Decline in Arctic sea ice thickness from submarine and ICES at records: 1958–2008. *Geophysical research letters* Vol. 36, L15501

Laxon S. W., Giles K. A., Ridout A. L., Wingham D. J., Willatt R., Cullen R., Kwok R., Schweiger A., Zhang J., Haas C., Hendricks S., Krishfield R., Kurtz N., Farrell S., Davidson M. (2013) CryoSat-2 estimates of Arctic sea ice thickness and volume. *Geophysical research letters*. VOL. 40, 1–6

Levine J. G., et al.(2014) Sea salt as an ice core proxy for past sea ice extent: A process-based model study. *Journal of Geophysical Research: Atmospheres*, 119.9: 5737-5756.

Lewis, E. L.; et al. (1996). "Springtime sensible heat, nutrients and phytoplankton in the Northwater Polynya, Canadian Arctic". *Cont. Shelf Res.* 16 (14): 1775–1792.

MacDonald, S. M. et al. A laboratory characterisation of inorganic iodine emissions from the sea surface: dependence on oceanic variables and parameterisation for global modelling. *Atmos. Chem. Phys.* 14, 5841–5852 (2014).

Maffezzoli, N., Vallelonga, P., Edwards, R., Saiz-Lopez, A., Turetta, C., Kjær, H. A., Barbante, C., Vinther, B., and Spolaor, A.(2018) 120,000 year record of sea ice in the North Atlantic, *Clim. Past Discuss.*

Maslanik J. A., Fowler C., Stroeve J., Drobot S., Zwally J., Yi D. and Emery W. (2007) A younger, thinner Arctic ice cover: Increased potential for rapid, extensive sea-ice loss. *Geophysical Research Letters.* 34(L24501).

Maslanik, J., J. Stroeve, C. Fowler, and W. Emery (2011) Distribution and trends in Arctic sea ice age through spring 2011. *Geophysical Research Letters, 38(L13502).*

Matoba, S., Niwano, M., Tanikawa, T., Iizuka, Y., Yamasaki, T., Kurosaki, Y., ... Sugiyama, S. (2018). Field activities at the SIGMA-A site, northwestern Greenland Ice Sheet, 2017. *Bulletin of Glaciological Research*, 36, 15-22. https://doi.org/10.5331/BGR.18R01

McEvoy, Augustin, et al. *(2003)* Practical handbook of photovoltaics: fundamentals and applications. *Elsevier.*

Debra M., et al. (1997) The Greenland Ice Sheet Project 2 depth-age scale Article. *Journal of Geophysical Research Atmospheres* 102(C12):26411-26423.

Millero F. J., et al. (2008) The composition of Standard Seawater and the definition of the Reference-Composition Salinity Scale. *Deep Sea Research Part I: Oceanographic Research Papers, 55.1: 50-72.*

Muller J., et al.(2009) Variability of sea-ice conditions in the Fram Strait over the past 30,000 years. *Nature Geoscience, 2.11: 772-776.*

Poliak L., et al. (2010) History of sea ice in the Arctic. *Quaternary Science Reviews.* 29.15: 1757-1778.

Pöhler, D., Vogel, L., Frieß, U., and Platt, U. (2010). Observation of halogen species in the Amundsen Gulf, Arctic, by active long-path differential optical absorption spectroscopy. *Proceedings of the National Academy of Science, 107(15):6582–6587.*

Perovich DK, Jones KF. The seasonal evolution of sea ice floe size distribution *Journal of Geophysical Research: Oceans.* 119: 8767-8777.

Pratt K. A., et al. (2013)Photochemical production of molecular bromine in Arctic surface snowpacks. *Nature Geoscience,* 6.5: 351-356.

Rankin A. M., Wolff E. W. (2003) A year-long record of size-segregated aerosol composition at Halley, Antarctica. *Journal of Geophysical Research: Atmospheres*, 108.D24.

Rasmussen S.O., Andersen K.K., Svensson A.M., Steffensen J.P., Vinther B.M., Clausen H.B., Siggaard-Andersen, M.-LJohnsen S.J., Larsen L.B., Dahl-Jensen D., Bigler M., Röthlisberger R., Fischer H., Goto-Azuma K., Hansson M.E., Ruth U. (2006) A new Greenland ice core chronology for the last glacial termination. *Journal of Geophysical Research* 111, p. D06102

Rasmussen S.O., Seierstad I.K., Andersen K.K., Bigler M., Dahl-Jensen D., Johnsen S.J.. (2008) Synchronization of the NGRIP, GRIP, and GISP2 ice cores across MIS 2 and palaeoclimatic implications *Quat. Sci.* Rev., 27, pp. 18-28

Rasmussen C., Lybrand R., Jardine A.B., Heidbuechel I., Troch P.A., Chorover J. (2010) Climate and landscape controls on chemical weathering - regional to pedon-scale analysis. *AGU Fall Meeting (Invited) Abstract EP42A-02.*

Rigor I.G., and Wallace J.M. (2004) Variations in the age of Arctic sea-ice and summer sea-ice extent. *Geophysical Research Letters* 31: L09401.

Rothlisberger, Regine, et al. (2010) Potential and limitations of marine and ice core sea ice proxies: an example from the Indian Ocean sector. *Quaternary Science Reviews*, 29.1: 296-302.

Rothrock D. A., Maykut Y. Yu G. A. (1999) Thinning of the Arctic sea-ice cover. *Geophysical Research Letters Vol26-23, 3469-3472*

Sadatzki H., et al (2019). Sea ice variability in the southern Norwegian Sea during glacial Dansgaard-Oeschger climate cycles. *Science advances, Vol. 5, no. 3,*

Saiz-Lopez, A., Blaszczak-Boxe, C., and Carpenter, L. (2015). A mechanism for biologically induced iodine emissions from sea ice. *Atmospheric Chemistry and Physics*, 15(17):9731–9746.

Saiz-Lopez, A., Chance, K., Liu, X., Kurosu, T. P., and Sander, S. P. (2007a). First observations of iodine oxide from space. Geophysical Research Letters, 34(12). Saiz-Lopez, A., Fernandez, R., Ordóñez, C., Kinnison, D., Gómez Martín, J., Lamarque, J., and Tilmes, S. (2014). Iodine chemistry in the troposphere and its effect on ozone. *Atmospheric Chemistry and Physics*, 14(23):13119–13143.

Saiz-Lopez, A., Mahajan, A. S., Salmon, R. A., Bauguitte, S. J.-B., Jones, A. E., Roscoe, H. K., and Plane, J. M. (2007b). Boundary layer halogens in coastal antarctica. *Science*, 317(5836):348–351.

Saiz-Lopez, A., Plane, J. M., Baker, A. R., Carpenter, L. J., von Glasow, R., Gómez Martín, J. C., Mc.gans, G., and Saunders, R. W. (2011). Atmospheric chemistry of iodine. *Chemical reviews*, 112(3):1773–1804.

Saiz-Lopez, A. and von Glasow, R. (2012). Reactive halogen chemistry in the troposphere. *Chemical Society Reviews*, 41(19):6448–6472.

Schonhardt A., et al. (2012) Simultaneous satellite observations of IO and BrO over Antarctica. *Atmospheric Chemistry and Physics*, 12.14: 6565-6580.

Schroeder W. H., et al. (1998) Arctic springtime depletion of mercury. *Nature*, 394.6691: 331-332.

Schüpbach S., Federer U., Kaufmann P., Albani S., Barbante C., Stocker T., and Fischer H.(2013). High-resolution mineral dust and sea ice proxy records from the Talos dome ice core. *Climate of the Past*,9(6):2789–2807.

Schüpbach, S., Fischer, H., Bigler, M., Erhardt, T., Gfeller, G., Leuenberger, D., Mini, O., Mulvaney, R., Abram, N. J., Fleet, L., Frey, M. M., Thomas, E., Svensson, A., Dahl-Jensen, D., Kettner, E., Kjaer, Seierstad, I., Steffensen, J. P., Rasmussen, S. O., Vallelonga, P., Winstrup, M., Wegner, A., Twarloh, B., Wolff, K., Schmidt, K., Goto-Azuma, K., Kuramoto, T., Hirabayashi, M., Uetake, J., Zheng, J., Bourgeois, J., Fisher, D., Zhiheng, D., Xiao, C., Legrand, M., Spolaor, A., Gabrieli, J., Barbante, C., Kang, J. H., Hur, S. D., Hong, S. B., Hwang, H. J.,

Hong, S., Hansson, M., Iizuka, Y., Oyabu, I., Muscheler, R., Adolphi, F., Maselli, O., McConnell, J., and Wolff, E. W.: Greenland records of aerosol source and atmospheric lifetime changes from the Eemian to the Holocene, *Nature Communications*, 9, 1476, 10.1038/s41467-018-03924-3, 2018.

Sturges, W. T. and L. A. Barrie (1988). "Chlorine, Bromine and Iodine in arctic aerosols." *Atmospheric Environment* (1967) 22(6): 1179-1194.

Schweiger O., Risto K. Heikkinen Alexander Harpke Thomas Hickler Stefan Klotz Otakar Kudrna Ingolf Kühn Juha Pöyry Josef Settele (2011) Increasing range mismatching of interacting species under global change is related to their ecological characteristics. *Global Ecology and Biogeography* Volume21, Issue1

Sihler H., et al. (2012) Tropospheric BrO column densities in the Arctic derived from satellite: retrieval and comparison to ground-based measurements.

Simpson W. R., et al. (2007) Halogens and their role in polar boundary-layer ozone depletion. *Atmospheric Chemistry and Physics*, 7.16: 4375-4418.

Spolaor A., et al. (2013) Sea ice dynamics influence halogen deposition to Svalbard. *The Cryosphere*, 7.5: 1645-1658.

Spolaor, A., P. Vallelonga, J. M. C. Plane, N. Kehrwald, J. Gabrieli, C. Varin, C. Turetta, G. Cozzi, R. Kumar, C. Boutron and C. Barbante (2013). "Halogen species record Antarctic sea ice extent over glacial-interglacial periods." *Atmos. Chem. Phys*. 13(13): 6623-6635.

Spolaor A., et al. (2016a) Canadian Arctic sea ice reconstructed from bromine in the Greenland NEEM ice core. *Scientific Reports*, 6.

Spolaor A., et al. (2016b) Halogen-based reconstruction of Russian Arctic sea ice area from the Akademii Nauk ice core (Severnaya Zemlya). *Atm.Chem.Phys*

St-Hilaire-Gravel D., Bell T.J., and Forbes D.L.(2010). Ryaised gravel beaches as proxy indicators of past sea-ice and wave conditions, low therisland, Canadian arctic archipelago. *Arctic*, 213–226.

Stein A.F., Draxler R.R, Rolph G.D., Stunder B.J.B., Cohen M.D., and Ngan F., (2015). NOAA's HYSPLIT atmospheric transport and dispersion modeling system, *Bull. Amer. Meteor. Soc*., 96, 2059-2077,

Thomas E.R., Abram N. J., (2016) Ice core reconstruction of sea ice change in the Amundsen-Ross Seas since 1702 AD. *Geophysical Research Letters* 43.10: 5309-5317.

Tschudi M. A., Fowler C., Maslanik J.A., Stroeve J. (2010) Tracking the movement and changing surface characteristics of Arctic sea ice. *IEEE J. Selected Topics in Earth Obs. And Rem*. Sens., 3(4).

Tschudi M. A., Meier W. N., and Stewart J. S. (2019) An enhancement of sea ice motion and age products. *The Cryosphere Discussion*.

Vallelonga, P., Maffezzoli, N., Moy, A. D., Curran, M. A., Vance, T. R., Edwards, R., Hughes, G., Barker, E., Spreen, G., Saiz-Lopez, A., et al. (2017). Sea-ice-related halogen enrichment at Law dome, coastal East Antarctica. *Climate of the Past*, 13(2):171.

Vallelonga, P., Barbante, C., Cozzi, G., Gaspari, V., Candelone, J.-P., van de Velde, K., Morgan, V. I.,Rosman, K. J. R., Boutron, C. F., and Cescon, P.: Elemental indicators of natural and anthropogenic aerosol inputs to Law Dome, Antarctica, Ann. Glaciol., 39, 169-174, 10.3189/172756404781814483, 2004.

Vallelonga, P., Barbante, C., Cozzi, G., Gabrieli, J., Schüpbach, S., Spolaor, A., and Turetta, C.: Iron fluxes to Talos Dome, Antarctica, over the past 200 kyr, Clim. Past, 9, 597-604, 10.5194/cp-9-597-1989 2013, 2013.

Vinther B. M., Andersen K. K., Jones P.D., Briffa K. R., and Cappelene J. (2006) Extending Greenland temperature records into the late eighteenth century. *Journal of Geophysical Research*, VOL. 111, D11105, doi:10.1029/2005JD006810.

Vogt, R., Crutzen, P. J., and Sander, R. (1996). A mechanism for halogen release from sea-salt aerosol in the remote marine boundary layer. *Nature*, 383(6598):327–330.

Yang X., Pyle J.A., Cox R. Sea salt aerosol production and bromine release: Role of snow on sea ice. *Geophysical Research Letters*, 2008, 35.16.

Zhao X., Strong K., Adams C., Schofield R., Yang X., Richter A., Friess U., Blechschmidt A.-M., and Koo J.-H.(2016). A case study of a transported bromine explosionevent in the canadian high arctic. *Journal of Geophysical Research: Atmospher*, 121(1):457–477.